

Task 13 Performance, Operation and Reliability of Photovoltaic Systems

S
P
V
P
S

Soiling Losses – Impact on the Performance of Photovoltaic Power Plants

2022



What is IEA PVPS TCP?

The International Energy Agency (IEA), founded in 1974, is an autonomous body within the framework of the Organization for Economic Cooperation and Development (OECD). The Technology Collaboration Programme (TCP) was created with the belief that the future of energy security and sustainability starts with global collaboration. The programme is made up of 6.000 experts across government, academia, and industry dedicated to advancing common research and the application of specific energy technologies.

The IEA Photovoltaic Power Systems Programme (IEA PVPS) is one of the TCPs within the IEA and was established in 1993. The mission of the programme is to “enhance the international collaborative efforts which facilitate the role of photovoltaic solar energy as a cornerstone in the transition to sustainable energy systems.” In order to achieve this goal, the programme’s participants have undertaken a variety of joint research projects in photovoltaic (PV) power systems applications. The overall programme is headed by an Executive Committee, comprising one delegate from each country or organizational member, which designates distinct ‘Tasks’ that may be research projects or activity areas.

The IEA PVPS participating countries are Australia, Austria, Canada, Chile, China, Denmark, Finland, France, Germany, Israel, Italy, Japan, Korea, Malaysia, Mexico, Morocco, the Netherlands, Norway, Portugal, South Africa, Spain, Sweden, Switzerland, Thailand, Turkey, and the United States of America. The European Commission, Solar Power Europe, Smart Electric Power Alliance (SEPA), and Solar Energy Industries Association are also members.

Visit us at: www.iea-pvps.org

What is IEA PVPS Task 13?

Within the framework of the IEA PVPS, Task 13 aims to support market actors working to improve the operation, reliability and quality of PV components and systems. Operational data from PV systems in different climate zones compiled within the project will help provide the basis for estimates of the reliability and performance of the current PV systems.

Task 13 provides a common platform to summarize and report on technical aspects affecting the quality, performance, reliability and lifetime of PV systems in a wide variety of environments and applications. By working together across national boundaries, we can all take advantage of research and experience from each member country and combine and integrate this knowledge into valuable summaries of best practices and methods for ensuring that PV systems perform at their optimum and continue to provide competitive return on investment.

Task 13 has established a framework for calculations of various parameters that provide an indication of the quality of PV components and systems. The framework, along with the results included in the high-quality reports, is useful to and appreciated by the solar PV industry.

The IEA PVPS countries participating in Task 13 are Australia, Austria, Belgium*, Canada, Chile, China, Denmark, Finland, France, Germany, Israel, Italy, Japan, the Netherlands, Norway, Spain, Sweden, Switzerland, Thailand, and the United States of America.

This report addresses global soiling of PV power plants with the aim to provide information on the impact of dust soiling and snow losses for various stakeholders. Further information and results of Task 13 can be found at: <https://iea-pvps.org/research-tasks/performance-operation-and-reliability-of-photovoltaic-systems/>.

* Belgium is no longer participating in IEA PVPS, effective from 01 July, 2022.

DISCLAIMER

The IEA PVPS TCP is organised under the auspices of the International Energy Agency (IEA) but is functionally and legally autonomous. Views, findings and publications of the IEA PVPS TCP do not necessarily represent the views or policies of the IEA Secretariat or its individual member countries.

COVER PICTURE

Soiling in a PV plant in Atacama Desert, Chile. Source: Fraunhofer ISE/Andreas Steinhüser

ISBN 978-3-907281-09-3: Soiling Losses – Impact on the Performance of Photovoltaic Power Plants



INTERNATIONAL ENERGY AGENCY
PHOTOVOLTAIC POWER SYSTEMS PROGRAMME

IEA PVPS Task 13
Performance, Operation and
Reliability of Photovoltaic Systems

**Soiling Losses – Impact on the Performance of
Photovoltaic Power Plants**

Report IEA-PVPS T13-21:2022
December 2022

ISBN 978-3-907281-09-3



AUTHORS

Main Authors

Christian Schill, Fraunhofer ISE, Freiburg, Germany
Anne Anderson, Research Institutes of Sweden AB (RISE), Sweden
Christopher Baldus-Jeursen, CANMET Energy Technology Centre, Canada
Laurie Burnham, Sandia National Laboratories, USA
Leonardo Micheli, Universidad de Jaén, Spain
David Parlevliet, Murdoch University, Perth, Australia
Eric Pilat, CEA INES, France
Bengt Stridh, Mälardalens högskola, Sweden
Elías Urrejola, Atamostec, Chile

Contributing Authors

Manjunath Basappa Ayanna, CSIR, South Africa
Gianluca Cattaneo, Centre Suisse d'Electronique et de Microtechnique, Switzerland
Sebastian-Johannes Ernst, Fraunhofer ISE, Germany
Anil Kottantharayil, NCPRE, IIT Bombay, India
Gerhard Mathiak, DEWA Research & Development Center, United Arab Emirates
Erin Whitney, University of Alaska Fairbanks, USA
Rosmarie Neukomm, Bern University of Applied Sciences, Switzerland
Delphine Petri, Centre Suisse d'Electronique et de Microtechnique, Switzerland
Lawrence Pratt, CSIR, South Africa
Lina Rustam, Fraunhofer ISE, Germany
Thomas Schott, Bern University of Applied Sciences, Switzerland

Editor

Ulrike Jahn, VDE Renewables, Alzenau, Germany



TABLE OF CONTENTS

Acknowledgements	7
List of Abbreviations	8
Executive Summary	11
1 Introduction.....	14
2 Physical and Chemical Principles of Soiling.....	20
2.1 Physical and Chemical Nature of Dust	20
2.2 Cementation, Caking, Capillary Aging	23
2.3 Dew-Driven Soiling Mechanisms	25
2.4 Review of Moisture in Soiling.....	27
2.5 Overview of Particle Deposition and Adhesion Forces: Van der Waals, Capillary, Electrostatic, and Gravitational Forces.....	28
3 Sensing Soiling and Snow	31
3.1 Soiling Metrics	31
3.2 Market Overview of Soiling and Snow Sensors	34
4 Soiling and Snow Models	41
4.1 Soiling Models	41
4.2 Snow Models.....	50
5 Estimation of Energy and Revenue Losses of Soiling at Utility Scale.....	56
5.1 Economic Impact of Soiling	56
5.2 Soiling Losses Worldwide: Resources and Variability	59
5.3 Case Study: Long-Term Soiling Losses in a Moderate Climate	60
6 Mitigation of Soiling Losses in PV Systems	63
6.1 Preventive Mitigation Methods.....	64
6.2 Corrective Mitigation Methods	71
6.3 Generic “Best-Time-to-Clean” Models	82
6.4 Snow Impact Mitigation Strategies.....	87
7 Snow Shading of Photovoltaic Systems.....	89
7.1 Introduction	89
7.2 Performance Factors for PV Systems at High Latitudes	90
7.3 Global Distribution of Snow	92
7.4 Focus Areas for Snow Research	94
7.5 Snow-Loss Metrics	95



7.6 Design Optimization for Snowy Climates	100
8 Conclusion.....	108
Appendix 1: Particle Composition and Solubility	110
Appendix 2: Dust Composition Survey	112
Appendix 3: Macroscopic, Controllable and Microscopic Factors Influencing Soiling	114
References.....	117



ACKNOWLEDGEMENTS

This paper received valuable contributions from several IEA-PVPS Task 13 members and other international experts, as outlined below.

This report is supported by the German Federal Ministry for Economic Affairs and Energy (BMWi) under contract no. 0324304A and no. 0324304B.

Part of this work was funded through the European Union's Horizon 2020 research and innovation programme under the NoSoilPV project (Marie Skłodowska-Curie grant agreement No. 793120).

Anil Kottantharayil would like to acknowledge co-workers S. Bhaduri, S. Chattopadhyay, S. Zachariah, and C. S. Solanki from NCPRE, IIT Bombay for contributions to the work reported in the subchapter “New Module- and Plant Concepts”.

Lina Rustam would like to acknowledge Klemens Ilse, Fraunhofer CSP, Germany, for contributions to subchapter “Anti-Soiling Coatings”.

Erin Whitney would like to acknowledge colleagues Christopher Pike, Michelle Wilber, Dr. Joshua Stein, Dayne Broderson, Rob Bensin, David Light, Henry Toal, Iris Tuller, and Christie Hauptert for their contributions to the University of Alaska Fairbanks Solar Test Site and data analysis efforts. The Solar Test Site and its resulting data were made possible through a Cooperative Research and Development Agreement (CRADA) between the University of Alaska and Sandia National Laboratories as well as generous support from the United States Department of the Navy, Office of Naval Research.

Many thanks go to Erin Whitney and colleagues for the editing of the executive summary, technical and language editing and proof-reading of this report, and also to Leonardo Micheli for technical editing and support. Your help and support is highly appreciated.



LIST OF ABBREVIATIONS

AFm	Alumina, Ferric Oxide, Mono-Sulfate
AI	Artificial Intelligence
Al	Aluminium
ANN	Artificial Neural Network
ANOVA	Analysis of Variance
AOD	Aerosol Optical Depth
ARC	Anti-Reflection Coating
ASC	Anti-Soiling-Coating
ASTM	American Society for Testing and Materials
BFH	Bern University of Applied Science
BoS	Balance of System
Ca	Calcium
CA	Contact Angle
CAMS	Copernicus Atmosphere Monitoring Service
Cd	Cadmium
CIS	Copper Indium Selenide
Cl	Chlorine
cm ²	Square-Centimetre
CMAQ	Community Multiscale Air Quality
CPL	Cost of Production Losses
CSP	Concentrating Solar Power
CWEEDS	Canadian Weather Energy and Engineering Data Sets
D	Particle Diameter
DNI	Direct Normal Irradiance
DOI	Digital Object Identifier
ECMWF	European Centre for Medium-Range Weather Forecast
EDS	Electrodynamic Shield
EDX	Energy Dispersive X-Ray
EMC	Electromagnetic Compatibility
EP	Electricity Price
EPC	Engineering, Procurement and Construction
ESD	Electrostatic Discharge
EVA	Ethylene-Vinyl Acetate
G	Gravitational Acceleration
GHCN	Global Historical Climatology Network
H	Hydrogen



HR	Hygrometry
IEA	International Energy Agency
IEC	International Electrotechnical Commission
IEEE	Institute of Electrical and Electronics Engineers
IPCC	Intergovernmental Panel on Climate Change
IR	Infrared
I_{sc}	Short Circuit Current
I-V	Current-Voltage
K	Potassium
kHz	Kilohertz
kV	Kilovolts
kWh	Kilo-Watthour
LCOE	Levelized Cost of Energy
LED	Light Emitting Diode
MERRA	Modern Era Retrospective-Analysis for Research and Applications
mg	Milligram
Mg	Magnesium
MW	Megawatt
N	Nitrogen
Na	Sodium
NASA	National Aeronautics and Space Administration
NCPRE	National Centre for Photovoltaic Research and Education
NNE	North-North-East
NNW	North-North-West
NOCT	Normal Operating Cell Temperature
NPV	Net Present Value
NREL	National Renewable Energy Laboratory
O	Oxygen
O&M	Operation & Maintenance
PA	Polyamide
PDF	Powder Diffraction File
PE	Polyester
PM	Particle Mass
PM10	Particulate Matter of Size of 10 Microns and Below
P_{mpp}	Maximum Power Point
POA	Plane of Array
PV	Photovoltaic



RH	Relative Humidity
S	Sulphur
SAM	System Advisor Model
SDS-WAS	Sand and Dust Storm Warning Advisory and Assessment System
SEM	Scanning Electron Microscopy
Si	Silicon
Soiling Rate	Daily Variation in Soiling Ratio while Soiling Deposits on PV Module Surface
Soiling Ratio SR	Current Soiling State of the System
SR	Spectral Response
STC	Standard Testing Conditions
SUNY	State University of New York
SVI	Soiling Variability Index
T_a	Ambient Temperature
TEM	Transmission Electron Microscopy
TSP	Total Suspended Particles
TSPM	Total Suspended Particulate Matter
VAC	Volts Alternating Current
VDC	Volts Direct Current
VDI	Verein Deutscher Ingenieure, Association of German Engineers
V_{oc}	Open Circuit Voltage
W	Watt
WD	Wind Direction
WMO	World Meteorological Organization
W_p	Watt Peak
WS	Wind Speed
XRD	X-Ray Diffraction
A	Temperature Coefficient
M	Dynamic Viscosity of Air
Mm	Micro-Metre
P	Particle Density



EXECUTIVE SUMMARY

On a global scale, the soiling of solar photovoltaic (PV) systems from dust and snow, and subsequent loss of energy yield, is the single most influential factor impacting system yield after irradiance. Especially in arid regions, soiling may affect large utility-scale PV plants to a significant extent – making it necessary to mitigate these effects by cleaning whole systems – and thus leading to a reduction of revenues, caused by higher operating and/or capital expenditures (e.g., for investments in anti-soiling coatings [ASC] or cleaning robots and their maintenance).

This report therefore summarizes aspects of soiling from different perspectives including particle types and global distributions (Chapter 1), mechanisms and contributing factors (Chapter 2), sensors and measurement techniques (Chapter 3), modelling approaches and results (Chapter 4), economic impacts (Chapter 5), mitigation strategies (Chapter 6), and special installation and operation considerations for snow shading as solar arrays increasingly proliferate into higher latitudes (Chapter 7). The report is intended to serve the communities of PV customers, PV industry, O&M companies, investors, asset managers, testing equipment developers, testing companies, standardization authorities and research institutions alike.

Chapter 1 (*Introduction*) provides an overview of particle sizes, types, and global distributions and impacts. In particular, global surveys show the highest total suspended particle densities (100-200 $\mu\text{g}/\text{m}^3$) in equatorial regions around Africa and Asia, not including snow shading effects at high latitudes.

Chapter 2 (*Physical and Chemical Principles of Soiling*) characterizes the factors contributing to dust particle deposition and adhesion on glass and PV module. Silt size particles in the range of 2 μm to 63 μm are the predominant contributors to soiling in arid and semi-arid climates, as can be seen from analyses in the Atacama Desert, Chile, and Qatar. Gravitational forces contribute to shorter airborne times for medium to large particles (>10 μm), while smaller particles (<5 μm) remain airborne longer due to air turbulence, and very small particles (<1 μm) are easily removed from the atmosphere by rain and do not deposit. The basic soiling formation processes of cementation, capillary aging, and caking are described, all of which have specific effects on the severity, persistence, and resistance to removal. Dew formation also plays a role, often increasing particle deposition rates as illustrated with an example from the Atacama Desert, in conditions of ambient high humidity combined with radiative cooling of PV modules due to the high infrared emissivity of solar glass. A review of deposition and adhesion forces asserts that particles smaller than 10 μm are rarely removed by wind from PV modules.

Chapter 3 (*Sensing Soiling and Snow*) provides insight into how to measure soiling, with what kind of sensors, their metrics, and different principles of operation, which can be categorised into electrical (short-circuit current and power) and optical (image processing cameras, LEDs, and reflectance measurements). This information is critical for predictions of future soiling rates and cleaning decision timelines. Metrics generally comprise a soiling ratio and soiling rate. Soiling does not always occur homogeneously over the whole module surface or plant, and tends to accumulate in the lower parts of modules. In particular, if soiling is not distributed uniformly, the short circuit current measurements may underestimate the actual impact of soiling on PV power. As such, an underestimated cost factor is the integration of multiple soiling monitors into the overall monitoring infrastructure to account for this heterogeneity. IEC Standard 61724 "Photovoltaic system performance - Part 1: Monitoring" provides recommendations of when and where to measure soiling on site and how often to clean sensors in order to produce reliable results. On a general note, with regard to soiling sensor measurement



accuracy, more study is needed to quantify measurement uncertainty of different soiling sensing products.

Chapter 4 (*Soiling and Snow Models*) summarizes efforts to develop methods of modelling soiling based on different sets of parameters. These models can be categorised as micro-, regional- and macro models, and all have their strengths and weaknesses. The report differentiates between linear-regression, semi-physical, artificial neural network, and geospatial models, all of which have their specific fields of application, advantages, and disadvantages. Most of the models are calibrated against local phenomena. To date, globally applicable models tend to forecast the correct trends for higher soiling losses but correlate poorly with minor losses. Snow shedding models are also discussed and differentiated into the two categories of direct energy loss prediction and snow coverage prediction. Chapter 4 concludes with a Canadian case study that estimates energy losses predicted by two different snow models as predictors for soiling phenomenon in high latitudes. More work is still needed to understand the causes of discrepancy and to validate the models with more sites.

To provide a better overview of the global and economic dimensions of the problem, the report estimates the energy losses for PV plants on a global scale in Chapter 5 (*Estimation of Energy and Revenue Losses of Soiling at Utility Scale*). It is estimated that in 2018, soiling caused a loss of the annual PV energy production of at least 3-4%, which corresponded to an economic loss in the order of three to five billion euros. It is expected that these kinds of losses will translate to 4-5% in energy production, leading to subsequent financial losses in the range of four to seven billion euros by 2023. This is due to several factors. For example, more PV modules are installed in high-insolation regions, such as China or India, which are also more exposed to soiling. The reduced price of electricity in some regions will make cleaning “less convenient” because revenues for recovered energy will be lower. And, lastly, under identical soiling conditions, more efficient modules are subject to larger energy losses compared to less efficient PV modules. Various economic models have been proposed to identify the best fitting cleaning schedule under different constraints, in order to minimize revenue losses. Chapter 5 and Chapter 6 examine these kinds of models and the promises they make.

Two categories of possible mitigation strategies are summarized in Chapter 6 (*Mitigation of Soiling Losses in PV Systems*). The first is preventive methods such as site assessment and planning, new module and plant concepts, as well as anti-soiling coatings. The second is corrective mitigation methods such as different types of cleaning (by wet/dry brushes, cleaning robots, electrodynamic cleaning, etc.). Chapter 6 also provides an overview of generic “Best Time-to-Clean” models as decision support tools for triggering cleaning operations on site.

PV systems in high latitudes are proliferating due to the advent of bifacial modules, higher system efficiencies, and lower costs. Chapter 7 (*Snow Shading of Photovoltaic Systems*) summarizes aspects of snow shading of PV systems, with an emphasis on performance factors like temperature, irradiance, albedo, and their global distribution. Focus areas for “snow research” are then highlighted, i.e., assessing snow losses, performance modelling, and performance optimization, as well as reliability aspects related to thermo-mechanical load stresses. These load stresses are exacerbated by extreme winter storms and freeze/thaw cycles that can crack solar cells, distort module frames, and damage coatings, resulting in under-performing and failed modules. Chapter 7 then defines snow loss metrics and finally suggests design optimisations for snowy climates by demonstrating that climate-specific technological and design choices can lead to measurable efficiency gains. Choices fall into categories like module architecture (e.g., frame vs. frameless, cell stringing, etc.), module technology (cell size, cell design, bifacial vs. mono-facial) and finally system design (module orientation, height above ground, tilt angle, clip design and placement). To mitigate production losses, promising



considerations for high latitude solar installations include frameless modules, steeper tilt angles, snow-shedding coatings, bifacial modules, and attention to array heights to minimize snow accumulation on the bottom edges of modules, among other factors.



1 INTRODUCTION

Especially in arid regions and snow prone areas, shading from mineral dust and snow and the subsequent losses in performance for PV installations present substantial challenges for the PV industry. Mitigation for these effects can lead to a reduction of revenues, caused by higher operating and/or capital expenditures (e.g., for the investments in anti-soiling coatings [ASC] or cleaning robots and their maintenance). The continued growth of the PV industry worldwide into arid and snowy regions requires an understanding of soiling processes, impacts, and mitigation measures.

Deposition of dust on inclined surfaces – either with or without anti-soiling coatings – is a complex and multidimensional phenomenon. The primary parameters are local environmental conditions like relative humidity and the occurrence of dew, wind speed and direction, precipitation frequency and intensity, soil type, and topography of the terrain [1]. However, there are also larger-scale effects such as dust transport over hundreds of kilometres. Other factors like land use and land cover are examples of anthropogenic activity that impact the potential for soiling, e.g., by agricultural activity.

The size of wind-blown dust particles are in the range of 1-100 μm , with PM10 and PM2.5, as shown in Figure 1:

Particle Size

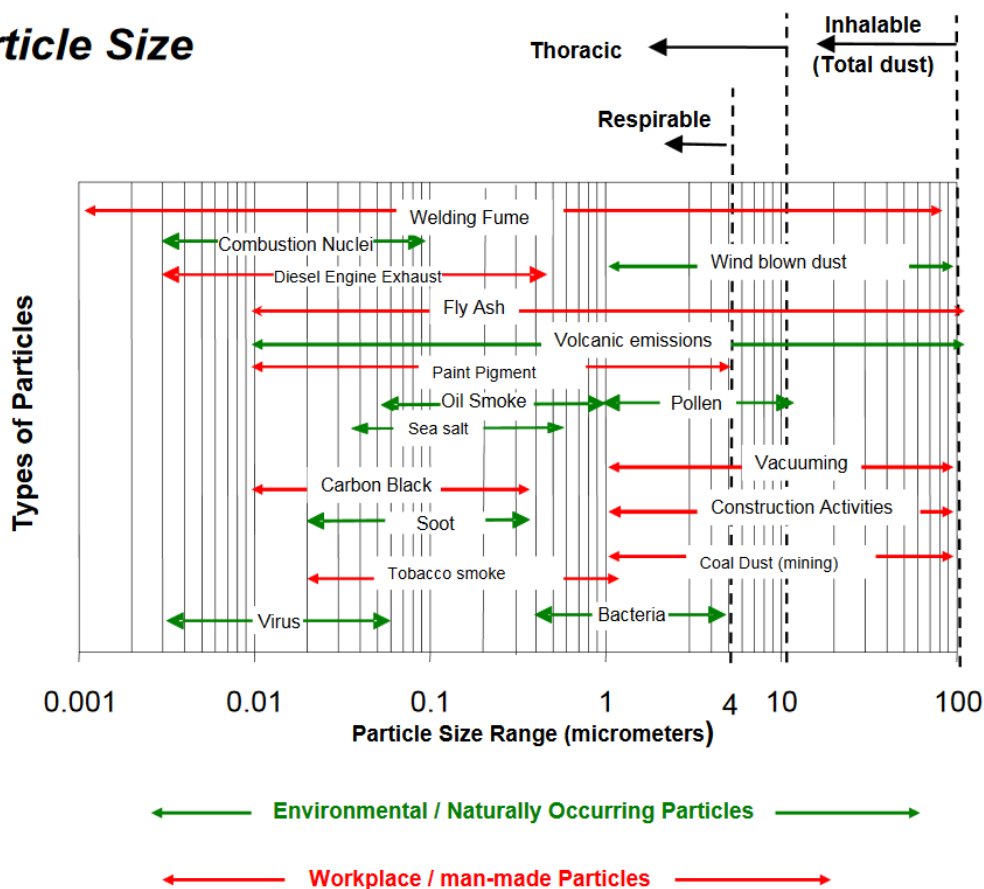


Figure 1: Particle size distributions, kind permission by TSI.



Particle sizes below $10\ \mu\text{m}$ or $2.5\ \mu\text{m}$, respectively, are among the best proxies to model soiling [2], [3], as detailed in Chapter 4. Soiling is a very site-specific problem and may vary seasonally and annually. [4], [2]. Javed and colleagues [1] have shown that environmental factors like the ones mentioned above have a loose correlation with the daily degree of soiling.

Figure 2 below shows the seasonal variation of airborne dust intensity around the world. It is derived from Aerosol-Optical-Depths (AOD) satellite time series measurements. The darker regions indicate areas with higher densities of dust. It is notable that Saharan dust plumes are transported hundreds of kilometres over the Atlantic to reach the Americas.

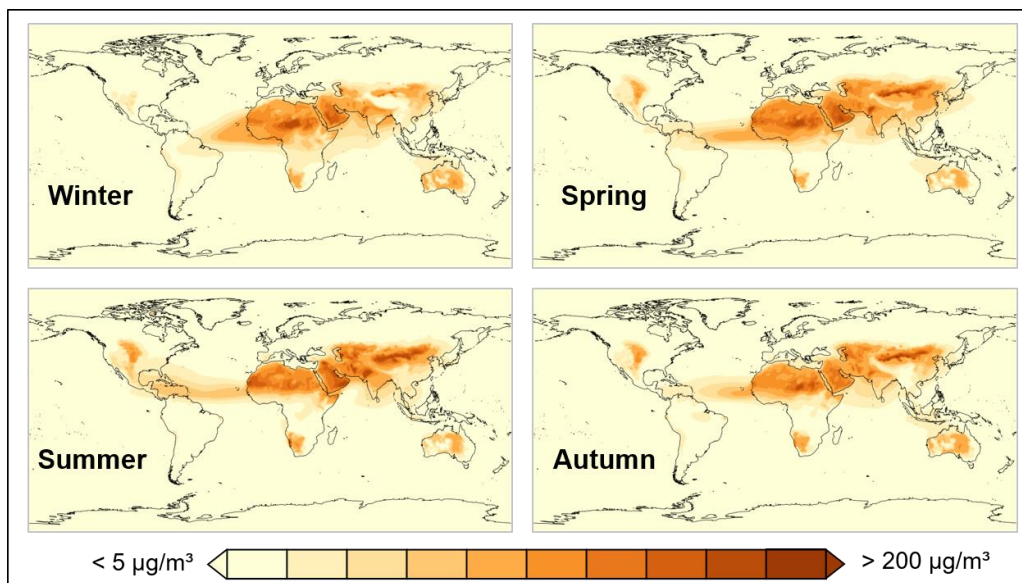


Figure 2: Total suspended particle density derived from a typical dust year.

The global dimensions of this phenomenon and especially the energy and revenue losses for PV installations are immense, as discussed further in Chapter 5.

Taking a closer look at its components, soiling consists of the accumulation of dust, dirt and contaminants on the glass surface of photovoltaic modules. The driving factors behind the formation of soiling are physical and chemical characteristics of the dust and processes known as cementation, caking and capillary aging. Humidity increases the adhesion and cementation of dust on PV surfaces [5], [6], [7]. Chapter 2 explores these basic principles of soiling.

The deposited soiling layer causes optical losses, reducing the number of photons that reach the solar cells and, consequently, diminishing performance. The optical losses are due to the absorbance, reflectance, and dispersion of the incident light because of the presence of dust (Figure 3) [8]. These effects can be partly mitigated by applying anti-soiling coatings (ASC).

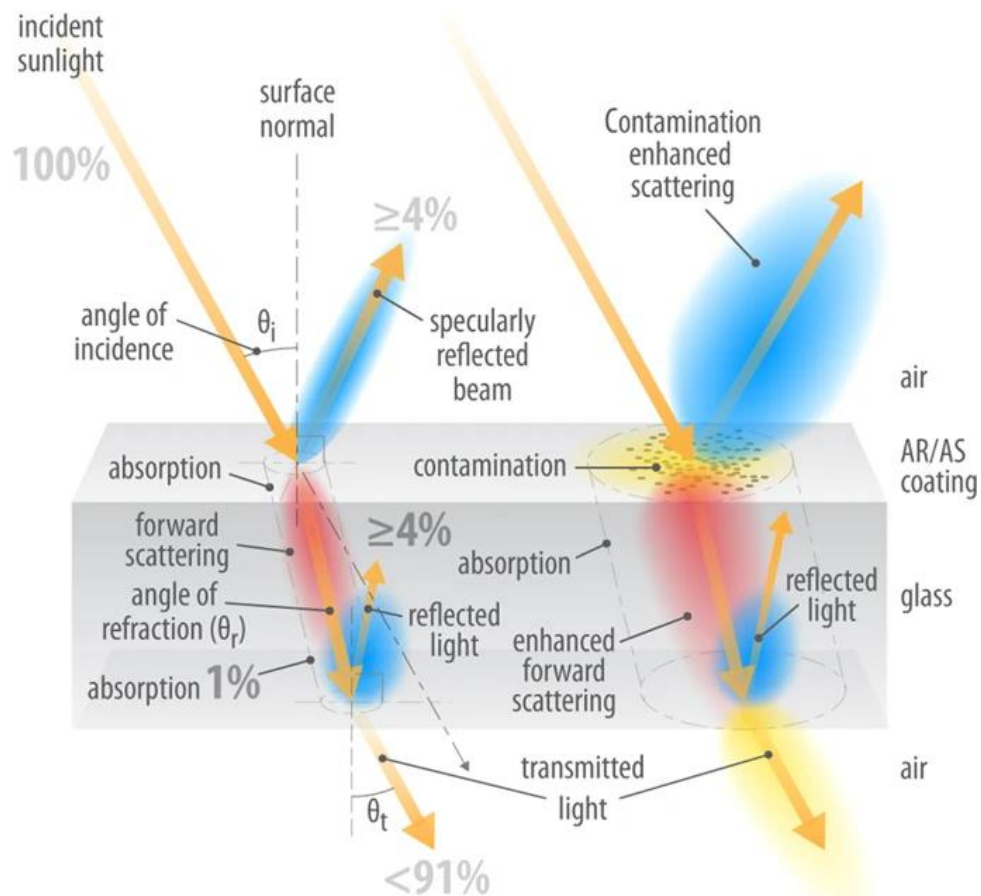


Figure 3: The impact on incident light from soiling on a photovoltaic glass. Diagram made by AI Hicks (NREL, USA) and sourced from [9].

Chapter 3 “Sensing Soiling and Snow” will detail the available sensor solutions on the market to assess the amount of soiling at PV sites. These sensors have quite different operating principles. Ideally, sensors should be maintenance free, as many PV sites will be unmanned in the coming years. Sensing soiling can serve different purposes, e.g., to find the best time to clean a plant or to determine the system losses, even on a global scale.

Although soiling is not recognized as a PV module failure [10], its detrimental effect on reducing the electrical output of PV solar panels is well known.

Many different case studies all over the world can be found in the literature, and several authors have compiled extensive overview lists with cases studies [11], [12] that have been extended with the NREL (National Renewable Energy Laboratory) soiling map of the US, NCPRE (National Centre for Photovoltaic Research and Education) soiling cases by J. Josephson, and other available sources in the literature. Figure 4 shows these studies in the world harmonized soil map for mid-range latitudes¹.

¹ <http://www.fao.org/soils-portal/soil-survey/soil-maps-and-databases/harmonized-world-soil-database-v12/en/>

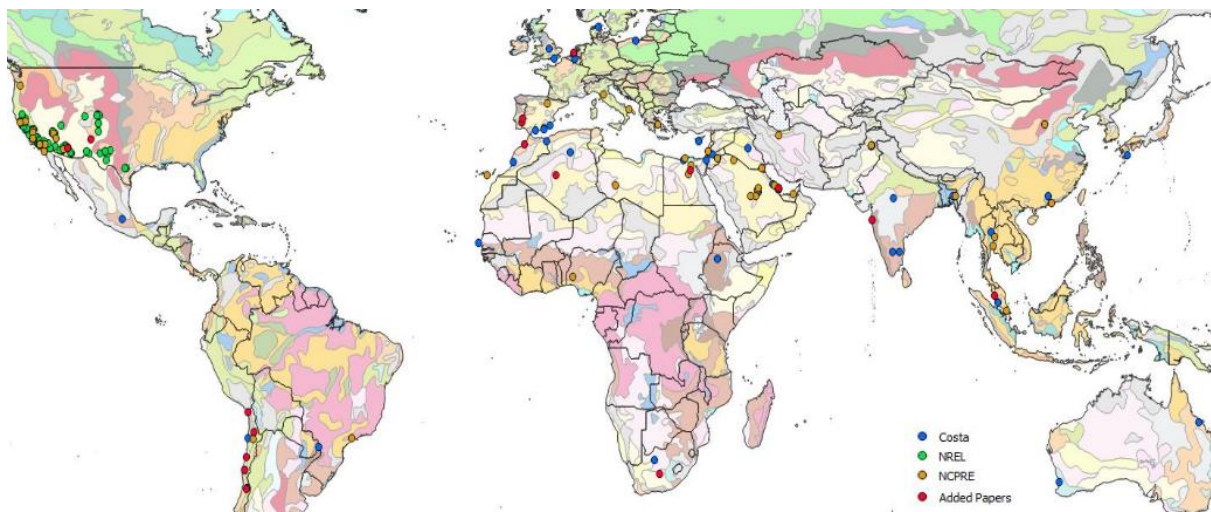


Figure 4: The soil classes of the world with selected soiling case studies.

These studies are difficult to compare and standardize, however, since different metrics may be used, and studies are sometimes conducted only for a short amount of time, e.g., several weeks. To compare soiling studies on a global scale, soiling studies should be conducted for at least a full vegetation growing cycle to account for seasonal and temporal aspects (see above).

To cite some examples from the literature,

- In Europe, the mean daily production losses in Malaga (Spain) caused by the accumulation of dust deposited on the surface of a PV module was around 4.4%, and in long dry periods of dust accumulation this value was higher than 20% [13].
- In Belgium, the power loss was between 3% and 4% in a period of 5 weeks [14].
- In Crete, the annual soiling losses were estimated to be 5.86% [15].
- In the countryside of Southern Italy, 6.9% and 1.1% monthly power losses were found for a plant built on sandy soil and a plant built on more compact soil, respectively [16].
- In Kuwait, soiling losses amounted to 45.8% over a three month period without cleaning [17].

The dust deposited on PV modules is detrimental in most places around the world, especially in arid areas [18]. In addition, regional or even local circumstances may have negative – but sometimes positive – side effects. For example, in deserts near the ocean, such as the Atacama Desert, a dense fog often appears in the morning. This fog reduces the direct component of solar radiation and supports adhesion based on the hygroscopic property of dust to attract humidity [8], [19], [20].

Arid areas with windy and dusty environments may intensify soiling. For example, studies have shown that for arid regions, a shorter time can lead to the same performance reduction generated after months in regions with more temperate and tropical climates. In semiarid and arid desert regions, rainfall is scarce so there is no natural cleaning of the modules [12].

On a global scale, losses from soiling do present a persistent problem to PV systems, with energy and monetary losses by far outplaying the breakthroughs in novel cell designs and efficiency world records.



In their models of solar power generation efficiency, Li et al. [21] combined PV performance modelling with long-term satellite-observation-constrained surface irradiance, aerosol deposition and precipitation rates. Their models provide a good impression of the global impact of these effects on PV generation. Figure 5 visualises the average reduction of the PV capacity factor (CF) due to atmospheric aerosols and soiling. The PV capacity factor is defined as “the actual annual generation divided by the total generation that would occur if the PV panels generated electricity at the nameplate capacity all year round” [21].

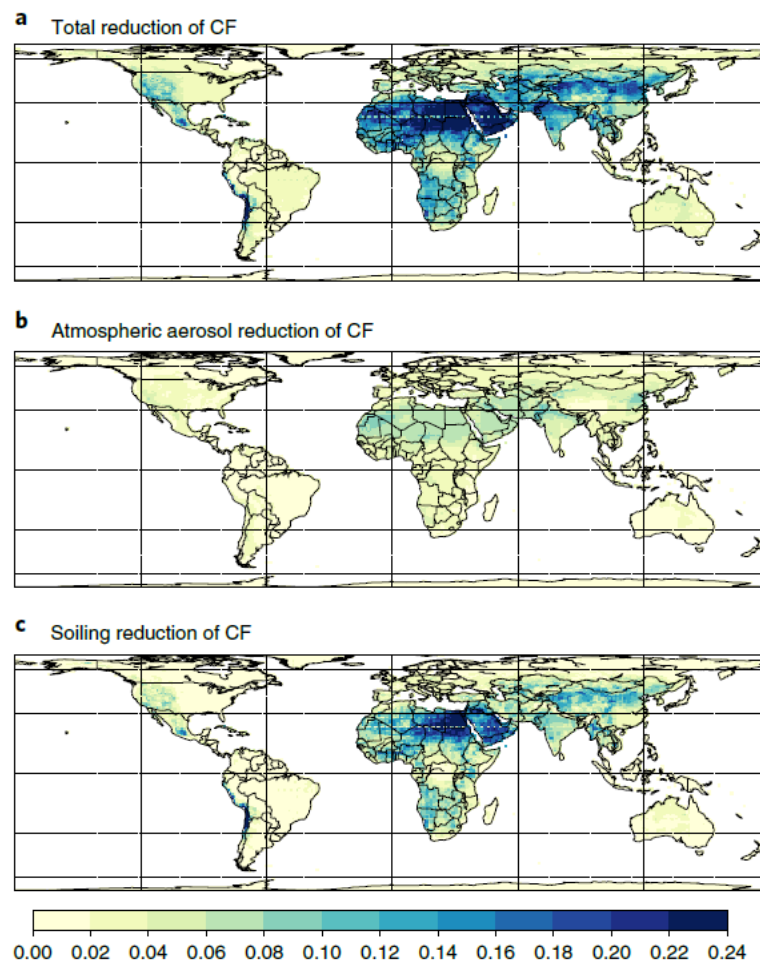


Figure 5: Average reduction of PV CFs due to aerosols, 2003–2014. Inset (a) shows the combined effect of atmospheric aerosols and soiling (resulting from aerosol deposition on PV panels). Insets (b) and (c) show the effects due to atmospheric aerosols alone (b) and soiling alone (c). It can be noted that the effect due to atmospheric aerosol attenuation is much less than the effect of soiling [21].

These studies show that it is worthwhile to prevent or mitigate soiling, which requires more accurate modelling, which is currently being developed by different researchers (Chapter 4.1 “Soiling Models”). Besides modelling efforts, anti-soiling techniques have been developed, including self-cleaning glazing products and anti-soiling photocatalytic coatings, in the hope of finding the “holy grail of soiling mitigation” (Chapter 6.1.2). The market for washing and cleaning devices is ever growing, with a strong tendency towards fully robotic dry cleaning, especially in regions with water scarcity and high ambient temperatures, as discussed in Chapter 6.2.1.



In August 2021, the IPCC “Climate Change Report 2021” [22] was published, with summaries of human-driven contributions to agricultural and ecological droughts. Figure 6 visualises the increase in drought events for many regions of the world, which will also further contribute to soiling increases.

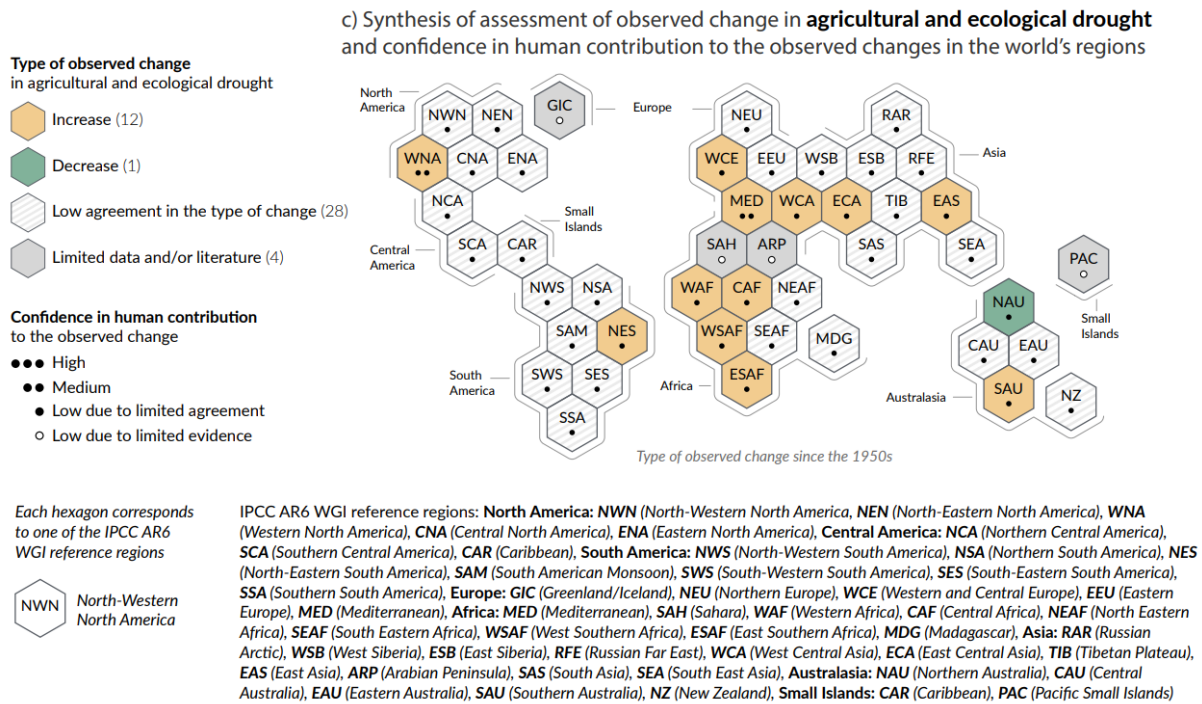


Figure 6: Observed changes in global droughts and human contribution, IPCC report 2021 [22].

A phenomenologically different accumulation than dust – snow and ice – leads to similar consequences in terms of performance losses. However, snow and ice require different modelling, mitigation and system designs that also come with high impacts on component reliability caused by mechanical load stresses. Chapter 7 (*Snow Shading of Photovoltaic Systems*) provides a summary of current snow research in the photovoltaic domain, complemented by case studies from Canada.



2 PHYSICAL AND CHEMICAL PRINCIPLES OF SOILING

2.1 Physical and Chemical Nature of Dust

Extensive reviews and scientific papers have presented the physical and chemical properties of dust in urban and desert areas and its impact on PV power plants [12], [23], [24]. This section discusses the physical and chemical nature of dust particles, their morphology, chemistry, and composition. We will focus mainly on desert areas due to the high irradiance levels and growth of PV plants in these areas.

2.1.1 Particle Size

Dust particle size is a fundamental parameter in deposition mechanisms of soiling affecting PV power plants. Particle sizes may vary over several orders of magnitude, as shown in Figure 1. Particle size also varies from location to location. Several studies have reviewed the size of dust particles for different PV installations. Since dust particle size is related to soil properties, several studies are found in diverse disciplines (not only on PV), where important information about the particle size can be found.

Scanning Electron Microscopy (SEM) is normally used for characterizing particle size above $0.2\ \mu\text{m}$ [25]. Lawrence and Neff [26] present a particle size classification, where particles are defined as clay ($<2\ \mu\text{m}$), fine silt ($2\text{--}20\ \mu\text{m}$), coarse silt ($20\text{--}50\ \mu\text{m}$), fine sand ($50\text{--}125\ \mu\text{m}$), and medium sand ($125\text{--}250\ \mu\text{m}$). But not all particles contribute to soiling, since inertia is a significant limitation for particles bigger than $500\ \mu\text{m}$, and therefore these larger particles generally do not rise and are less affected by wind [27].

Since the mechanism of deposition of dust particles depends mostly on particle size, Mohan [25] has reviewed the influence of size on the deposition of dust particles and found that large particles ($>150\ \mu\text{m}$) remain airborne for a very short time. Gravity has a higher impact on large particles ($>10\ \mu\text{m}$) because smaller particles ($<5\ \mu\text{m}$) are more affected by air turbulence. The smallest particles ($<1\ \mu\text{m}$), meanwhile, are easily removed by rain and do not deposit [25].

The silt size particles in the range of $2\ \mu\text{m}$ to $63\ \mu\text{m}$ are the predominant contributors to soiling in arid and semi-arid climates, although bigger particles can also be lifted due to higher winds [23]. From analysis performed in dust collected from several sites in the Atacama Desert, Chile, 98% of all particles are smaller than $50\ \mu\text{m}$ [28], with an average shape factor between 1.2 and 1.5. Silt size particles are the predominant category for both coastal desert and inland desert locations [29]. Similarly, in Qatar the predominant size for dust present on PV modules was between 10 and $30\ \mu\text{m}$ [30].

Elsewhere, it has been concluded that finer particles affect PV efficiency more considerably than coarser particles [31], and that up to 33% reduction in current has been predicted for a dust concentration of $4.25\ \text{mg}/\text{cm}^2$ [18]. Therefore, it is difficult to make conclusions about the size of dust particles that most affect PV performance. We have shown that many natural parameters affect the particle size range, and their physical properties are influenced by location, and even human influence, since the published results also depend on the capture methodology, accumulation surface (glass), distance to the source, etc. On PV there is no solution yet other than mitigation, including manual, semi-automatic, or automatic-cleaning.

Chemical Composition

Utility scale and small PV installations experience soiling around the globe due to natural sources (e.g., deserts) or due to anthropogenic activities such as mining, industry, agriculture,



etc. Thus, the chemical nature and size of aeolian dust strongly varies depending on the location of the PV array and on natural parameters such as the source of dust, the wind, gravitational effects, etc. as shown in Figure 1. Particles from industrial sources may include concrete, fibreglass, carbon fibres, and brick, among other elements coming from construction sources. Natural sources may include pollen, bacteria, volcanic emissions, and much more. Urban sources may include carbon, oil smoke, diesel engine exhaust, and other pollutants. The pollution coming from contamination sources is a significant factor influencing the amount of soiling and the effort needed for cleaning PV assets [32], [33].

In order to understand the chemical nature of dust, one needs to consider that sand may come from different sources and locations due to wind transport that can vary in scale from local (hundred metres) to global (thousands of kilometres) [34]. One way to ensure an accurate analysis is to collect dust samples and analyse them following a standardized protocol. This information could be used to assess the cleaning procedure of PV plants in the O&M plan, to understand the impact of dust on the degradation process of the PV panels, and, most importantly, to assess output power losses.

Many studies examine the various phenomena that influence the rearrangement, aggregate formation, and accumulation of dust. However, the chemical aspect is rarely discussed despite being the root cause of soiling.

Later sections of this chapter describe the caking phenomena. In short, interstitial compounds in the form of platelets fill the spaces between particles and the glass surface (Figure 9). Additional details may be found in the Appendix. In one case from the Atacama Desert [35], these platelets were Kaolinite minerals. However, the chemical formation process $\text{Al}_2\text{Si}_2\text{O}_5(\text{OH})_4$ of this mineral was not explained.

Gypsum $\text{CaSO}_4(\text{H}_2\text{O})_2$ and Palygorskite $(\text{Mg},\text{Al})_2\text{Si}_4\text{O}_{10}(\text{OH})(\text{H}_2\text{O})_4$ also form strong crystalized bridges. This agglomeration phenomena is called cementation. But the formation of this mineral or their interactions with some elements in the surface of the glass is not explained in detail. The aim of this chapter is not to list every possible chemical formula and equation, but to provide an overview of the main chemical factors that induce the accumulation of dust and increase the difficulty of cleaning it.

Later sections also highlight the predominant role of water in the soiling process. In order to understand its effects, we must first consider two chemical properties: solubility and hygroscopicity. Solubility corresponds to the ability of a material to attract and retain water molecules from the surrounding medium. Hygroscopic behaviour manifests through either adsorption, i.e., attraction and retention of water molecules on the surface, or absorption, i.e., penetration inside the material pores. As a rule, part of the dust found on PV modules is made of salts, which indicates ionic compounds. Many of those ionic compounds are metastable and exhibit significant solubility in water. Once in solution, they dissociate into anionic and cationic components. Those ionic components or elements will interact with each other to form new insoluble compounds, thus causing setting and hardening of the material.

Therefore, this solubility characteristic is a chemical factor. Appendix 1 summarizes some mineral families with high levels of solubility, or which are highly hygroscopic.

Mineral Identification

Dust mineralogy composition can vary greatly by geographical location. Fine particles of minerals can travel on the wind at the troposphere level over very long distances. For instance, the “El Niño” climatic phenomenon causes the finest mineral particles to be raised from the Sahara Desert and travel over the Atlantic Ocean, aggregating with organic particles and then



falling on the South American continent, thus contributing to the fertilization of the Amazon Rainforest. But the local situation can also influence this mineral composition; urban-industrial pollution, road traffic, mining or construction sites, or intensive agriculture generate airborne particles, the heaviest of which travel only a few meters or kilometres. Analysing the composition of airborne dust is complex and time-consuming. The simplifying assumption, accepted by the scientific community, is that this composition is strongly linked to the ground dust composition. Based on that assumption, the large investigation of Engelbrecht et al. [36], who collected and analysed dust from over 60 different ground sites throughout the world, provides a good overview of expected mineral compositions.

Carbonates

The survey by Engelbrecht et al. shows that 62% of global airborne mineral dust mass is emitted from North Africa, while 15% comes from Asia and 11% from the Arabian Peninsula.

In the Atacama Desert, for example, the mineral compositions of the dust collected from the ground and module glass contained diverse minerals, such as albite ($\text{NaAlSi}_3\text{O}_8$), anorthite ($\text{CaAl}_2\text{SiO}_8$), calcite (CaCO_3), cristobalite (SiO_2), gypsum ($\text{CaSO}_4 \cdot 2\text{H}_2\text{O}$), halite (NaCl), quartz (SiO_2), muscovite $\text{KAl}_2(\text{AlSi}_3\text{O}_{10})(\text{OH})_2$ and orthoclase (KAlSi_3O_8) [28]. Another study performed at the same site found that the collected dust was formed by minerals such as quartz (SiO_2), sulfates of gypsum/bassanite ($\text{CaSO}_4 \cdot 2\text{H}_2\text{O} / 2\text{CaSO}_4 \cdot \text{H}_2\text{O}$), albite/feldspars, and very small amounts of muscovite, amphibole, chlorite, hematite, and clinocllore [23]. In Yungay, near the ATAMOSTEC installations (a site in the Atacama Desert), another study found that dust contains mainly quartz, clay (illite, montmorillonite), gypsum, anhydrite, plagioclase, calcite, orthoclase, biotite, and amphibole [36].

Dust on Glass

Dust solutions attack the glass surface while altering the surface texture and the molecular vibrational states in the surface region. In addition, the diffusion of potassium into the surface region causes surface toughening, while increasing the surface microhardness of the glass. The optical transmittance of the glass decreases after the removal of the mud; this reduction is associated with (i) mud residues that remain after cleaning the glass surface and (ii) chemical changes in the glass surface due to the alkali and alkaline earth hydroxide attacks. The adhesion and cohesion work required to remove the mud from the glass is higher than the frictional work performed against the glass surface [24].

An overview of macroscopic, controllable and microscopic factors influencing soiling has been provided [23] (see Figure 7). A detailed discussion of this figure is provided in Appendix 3.

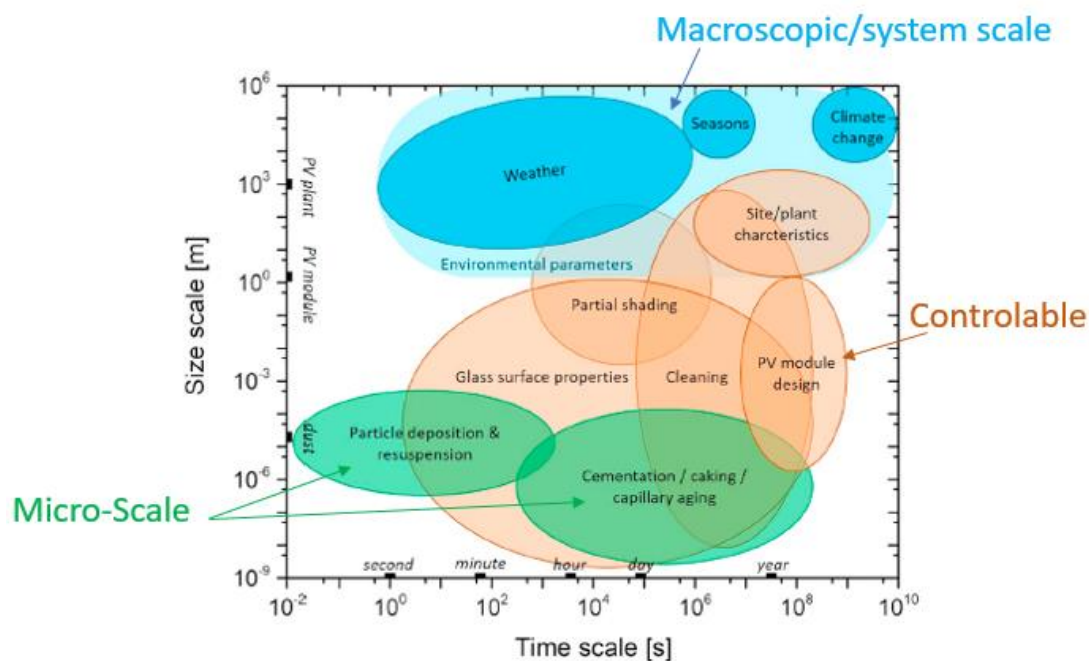


Figure 7: Complexity of the soiling process due to many influencing factors with variation in particle size and deposition time [23].

At the microscopic level, the properties of airborne dust have a significant influence. These properties, including size distribution, shape, and chemical and mineralogy composition, can vary greatly from one location to another. Soiling is mostly attributed to airborne particles with diameters between 2 and 63 μm , since larger particles are too heavy to be lifted and transported in air. Furthermore, it is assumed that there is a correlation between airborne size distribution and particle size distribution of dust deposited on PV modules. Depending on the specific location, there may be a great difference in the mineral dust composition, especially concerning the individual proportions of the main constituents such as quartz, calcite, dolomite, kaolinite or hematite. The mineralogical composition of the particles can strongly influence the optical behaviour and corresponding transmission losses [12], [37], [38], [39]. Furthermore, the light transmission losses caused by accumulated dust on glass surfaces are strongly influenced by the particle size distribution, depending on the irradiance level [40].

2.2 Cementation, Caking, Capillary Aging

Water is the common factor in cementation, caking, and capillary aging, which can all be the result of physical and chemical reactions or simply physical consequences.

2.2.1 Cementation

In high humidity conditions or below dew point conditions, cementation occurs when soluble fractions of the deposited dust are partly or completely dissolved by water present at the surface of the PV module. Besides the dissolution of some ionic compounds like sodium chloride (NaCl) or minerals like gypsum ($\text{CaSO}_4(\text{H}_2\text{O})_2$), this could also involve the hydrolysis of silicates and carbonates included in the PV module glass itself. This hydrolysis is promoted by carbonic, sulfuric or nitric acids, which are typically present in water films on outdoor surfaces due to



dissolution of airborne CO_2 , SO_2 or NO_2 . More details on these phenomena are in various publications [41], [42], [43].

During the subsequent drying process, dissolved material precipitates, causing the formation of solid crystallised bridges between non-dissolved fractions or insoluble minerals and the glass surface, as shown in Figure 8.

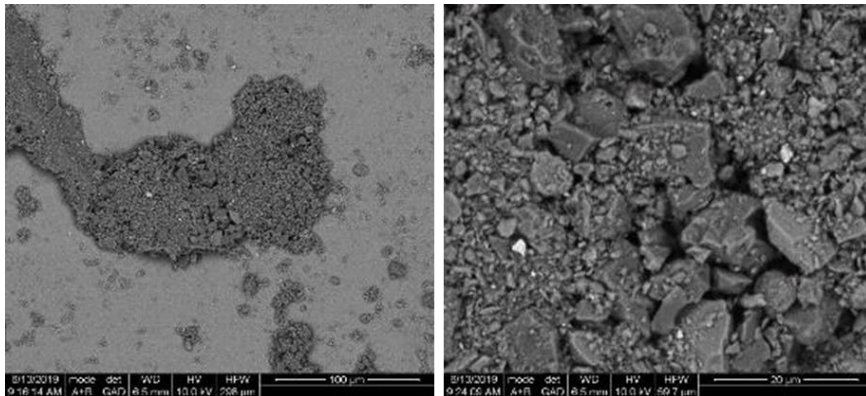


Figure 8: SEM images of particles deposited on a glass substrate in dew configuration, on the left low magnification, on the right high magnification.

These solid bridges result in increased particle adhesion [23], [5], [44], [45], [46].

2.2.2 Caking

Caking is the rearrangement, aggregation and compaction of particles that occurs when particles adhere during wet conditions, such as dew events (Figure 9). This process of particles caking can be illustrated by soiling processes as observed on outdoor exposed glass samples in the Atacama Desert in Chile [35].

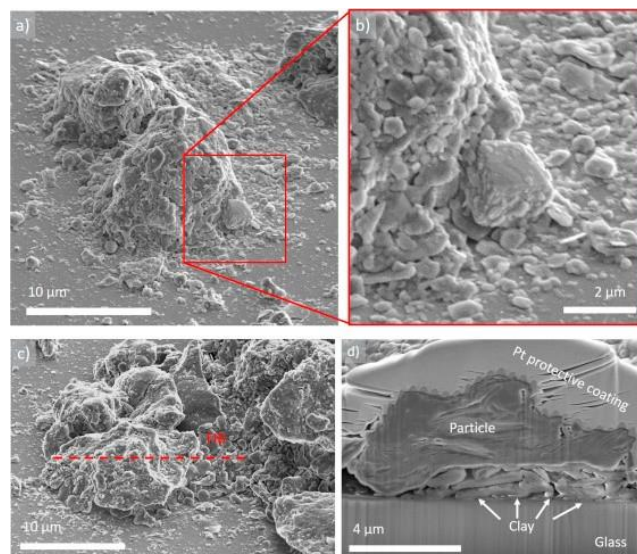


Figure 9: SEM images of bigger dust particles, which became caked to the surface of the glass [23].



2.2.3 Capillary Aging

When liquid bridges between particles and surfaces are drying, the corresponding capillary forces press the particles against the surface, resulting in an increased effective contact area and adhesion [47]. Accordingly, adhesion forces – such as van der Waals forces – can significantly increase after drying.

The process of capillary aging can occur even if there is no macroscopic dew formation detected, because nano and microscopic water films can form between particles and surfaces at low relative humidity levels due to capillary condensation [45].

2.3 Dew-Driven Soiling Mechanisms

Dew formation on PV modules is frequently reported for different desert locations (Figure 10). This phenomenon can be attributed to ambient high humidity but also radiative cooling of PV modules. This cooling is due to the high infrared emissivity of solar glass.

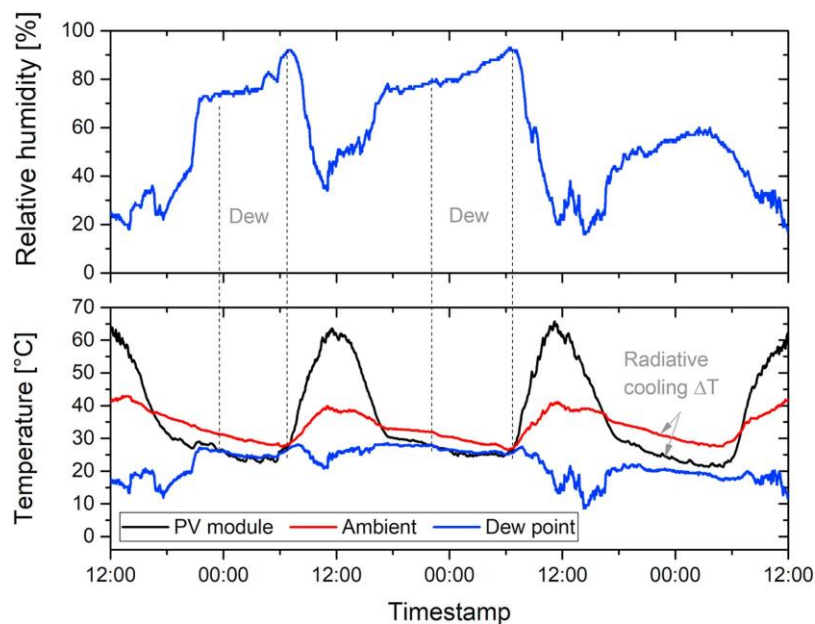


Figure 10: Typical dataset for relative humidity and temperatures of PV modules, ambient as well as calculated dew point temperature over the duration of three nights in October 2015 at the solar test facility, Doha [23].

Figure 11 shows one model dataset for temperatures in the Atacama Desert, which demonstrates that at night the front surface of PV modules cool down below ambient temperature, especially during clear skies. This phenomenon is described in many articles [1], [48], [49], [41], [23].

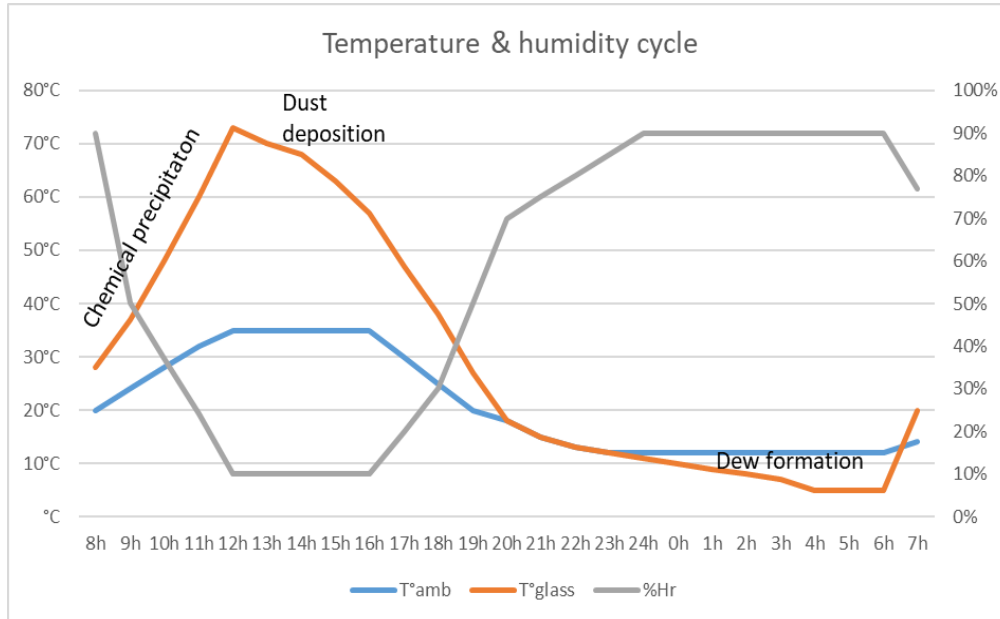


Figure 11: Simulation of temperature and humidity cycle of one full day in the Atacama Desert.

In Figure 11, the ambient temperature (T_{amb}) and the hygrometry percentage (%Hr) are the means of the daily measures for each hour during one year.

The temperature on the glass of the PV module (T_{glass}) is calculated assuming that this temperature is similar to the temperature of the cells inside the panel.

$$T^{\circ}glass = T^{\circ}amb + \frac{NOCT - 20}{80} \times S \tag{1}$$

Where:

- NOCT is the Normal Operating Cell Temperature which is specified on the PV module label.
- S is the solar irradiance in the plane of array. This irradiance is the calculated mean of the daily irradiance for each hour during one year.

At night, the temperature of the glass depends mainly on the radiative cooling phenomena. The French Research Institute CEA-INES monitors several photovoltaic installations, and it has been noted that on average, just after sunset, the temperature of the glass drops rapidly to $-3^{\circ}C$ below ambient temperature and decreases further to $-7^{\circ}C$ just before sunrise. This rough model could be improved by taking into account meteorological conditions, which have a direct impact on the clear-sky characteristics and therefore on the radiative phenomena.

As soon as the glass temperature reaches the dew point, water condenses on it. This dew point can be calculated using the following Equation 2:

$$Tp = \frac{b \left(\frac{aT}{b+T} + \ln RH \right)}{a - \left(\frac{aT}{b+T} + \ln RH \right)} \tag{2}$$

Where:

- a = 17.27, dimensionless
- b = 237.7 °C



- RH: relative humidity in [%]

Condensing water can increase the particle deposition rate. Furthermore, once dew is present on the PV module surface, the water can interact with dust particles and the glass surface, until it evaporates during the day when the surface temperatures of the PV modules rise to high levels. Besides temporarily increasing capillary forces, the water particle interaction promotes different processes with permanently increased particle adhesion, such as cementation, particle caking, and capillary aging as described previously.

2.4 Review of Moisture in Soiling

As already mentioned, soiling is a complex phenomenon governed by interrelated parameters. Particle adhesion is mainly the result of capillarity, caking and cementation. In each of those processes, moisture plays a key role. Some studies have endeavoured to correlate chemical composition of dust particles and chemical physical adhesion mechanisms. The aim of this chapter is to give an overview of the different phenomena caused by moisture in the whole soiling process. An overview of the different adhesion forces is given in Chapter 2.5.

- Gravitational force acting on a dust particle is dependent on the mass of the particle, which may increase because of moisture ingress.
- Capillary forces occur in the presence of moisture. A thin layer of water covers the module surface, and the resulting capillary forces are a combination of two conditions: surface tension and a difference of pressure between the air and the water surrounding the particles, causing “water meniscus”. As a result, the water capillary forces cause particles to adhere to the module surface.
- Van der Waals forces are dominant at very low relative humidity. Van der Waals forces arise from interatomic attraction. Thus, interatomic forces can occur between dust particles and the surface, leading to an increase of adhesion. The water acts as a physical barrier between those particles, thus decreasing or even cancelling the resulting attractive forces.
- Electrostatic interactions are caused mainly by collision between airborne particles. These provide an electric charge and thus produce electrostatic attraction or repulsion. Since there is less moisture vapor in the air, ESD (Electrostatic Discharge) is more common in environments with low relative humidity. Normally, the airborne moisture helps to dissipate static electricity. Water is conductive which allows electricity to travel freely throughout the air and minimizes ESD build-ups.
- Caking is a mechanism involving water. Water droplets that flow on the module surface can drag particles and bring them together, thus forming aggregates. Small particles can also fill interstices between larger particles. This results in the formation of a more cohesive structure and small particles act as “sticking” components between the surface and larger particles.
- Cementation is one of the most reported mechanisms explaining dust adhesion. Chemical reactions form a new compound that crystallises and covers dust particles, creating solid bridges between them and the surface, which drastically increases adhesion. Ilse et al. [23] has analysed and identified the major role of the mineral palygorskite in the soiling process in Qatar. Palygorskite, which has a needle-like shape (Figure 12), is probably the result of a dissolution-precipitation process. Palygorskite first dissolves in water produced from condensation, then evaporation enables it to recrystallize.

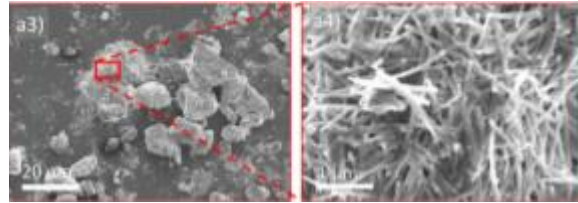


Figure 12: Palygorskite needle structure, SEM images [50].

The cementation process has also been highlighted in one area of the Atacama Desert [29]. This study revealed particles with silica covered by particles in the form of gypsum. This encapsulation of particles by gypsum increases dust fixation and encourages soiling. This result also suggests a dissolution-recrystallization process like palygorskite, which is corroborated by the prismatic shape of the monoclinic gypsum. Even if the exact formation process remains unclear, it is obvious that moisture plays an essential role.

2.5 Overview of Particle Deposition and Adhesion Forces: Van der Waals, Capillary, Electrostatic, and Gravitational Forces

The rate at which dust particles accumulate on the PV surface can be considered the net result of the following three processes [30]:

1. Deposition: particles from the atmosphere impacting the surface
2. Rebound: immediately rebounding from the surface without adhering
3. Resuspension: later being resuspended by wind

$$\text{Accumulation rate} = \text{Deposition rate} - \text{Rebound rate} - \text{Resuspension rate} \quad (3)$$

The deposition of particles is mostly controlled by gravity (sedimentation) and turbulence of the airflow (inertial deposition). If wind speed is above approximately 3 m/s, the particle deposition rate can be adequately explained by sedimentation alone. This sedimentation process can be roughly modelled by the Stokes settling velocity in Equation (4):

$$v_{\text{Stokes}} = \rho d^2 g / 18\mu \quad (4)$$

Where

- ρ : particle density
- d : particle diameter
- g : gravitational acceleration
- μ : dynamic viscosity of air

The deposition flux rate for each particle size category is obtained by multiplying that velocity by the airborne concentration of particles of that size. There is no widely used predictive model for the rebound of particles. Theoretically, particles are predicted to rebound from the surface if their kinetic energy on impact exceeds the work of adhesion between the particle and surface. Therefore, the rebound fraction is expected to be greater for large particles, high wind speed, and low humidity. For resuspension (particle removal by wind), three different mechanisms are considered: rolling, sliding and direct lift-off.

Typical particle adhesion forces include those listed below in decreasing order of importance:



- Capillary forces for hydrophilic (contact angle = 0°) and hydrophobic (contact angle $> 150^\circ$) glass surface properties;
- Van der Waals forces for a smooth and a rough glass surface;
- Gravity (weight of sphere);
- Electrostatic forces assuming mean particle charging at the Boltzmann equilibrium.

In addition, possible detachment modes in case of strong wind ($>10\text{m/s}$ or 36 km/h) include:

- Rolling
- Sliding
- Lift off

Surprisingly, in comparison with capillary and van der Waals adhesion forces, gravity and electrostatic forces can be omitted. We can also conclude that the sliding and rolling forces increase considerably depending on the particle size. The lifting force is negligible when particles have a diameter less than $50\text{ }\mu\text{m}$.

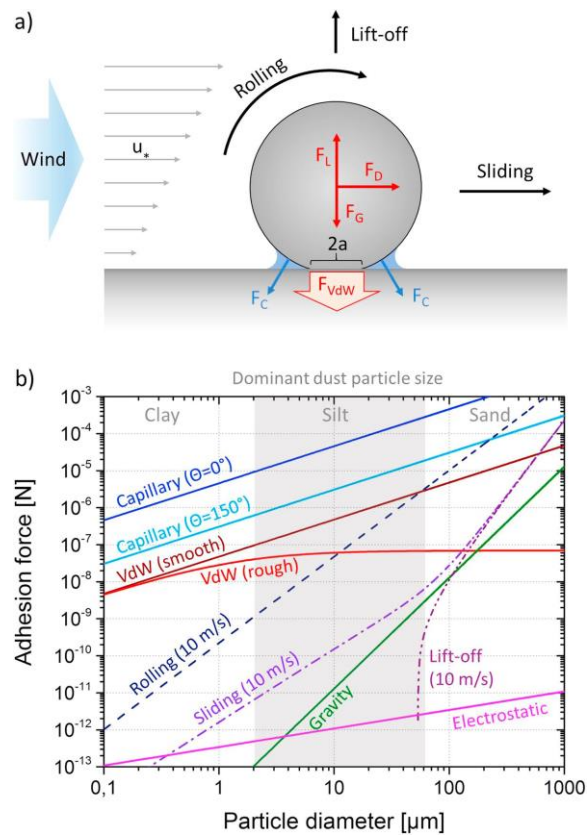


Figure 13: a) Schematic illustration and simulation of particle adhesion and removal for a SiO_2 sphere on solar glass. b) Adhesion forces and removal forces (dashed lines) are shown as a function of particle diameter [23].

The size scale of roughness is very important: asperities should be significantly smaller than particle diameter (about three orders of magnitude) to reduce adhesion. Particles may become trapped on surfaces whose surface roughness is comparable to particle size.

In wet environments, van der Waals forces are considerably decreased because of the reduction of the Hamaker constant by the interstitial water.



Solid bridge bonds, including chemical bonds as well as entanglements such as mechanical interlocking, are excluded in the comparison of adhesion forces (Figure 13) but can be assumed to be orders of magnitude higher than the given values for capillary and van der Waals forces [45]. These solid bridge bonds play an essential role in the phenomenon of cementation, which involves rather complex chemical interactions.

The simulated force ranges strongly support the assertion that particles smaller than 10 μm are rarely removed by wind [47].



3 SENSING SOILING AND SNOW

Soiling is a site-specific issue that causes reversible power and energy losses to PV systems worldwide. If not adequately tackled, it can lead to significant missed revenues and, in the worst cases, even turn profits into economic losses. In contrast to irreversible PV reliability and performance issues, soiling can be mitigated through a number of solutions that are described in Chapter 6, although soiling mitigation has to be adapted to the specific conditions of each site, which can also change with time.

Indeed, soiling not only varies from site to site, but can have dissimilar effects on systems that are located nearby and, in some circumstances, also on different parts of the same system. In addition, the rate of soiling and the frequency of natural cleaning events, such as rainfall, can change with the seasons and the years. For all these reasons, and because of the high economic value associated with the losses, it is critical to continuously measure and monitor the level of soiling on a PV plant. This can be done through a range of commercially available solutions, and through monitoring of the output of the PV plant and how it evolves with time. The measurements of these soiling sensors can then be used to determine the most profitable time to clean (see Chapter 6.3).

This chapter is structured as follows. First, in Chapter 3.1, the most common indexes used to quantify the effect of soiling on PV module performance are described. In Chapter 3.2, currently available soiling and snow sensors are listed. Ideally, soiling can also be extracted from performance ratios, but the effects of soiling on irradiance sensors have to be estimated in this case, as detailed in Chapter 3.2.3.

3.1 Soiling Metrics

Typically, the soiling profile of a PV system can be described as an alternation of soiling deposition periods and cleaning events. Soiling occurs on the surface of PV modules at rates that are affected by factors such as particulate matter, wind speed and relative humidity (Chapter 2), and soiling is washed off by rain or other natural cleaning events. For this reason, soiling has to be described by at least two metrics: one to quantify the current losses and a second to describe the daily variation in losses due to soiling deposition and resuspension. While the first metric (commonly called the *soiling ratio*) assesses the current state of the system, the other metric (commonly called the *soiling rate*) can be used in combination with cleaning event patterns to predict near-future losses.

The soiling ratio is defined by the IEC-61724 standard as the ratio of the power of a PV array in soiling conditions to the power of the same PV array in clean conditions. It has a value of one in conditions of no soiling and decreases while soiling accumulates, reducing the electrical output of the PV modules. A soiling ratio of zero occurs if soiling is blocking all light from reaching the PV cell. The fractional loss due to soiling (i.e., the soiling loss, also defined as “Soiling Level” in the IEC-61724) can be calculated as one minus the soiling ratio. The soiling ratio has been used to express the daily, seasonal, or annual impact of soiling on the energy yield. Also, depending on the application, it has been calculated as an irradiance-weighted average to give higher influence to the soiling occurring during the most irradiance-intense periods. In literature, indices similar to the soiling ratio can be found, including “Cleanness Index”, “Soiling Factor”, or “Soiling Loss Factor.” They are all based on the same concept (i.e., comparing the actual and the expected output of a PV device) even though the data used for their calculation might differ.



The electrical impact of soiling changes with the time of the day (Figure 14) because of the variation in angle of incidence and the components of light [13]. The IEC-61724 standards recommend measuring soiling within two hours of solar noon (if the PV devices are fixed) or for angle of incidence $< \sim 35^\circ$ (if the PV devices are tracked). Considering only the central hours of the day also limits the potential bias due to misalignments and to morning or evening shadings [51], [52]. On the other hand, some authors have been using 24-hour data, as this approach provides a more direct measure of the impact of soiling on the PV module energy yield [53].

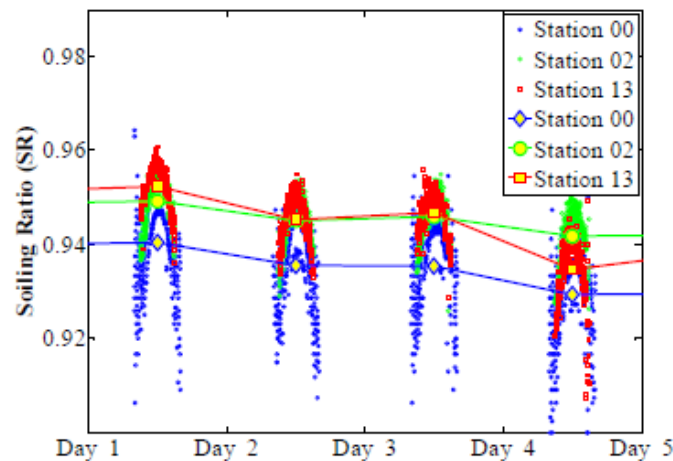


Figure 14: Time variation of the soiling ratios recorded at one-minute steps. The daily average values are marked by the large markers [51].

In most cases, the soiling ratio is approximated as the ratio of the short-circuit current of a soiled and reference PV device, instead of being calculated from the energy or the power outputs. When all cells in a PV module are uniformly soiled, the temperature-corrected short-circuit current is proportional to the power output. However, light rain or condensation can cause partial cleaning of tilted modules and the accumulation of soiling at the bottom row of cells. In this case, soiling also affects the shape of the PV module I-V curve, reducing the short-circuit current and the maximum power by dissimilar factors. In particular, if soiling is not distributed uniformly, the short circuit current measurements might underestimate the actual impact of soiling on the PV power. This underestimation occurs when a string of soiled cells is opened by the bypass diode, resulting in a power loss, but not in a change of the module's short-circuit current [54] as shown in Figure 15.

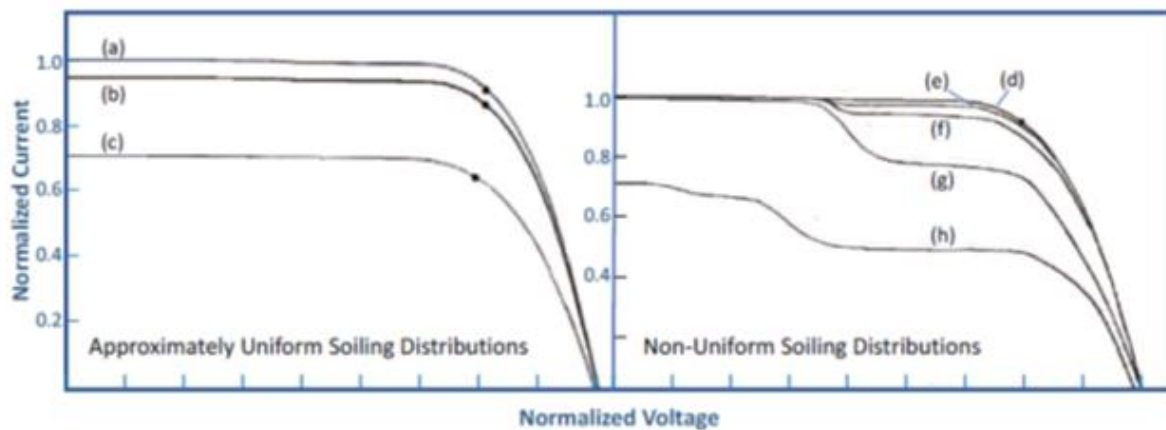


Figure 15: IV Characteristics of several soiling conditions and patterns for crystalline Si module [55]. (a) and (d) clean conditions; (b) and (c) “uniform” soiling conditions; (e) and (f) non-uniform soiling on the sides and bottom of the frame; (g) high non-uniform soiling at sides and corners; (h) blotch covering several cells near centre of module with high-level edge build up.

The second common metric used in soiling analysis is the soiling rate, which describes the daily variation in soiling ratio while soiling accumulates on the PV module surface. It is expressed as %/day and conventionally reported as negative. A rate of 0%/day expresses that the soiling ratio is not changing and generally occurs if no soiling is depositing. The steeper the soiling ratio profile, the higher the absolute value of the soiling rate. Commonly, the soiling rate is assumed to be constant in between cleaning events, even if some authors have suggested that the soiling loss profiles might follow an exponential function [56] or that they might be more accurately modelled through multiple linear functions.

The most common way to calculate the soiling rate is to determine the slope of the soiling profile in between cleaning events and this can be done by using a least-square regression [57]. However, this approach has been found to be potentially biased by outliers and unaccounted cleaning events. The Theil-Sen estimator and a bisquare weighted least square regression have been employed in previous studies to overcome this issue [58], [59]. In addition, Deceglie et al. [58] and Besson et al. [59] have suggested calculating soiling rates only for periods of at least 14 days with no cleaning events, to avoid fitting trends with a limited number of data points. Additional metrics are available in literature as an alternative to the soiling rate, such as the change in cleanness index [53].

In most cases, a single soiling rate is identified for each PV site and considered constant throughout the year. This can be determined as the soiling rate of the longest dry period [57], or as the median of the slopes of all the dry periods [58]. This value can then be used, in combination with the rainfall or natural cleaning event patterns, to generate the soiling loss profile of the investigated site. Recently, the use of monthly (rather than annual) soiling rates or, at least, the calculation of an average annual soiling rate, weighted according to the length of each dry period, was suggested as a way to improve the characterization of soiling and of its seasonality at a site [60].



3.2 Market Overview of Soiling and Snow Sensors

3.2.1 Monitoring Soiling

There are distinct seasonal variations of soiling [61], as shown in Figure 2. With this seasonal variation, it makes sense to monitor soiling continuously throughout the year. The location and environmental factors dictate how the particle concentration in the atmosphere, and hence dust deposition, change throughout the year. The different locations can affect the degree of soiling since different types of dust transmit different spectra of light [30]. The soil composition of the location contributes to the type of dust on the surface of the module and hence the light transmission spectrum. Some parts of the world will have greater average soiling rates than other regions. This is largely due to prevailing weather conditions [62], with more arid areas likely to have higher soiling rates.

One of the key messages from an investigation of the literature is that soiling rates can vary greatly from location to location as well as seasonally. For example, at two locations in the US, soiling rates can be as high as 11.5% per month in heavy agricultural areas [63]. There is also a link with human activity, with the soiling rates in agricultural areas being significantly higher than in natural deserts.

Table 1: Soiling rates per month (%/Month) [63].

Region Type	Winter	Spring	Summer	Autumn
Natural Desert	0-1.2	0.8-2.0	0.9-1.1	0-1.0
Dry Agricultural	0.3-3.6	1.3-5.5	2.2-10.9	0-11.5

Most soiling studies cover fairly short-term periods of days to a few years [64]. However, these data indicate that there is seasonal variation in the soiling of PV modules. When predicting soiling rates, it needs to be noted that yearly, or even monthly, average soiling data may not be sufficient for accuracy. To further complicate matters, soiling rates can be uneven within an array [64], or even on an individual module. For example, modules on upper racks tend to exhibit more soiling on average, as lower modules get rain runoff from the modules on the upper racks. The direction of the wind can directly impact the pattern of soiling [30] as shown by the uneven soiling in Figure 16, which is from the Atacama desert in Chile and demonstrates the effect of a dominant wind direction.



Figure 16: Soiling pattern demonstrating dominant wind direction.

Other studies have also documented these uneven soiling rates across larger PV power plants. The relative power reduction in one plant varies from 0.89 to 0.95 [51]. The soiling deposition rates within different locations of the same site can vary in between 1.5x and 2x, depending on the prevailing winds and the distribution of dust sources [4].



Figure 17: Data showing uneven power reduction across a large PV plant [51].

With uneven distribution across a PV plant, it is recommended to have several soiling stations distributed around the site to give accurate results. The IEC 61724-1 standard recommends more than one soiling sensor for any PV site of capacity larger than five MW and with expected yearly losses of more than two percent. The data from soiling stations can be mapped and spatially averaged to provide a metric for the site, which can then be used to predict future soiling rates or inform the operator of the best time to clean the PV system.



3.2.2 Technologies for Sensing Soiling

Soiling sensors are devices specifically designed to return a soiling loss measurement. The currently available soiling sensing methods can be divided into electrical techniques, which measure the modules' current or power, and optical techniques examining reflectance or transmittance losses due to accumulated dust on the sensor surface.

As described before, soiling quantification is based on a comparison of the electrical outputs in soiled and clean conditions. Electrical methods achieve that by measuring the current or power outputs from two side-by-side PV devices, where one is regularly cleaned and the other is allowed to soil normally. As shown in Table 2, non-exhaustive examples of manufacturers are Atonometrics, Campbell Scientific or NRG Systems. Electrical configurations can consist of two reference cells, two modules, or a cell-module combination. The identical reference cell method is relatively low cost since racking requirements are minimal. However, reference cells may not soil in the same way as modules since the cover glass may be different. For example, it was shown in a recent study that textured cover glass soiled up to 7% more than regular glass [65]. By contrast, some antireflection coatings may reduce soiling by as much as 60% depending on geographic conditions [66]. Furthermore, a soiled reference cell will not capture the non-uniform distribution that can develop on module surfaces. Alternatively, a soiling system using the module-module configuration accounts for non-uniform soiling but incurs higher maintenance costs since one module must be cleaned regularly, either with automated methods or by on-site personnel. By contrast, a soiling system using a cell-module configuration allows simple automated cleaning of the reference cell with the benefit of having a module that takes into account non-uniform soiling and is representative of the whole array.

The reference device is preferably cleaned every morning, as most of the soiling deposition is found to occur at night [23]. However, in real cases the reference device is often cleaned weekly, if cleaning is not fully automatic. When the costs and the benefits of a soiling sensor's cleaning schedule is assessed, it should be considered that an inadequate cleaning frequency can produce a significant underestimation of the soiling ratio [67].

Whether the soiling configuration is cell-cell, module-module, or cell-module, another important consideration is whether to measure only the short-circuit current or also the power. Indeed, as aforementioned, the non-uniform distribution can cause a disproportionate power loss relative to the change in short-circuit current, reduce the fill factor and even potentially lead to hot-spots that permanently damage the PV cells [64], [68]. Thus, soiling stations based on electrical measurement should ideally collect both short-circuit current and power data in order to address the complexities of non-uniform soiling.

While some soiling systems differ in terms of using modules or reference cells, the general method of short-circuit current measurement is the same: a temperature-compensated short-circuit current with back-of-module temperature measurements are used to determine the effective irradiance using the methods outlined in IEC 60891 edition 2 [69]. In order to minimize degradation, the clean and soiled PV devices may be kept at open-circuit between measurements. Usually, computations are only performed for the central hours of the day during clear-sky conditions and when effective irradiance is greater than 500 W/m². This minimizes the effects of zenith angle, air mass, and spectral differences. Other filtering techniques involve the exclusion of data when the rate of change of short-circuit current is high due to passing clouds [70]. The Soiling Ratio is calculated using the short-circuit currents of the clean, I_{sc1} , and soiled, I_{sc2} , devices with respective short-circuit current temperature coefficients given by α_1 and α_2 . The subscript M indicates measurements made at the time of soiling, and M' refers to measurements made at calibration [71].



$$SR = \frac{I_{sc2,M} (1 - \alpha_2 (T_{2,M} - T_{ref}))}{I_{sc1,M} (1 - \alpha_1 (T_{1,M} - T_{ref}))} \cdot \frac{I_{sc1,M'} (1 - \alpha_1 (T_{1,M'} - T_{ref}))}{I_{sc2,M'} (1 - \alpha_2 (T_{2,M'} - T_{ref}))} \quad (5)$$

Where:

- SR : Spectral Response
- $I_{sc1,M}$: Short Circuit clean device, time of soiling
- $I_{sc2,M}$: Short Circuit soiled device, time of soiling
- $I_{sc1,M'}$: Short Circuit clean device, time of calibration
- $I_{sc2,M'}$: Short Circuit soiled device, time of calibration
- α : Temperature coefficient
- T : corresponding temperatures, T_{ref} typically 25°C

A similar equation can be written for the soiling ratio using the power temperature coefficient and substituting short-circuit current with power output from clean and soiled devices.

Furthermore, in order to minimize degradation between soiling measurements, the load to which a module is connected can have important non-linear effects on the degradation rate and is technology specific. Multi and mono-crystalline silicon modules show reduced degradation rates under open-circuit compared to grid-connected operation at maximum power point [72]. By contrast, several studies reveal that thin film technologies such as a-Si:H [73] and CdTe [74] show higher degradation rates under open-circuit relative to grid-connected conditions.

In contrast to electrical measurements, dust sensors employing optical methods are provided by Kipp and Zonen and Atonometrics. Kipp and Zonen's Dust IQ sensor uses a pulsed blue LED to measure the scattered light reflected from dust particles. The transmission loss is converted into an equivalent loss in short-circuit current and power. However, dust scattering properties vary with test location. The Dust IQ is initially calibrated with Arizona quartz dust but should be recalibrated for site-specific soiling conditions by allowing local dust to accumulate until the transmission loss is between 5 to 10%. In addition to the photodiode, Dust IQ calibration involves measuring the short-circuit current of an internal silicon cell under clean and soiled conditions within two hours of solar noon [75]. An alternate optical method is provided by Atonometrics' Mars Soiling Sensor. The Mars device uses a sensor and image processing software to calculate transmission loss due to soiling. The sensor is located behind a diffuser, and the cover window has black and white marks on the inside surface for self-calibration. An overview of suppliers offering soiling systems is given in Table 2.



Table 2: A partial list showing several products available for quantifying losses due to soiling. Manufacturers are in alphabetical order. All equipment prices in this report are estimates from the year 2019. The manufacturer should be contacted for exact costs.

Soiling Sensors					
Manufacturer	Atonometrics	Atonometrics	Campbell Scientific	Kipp and Zonen	NRG Systems
Model name	Soiling Measurement System	Mars Soiling Sensor	CR-PVS1	Dust IQ	Soiling Measurement Kit
Method	Short-circuit current and power	Optical (image processing camera)	Short-circuit current	Optical (LED)	Short-circuit current
Module power range	Up to 450 W	Not applicable	Up to 300 W	Not applicable	3 panels of 15 W each
Power supply	10 to 30 VDC or 100 to 240 VAC	10 to 30 VDC	16 to 32 VDC	12 to 30 VDC	5 to 15 VDC
Output options	Ethernet	RS-485, Ethernet	RS-232	RS-485	Available upon request
Approximate Cost: Euro / USD	€ 6078 / \$ 6900	€ 2600 / \$2950	€ 2334 / \$ 2649	€ 3807 / \$ 4320	Available upon request

In terms of measurement accuracy, more study is needed to quantify measurement uncertainty of different soiling sensing products. In particular, it would be beneficial if soiling sensing products were referenced to the International Guidelines of Uncertainty in Measurement with reference to standard and expanded uncertainties for different devices. For the short-circuit current soiling ratio, both the clean and soiled cells or modules can be simultaneously calibrated with a reference PV device. Soiling ratio accuracy is thus dependent only on uncertainties in short-circuit current, temperature (with a difference between back-of-module and cell) and short-circuit current temperature coefficient. In addition to these uncertainties, clean and soiled modules may not be exactly co-planar, leading to tilt and azimuth angular alignment errors. The azimuth and tilt misalignment can be minimized by making measurements within a few hours of solar noon when angle of incidence is small. Furthermore, azimuth misalignment can be minimized by averaging data shortly before and after solar noon, taking advantage of the sign change in soiling ratio that occurs at noon. In addition, field-based calibrations should be made under realistic operating temperatures to minimize the contribution of uncertainty from short-circuit current temperature coefficients. It has been shown [71] that with careful calibration and filtering of data, short-circuit current soiling ratio measurements can have an uncertainty of approximately $\pm 1\%$. The most accurate measurements (1 to 2% uncertainty) are possible using the cell-module or module-module configuration when measuring power. Short-circuit current measurements in cell-module or module-module configuration are less accurate (around 3 to 5%) since they do not take into account non-uniform soiling. The least accurate methods (uncertainty around 4 to 7%) are short-circuit current cell-cell configuration and optical methods since they may use different cover glass compared to the array and will not capture



non-uniform soiling. Nevertheless, cell-cell and optical methods are the least costly, allow for simple installation and multiple measurement points, and have little or no maintenance costs. However, it must be emphasized that the magnitude of the uncertainties for different soiling sensors described in this report are estimates [76] and that also the reference device's cleaning interval can bias the soiling measurement [67]. Additional studies are needed to reinforce these figures.

3.2.3 Soiling Characteristics of Irradiance Sensors

Irradiance sensors are subject to soiling. In this section, the soiling rates of standard pyranometers with a characteristic dome shape are compared to soiling rates of reference cells with a characteristic flat plate surface. Regardless of sensor type, the international standard IEC61724 recommends irradiance sensors be cleaned weekly [77]. The temperature-corrected Performance Ratio can provide a good estimate of soiling rates and soiling loss during dry seasons, so long as the POA irradiance sensor is cleaned and maintained. The absolute uncertainty of the soiling sensor is irrelevant, so long as the short-term stability of the irradiance sensor is adequate.

Soiling losses depend on dust composition, local climate conditions, and exposure time. In addition, soiling losses also depend on tilt angle [78], [79]. Soiling losses typically decrease as tilt angles increase for a given location because the effective area of the surface decreases relative to the zenith angle and gravitational forces, at least in areas where the wind does not play a significant role in removing dust. The reduction in effective surface area is analogous to the cosine loss on irradiance due to the angle of incidence, which quantifies the decrease in the effective area of the modules as seen by the direct beam of sunlight.

The tilt angle should also influence soiling rates on irradiance sensors in some way. There are two basic surface geometries for irradiance sensors. Reference cells typically consist of silicon devices packaged under flat plate glass, and pyranometers typically consist of thermopile sensors packaged under single or double domed glass. The soiling rates for reference cells should be similar to soiling rates on other glass surfaces, including PV modules, assuming the glass coatings are also similar. However, tilt angle should influence the soiling rates on pyranometers differently given the dome shape. The dome shape presents the smallest possible horizontal surface at every tilt angle relative to the force of gravity, so theoretically soiling rates should be smaller on pyranometers.

Two published papers support lower soiling rates on pyranometers compared to flat plate devices. In one study conducted in the Western United States, soiling rates on pyranometers measured 50% less than soiling rates on modules [80]. While this is not a direct comparison between pyranometers and reference cells, the soiling rates on flat plate reference cells should be similar to soiling rates on the modules, given similar surface coatings and metrics. Soiling rates will also depend on the choice of metric, i.e., I_{sc} versus P_{mp} , so a direct comparison of reference cells and pyranometers should be based on the I_{sc} of the reference cell. In another paper, the soiling loss on a pyranometer was shown to be less than the soiling loss on a DNI pyrhelimeter [81]. Once again, this is not a direct comparison of the two sensor types, but the pyrhelimeter is also a flat plate surface device, albeit protected somewhat by a shield to limit the field of view.

The outdoor testing facility on the Council for Scientific and Industrial Research (CSIR) campus in South Africa maintains both silicon reference cells and pyranometers to monitor



irradiance, so a more direct comparison can be evaluated. The energy yield test bed is one of three different testing platforms available for research on modules and systems. The energy yield test bed connects individual modules to electronic loads with grid connection to recover the energy in between regularly scheduled I-V curves. The test bed is equipped with a silicon reference cell in the plane of array (due north, 25° tilt), a pyranometer in the plane of array, and a second pyranometer for albedo. The irradiance sensors are cleaned in the morning with a dry cloth to remove the dust, roughly once per week.

Figure 18 shows the difference in daily insolation as measured by a pyranometer and a silicon reference before and after a weekly clean cell over 11 weeks during the dry season in 2019, from 20 June to 04 October. The y-axis shows the block-centred difference in daily insolation measurements between the pyranometer and the silicon reference cell on the day before the clean and the day of the clean, blocked by week to remove the variability in daily insolation, which ranged from 5500-7500 Wh/m²/day during this period. After cleaning, the distribution of the differences in daily insolation as measured by the two sensors was significantly less than the day before the cleaning (two-tailed p-value – 0.01). The reduction in the difference can be attributed to the cleaning, and likely explained by the increased soiling loss on the reference cell (flat plate) compared to the pyranometer (domed). The dataset does not lend itself to further analysis since the cleaning was done in the early morning when the irradiance was changing rapidly, nor was the exact minute of cleaning recorded. The difference of the differences measured 42 Wh/m², or 0.6% of the average daily insolation of 6520 Wh/m²/day. The 95% confidence interval for the difference was 10-74 Wh/m²/day, or 0.2-1.1%. This 0.6% per week is a reasonable approximation of the additional soiling rate on the silicon reference cell (flat plate) compared to the pyranometer (dome-shaped) during this period.

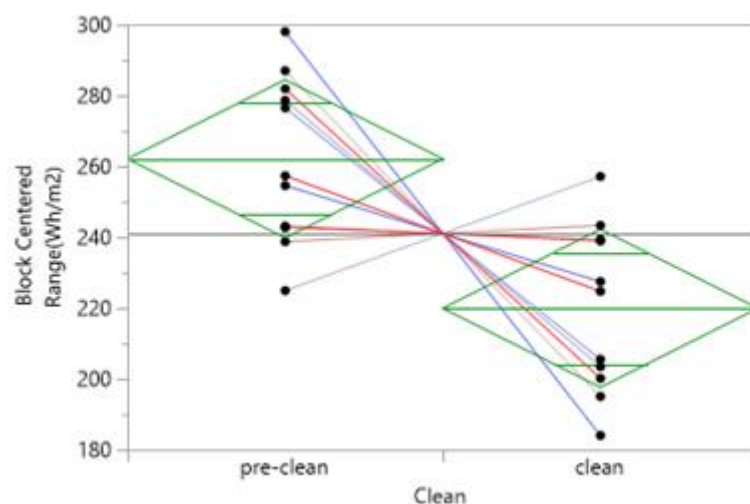


Figure 18: Analysis of variance (ANOVA) showing the difference in daily insolation as measured by a flat-plate reference cell and a pyranometer before and after cleaning.

In conclusion, soiling rates are likely lower on pyranometers compared to flat plate reference cells. However, irradiance sensors should be cleaned weekly to minimize the impact of soiling on ground-based irradiance measurement, as per the IEC 61724 standard.



4 SOILING AND SNOW MODELS

4.1 Soiling Models

Along with monitoring, it is also important to understand in advance the potential impact of soiling on the energy yield and on the O&M costs of a proposed PV plant. This can be accomplished by direct measurement of soiling levels at the site prior to installation and operation. This measurement would require setting up a soiling sensor for at least a year. Although, if the soiling level could be determined from other parameters whose values were already available, it would be possible to assess the energy and economic impact of soiling while selecting the site for a new PV installation.

Several weather and pollution factors influence soiling deposition and cleaning. In addition, inherent macroscale factors (e.g., Land use/Land Cover, NDVI, agricultural activity, prevailing soil type, etc.) can also influence the soiling profile. Out of all these parameters, the most prominent factors (or at least the most recurring ones in this research area) are the particle mass concentrations PM10 and PM2.5, the wind speed and direction, the frequency of wind gusts, the relative humidity, and the rain intensity and frequency [1]. PM10 and PM2.5 represent the concentration, in mass per m³ of air, of suspended particles of sizes ≤ 10 μm and ≤ 2.5 μm, respectively, with PM2.5 being a subset of PM10.

There are extensive literature sources available that describe efforts to model the deposition of suspended particulate matters on PV and CSP. A bibliometric survey done on Web of Science in 2019 gave a dedicated overview over research areas, outstanding publications, and their authors as well as their subdomain, as can be seen in Figure 19. The present chapter summarises the development and applications of models to predict the deposition of soiling without the need of specific soiling data or of PV performance from the site of interest.

A non-exhaustive overview of the currently available models is reported in the following subsections. The models have been classified into four categories: linear regression models, semi-physical models, artificial intelligence models and geospatial models. Subchapters 4.1.1 to 4.1.4 each focus on a different category. A summary of the existing models and of the current challenges are reported in subchapter 4.1.5.



Figure 19: Bibliometric analysis [82] of soiling model literature in Web of Science.

4.1.1 Linear Regression Models

The soiling profile can be modelled through a linear regression of one or more environmental parameters. The spatial resolution of the models ranges from single PV systems based on local meteorological conditions like wind direction and wind speed, relative humidity, and deposition velocities to small scale resolutions like particulate matter densities derived from satellites.

In the simplest approaches, an electrical or transmittance loss is estimated from exclusively the suspended particle concentration. Rainfalls are generally assumed to restore the soiling loss to 0% (i.e., soiling ratio to one). The method proposed by Boyle [83] uses total suspended particle concentration (TSP) to estimate the transmittance loss ($\Delta\tau$, expressed in %) on a PV glass after i days of outdoor exposure:

$$\Delta\tau(i) = 0.005 \cdot \overline{TSP} \cdot i + 0.22 \quad (6)$$

Where:

- \overline{TSP} represents the average concentration of particles of size $\leq 100 \mu\text{m}$
- i = days of outdoor exposure

The most common approach is multi-variate regression, where soiling is modelled through a large number of variables. Toth [84] calculates the electrical loss due to soiling (SL) only from PM_{10} and $\text{PM}_{2.5}$:

$$SR = A_{10-2.5} \cdot C_{10-2.5} + A_{2.5} \cdot C_{2.5} \quad (7)$$



Where:

- $C_{10-2.5}$ is the cumulative sum of coarse particles (calculated as difference between PM_{10} and $PM_{2.5}$) since the last day of rainfall
- C_{25} is the cumulative sum of $PM_{2.5}$ since the first day of data collection and
- $A_{10-2.5}$ and $A_{2.5}$ are constant conversion factors that have to be determined. These two factors are specific to the instrument used for the PM monitoring, and are also expected to vary depending on the site's configuration and local conditions.

Compared to other approaches, categorized as Semi-Physical models, the factors are determined through the fitting of the data, with no research for physical meaning.

In other cases, multi-variate regression is employed to take into account non-particulate matter related variables. For example, Guo [85] proposed a linear equation

$$SR = a + b * PM10 + c * WS + d * RH \quad (8)$$

Where:

- PM_{10} : Particle mass below 10 microns
- WS : Wind speed
- RH : Relative humidity (%)
- a, b, c, d : constant parameters, whose values were determined by fitting the data

In a later study, Javed et al. [1] tested a multi-linear approach with 10 variables in input. In 2018, Figgis [48] described the mass of deposited soiling considering only wind speed (WS) and PM_{10} :

$$Accumulation = 10.6 - 4.99 * WS + 274 * PM10 - 73.4 * WS * PM10 - 14.9\Delta WS1hr \quad (9)$$

Where:

- $\Delta WS1hr$ was the difference between WS of the observation period and average WS of the preceding hour.

In the same work, the authors also reported equations to describe the different phenomena that influence soiling accumulation: deposition, rebound and resuspension.

Particle size and compositions are also known to have an impact on the soiling losses. In this light, Pulipaka et al. [86] used a multilinear regression to estimate the power loss from the particle size.

Linear regression was also used by a NREL team [87], [3] to rank the severity of annual soiling losses at multiple sites in the USA. Compared to the aforementioned studies, which aimed to replicate daily soiling loss profiles, in this case long-term averages of the soiling losses were modelled. The authors compared the data of initially 20 and later 41 soiling stations with more than 100 micro- and macroscopic parameters describing the systems' characteristics and the local environmental conditions. The investigations found that PM_{10} , $PM_{2.5}$ and rainfall statistics were the only factors with significant correlations to the annualized soiling losses. However, they also showed how the data sourcing and processing could affect these correlations. In particular, ground-measured PM data were found to correlate better than satellite-derived concentrations, especially if measured within 30 to 50 km of the site.



Using a similar approach, Cordero et al. [88] found good linear correlations between the Aerosol Optical Depth (AOD) and the daily soiling rates measured at six locations in Chile. Even in this case, the ground-measured outperformed the satellite-derived data.

In contrast to the other soiling estimation approaches, the model proposed by Kimber et al. [57] makes use of PV power data and rainfall information to generate the soiling loss profile. In this case, the value of the soiling rate of the longest dry period is determined through linear regression, and then the same rate is applied to any dry period in the time series, assuming that rainfalls completely remove soiling from the PV modules. This method requires, before its application, the determination of two values: the minimum cleaning threshold (minimum amount of rain able to wash the PV modules) and the length of the grace period (number of days following a rain event after which soiling resumes depositing).

4.1.2 Semi-Physical Models

Semi-physical models try to replicate the non-necessarily linear relations occurring in the soiling process. These models generally require determining the particle deposition or settling velocity from local conditions, including, but not limited to, the relative humidity and wind speed values.

Guo et al. [85], [53], proposed a semi-physical model calculating the soiling loss as a function of the daily deposition and resuspension rates. These were calculated from ambient dust concentration, deposition velocity (function of wind speed), wind speed and relative humidity.

In an analysis of soiling occurring in seven cities worldwide, You et al. [89] assumed a linear correlation between deposited dust density (w) and the PV efficiency drop. In this case, the dust density (w) was calculated from the concentration of suspended particles of diameter within 20 μm and 50 μm (PM_{50-20}):

$$w = ND * PM_{50-20} * Vd * 10^{-6} \quad (10)$$

Where:

- ND = number of days since the last rainfall
- Vd = deposition velocity, determined based on the local environmental conditions.

Coello and Boyle [90] calculate the electrical soiling loss from the transmittance loss using an equation proposed by Hegazy [78] in 2001. In this case, the loss in transmittance is modelled as an error function of an exponentiation of base equal to the accumulated dust mass and of power < 1 . In particular, the mass accumulated at a time t as:

$$m = (v_{10-2.5} * PM_{10-2.5} + v_{2.5} * PM_{2.5}) * t * \cos(\vartheta) \quad (11)$$

Where:

- $PM_{10-2.5}$ = the concentration of coarse particles, of size in between 10 μm and 2.5 μm
- ϑ = tilt angle
- $v_{10-2.5}$, $v_{2.5}$ = deposition velocities.

The researchers considered three different approaches to determine the value of the deposition velocities: the deposition is considered in one approach, while fixed velocities were considered in the other two. The fixed velocities were either equal to the settling velocity or



determined from values observed at nearby stations. The best results were found for the static settling velocity approach.

Bergin et al. [91] calculates the daily loss in transmittance recorded for an installation in India by considering the particulate matter. In this case, differently from before, the concentration and the absorption and scattering efficiencies of each component of the particulate matter were considered.

A more complex model was proposed by Qasem et al [18], which took into account the ambient conditions, the system's characteristics, the rainfall pattern and the dust's spectral transmittance to calculate the soiling loss for different PV technologies.

4.1.3 Artificial Neural Network Models

Compared to linear regression and semi-physical models, Artificial Neural Network (ANN) models do not require an understanding of the physical principles of soiling. Instead, the models iteratively self-train to identify the correct algorithms that convert the inputs into the expected output (i.e., the soiling ratio profile). The main challenge for developers is the identification of key inputs, and of the best performing architecture (i.e., number of hidden layers and nodes).

Javed et al. [1] developed an ANN model to estimate the soiling losses of a site in Qatar. The network was made of one hidden layer and twenty neurons, requiring an input of 10 variables describing the environmental conditions of the site. The model returned an R^2 of 0.54 when compared to the measured data points. A different ANN model was proposed by Laarabi et al. [92] for a site in Morocco. In this case, the ANN had six inputs and one hidden layer of 35 nodes and returned an $R^2 > 0.90$.

In a different approach, Pulipaka et al. [86] used an ANN model to predict the soiling losses based on particle composition. Shapsough et al. [93] employed ANN to estimate the impact of soiling using irradiance and rainfall data.

4.1.4 Geospatial Models

Micheli et al. [94] investigated the possibility of estimating soiling based on PV or soiling data from nearby locations using spatial interpolation techniques. Inverse-distance based methods returned the best results, with $R^2 > 0.7$ if soiling is estimated from sites within 50 km. The results were even better if soiling data from only those systems with similar characteristics to the investigated sites were used. A similar technique was used by Gostein et al. [4], to map the soiling loss distribution within large utility-scale PV systems.

It should be noted that any of the previously listed models could be used to generate soiling maps, so long as the input data were widely and systematically available. For example, based on the correlation found between daily soiling rate and AOD, Cordero et al. [88] generated a soiling rate map for Chile. In a different study, Li et al. [21] made use of the Bergin model [91] to create maps of the soiling mitigation benefits, in terms of recovered energy, for different PV tracking configurations. The authors used the PM type and rainfall data of the MERRA-2 reanalysis dataset from 2003 and 2014. The same approach could be repeated for any of the previous models.

4.1.5 Models' Overview and Validation and Application Limits

Table 3 shows a summary of the four model types. Most studies are based on single locations, whereas the soiling of multiple locations has been investigated in only a few studies. The



literature is still lacking comparative works, where different approaches are tested against soiling measurements for more than one location. This makes it difficult at this time to evaluate the validity and robustness of each model in different soiling and environmental conditions.

Only the study by Pelland et al. [95] compared the performance of two models in the estimation of the average soiling losses for 20 locations worldwide. The models were found to correlate poorly for sites with average losses of less than 5% but performed well for sites with higher soiling losses. In addition, the study showed that the results of the same model could vary if particulate matter from different datasets were given as inputs.

Zhou et al. [96] employed the model proposed by Bergin et al. [91] to calculate the soiling losses for three locations in the USA. The authors used particulate matter data from the US Environmental Protection Agency's Community Multiscale Air Quality (CMAQ) model. The results showed that CMAQ overestimated $PM_{2.5}$ and underestimated the PM_{10} concentrations compared to the ground-measurements at the three investigated sites. In addition, the soiling losses were underestimated compared to the on-site measurements.

In some studies, researchers have proposed and compared two models for the same location. This is particularly common in studies that used ANN models. Both Pulipaka et al. [86] and Javed et al. [1] found better results with ANN models than with multilinear models fed with the same number of inputs. On the other hand, Shapsough et al. [93] found no significant difference between the results of a multilinear model and an ANN model used to estimate soiling losses from irradiance and rainfall. In a comparison of a linear regression model and a semi-physical model, Guo et al. [85] found that they performed similarly.

Some studies, such as Pelland et al. [95], have also investigated the performance of the same model for differently sourced or differently processed inputs. In general, when available, ground-measured data have been found to lead to better soiling estimation than satellite-derived data. Micheli et al. [3], Cordero et al. [88], and Coello et al. [90] have shown how the value set for the deposition velocity can affect the soiling estimation. Different results can also be found when soiling is extracted from PV performance data [57] because of the lack of agreement on the values of factors such as grace periods and cleaning thresholds.

For all these reasons, additional studies are still needed before a universally valid soiling model can be proposed. In particular, there need to be more comparative studies that identify the strengths and weaknesses of different approaches under various conditions of weather and soiling.

Table 3 gives an overview of soiling estimation models. The models are detailed in subchapters 4.1.1 to 4.1.4. The following acronyms are used:

- Ambient Temperature (T_a)
- Wind Speed (WS)
- Wind Direction (WD)
- Total Suspended Particles (TSP)
- Relative Humidity (RH)

**Table 3: Overview of soiling estimation models.**

Lead Author	Model Class	Year	Aim	Key Parameters	Main Findings	Reference
Kimber	Linear	2006	Extracting soiling loss from PV performance data.	PV Performance Ratio, Rainfall	The model generates a soiling loss profile based on the rainfall pattern and on the soiling rate recorded during the longest dry spell. It requires the identification of a minimum cleaning threshold and of the length of dry period.	A. Kimber, L. Mitchell, S. Nogradi, and H. Wenger, 'The Effect of Soiling on Large Grid-Connected Photovoltaic Systems in California and the Southwest Region of the United States', in 2006 IEEE 4th World Conference on Photovoltaic Energy Conference, Waikoloa, HI, 2006, pp. 2391–2395, doi: 10.1109/WCPEC.2006.279690.
Qasem	Semi-Physical	2012	Modelling soiling loss profile using weather data	Ta, WS, WD, dust, tilt, rainfall	A model is developed to estimate the dust accumulation based on weather conditions and to convert this into an electrical loss based on the PV module characteristics and on the dust spectral transmittance	H. Qasem, T. R. Betts, and R. Gottschalg, Soiling Correction Model for Long Term Energy Prediction in Photovoltaic Modules. New York: IEEE, 2012.
Boyle	Linear	2015	Modelling a daily soiling profile measured at five U.S. Locations	TSP	A linear model is developed where the transmittance loss is a function of TSP and of the exposure time.	L. Boyle, 'don't soil your chances with solar energy:experiments of natural dust accumulation on solar modules and the effect on light transmission'.
Guo	Linear & Semi-Physical	2016	Modelling a daily soiling profile of a soiling measurement system in Qatar.	WS, PM10, RH	A multi-linear and a semi-physical model are developed and compared. Both models were found to return estimation with < 16% uncertainty when used to estimate the daily soiling loss profile.	Guo B, Javed W, Khan S, Figgis B, Mirza T. Models for Prediction of Soiling-Caused Photovoltaic Power Output Degradation Based on Environmental Variables in Doha, Qatar. ASME 2016 10th Int. Conf. Energy Sustain., 2016, p. 1–8. https://doi.org/10.1115/ES2016-59390 .
Pulipaka	ANN & Linear	2016	Soiling loss is estimated from particle size composition	Particle size	Multi-linear regression and ANN are used to estimate the soiling losses based on particle size composition of the soil. ANN are found to perform better.	S. Pulipaka, F. Mani, and R. Kumar, 'Modeling of soiled PV module with neural networks and regression using particle size composition', Sol. Energy, vol. 123, pp. 116–126, Jan. 2016, doi: 10.1016/j.solener.2015.11.012.



Javed	ANN & Linear	2017	Modelling a daily soiling profile of a soiling measurement system in Qatar.	Same-day PM10, WS, WD, Ta, RH, Previous-day PM10, WS, RH, Wind Gust frequency and exposure time	A 10-input ANN model was able to significantly model the soiling loss trends, returning better results than a multilinear approach based on the same inputs. PM10, WS and RH were found to be parameters better correlated with soiling.	W. Javed, B. Guo, and B. Figgis, 'Modelling of photovoltaic soiling loss as a function of environmental variables', Solar Energy, vol. 157, pp. 397–407, Nov. 2017, doi: 10.1016/j.solener.2017.08.046.
Bergin	Semi-Physical	2017	Modelling the profile of a soiling measurement in India	PM components concentrations	The soiling profile is modelled based on the concentration of each PM10 and PM2.5 components, taking into account each specific component's absorption and scattering efficiency.	Bergin MH, Greenwald R, Xu J, Berta Y, Chameides WL. Influence of aerosol dry deposition on photosynthetically active radiation available to plants: A case study in the Yangtze delta region of China. Geophys Res Lett 2001;28:3605–8. https://doi.org/10.1029/2001GL013461 .
Micheli	Linear	2017	Ranking the average soiling losses of 20 soiling station in the USA.	PM10, PM2.5, Rainfall	PM10, PM2.5 and rainfall are found to be the best soiling predictors, out of 100+ potential variables, when the average losses of different sites are compared.	Micheli L, Muller M. An investigation of the key parameters for predicting PV soiling losses. Prog Photovoltaics Res Appl 2017;25:291–307. https://doi.org/10.1002/pip.2860 .
Figgis	Linear	2018	Modelling soiling deposition and resuspension	WS, PM10	Multilinear relations are proposed to estimate soiling accumulation, deposition, resuspension and rebound rates	Figgis B, Guo B, Javed W, Ahzi S, Rémond Y. Dominant environmental parameters for dust deposition and resuspension in desert climates. Aerosol Sci Technol 2018;52:788–98. https://doi.org/10.1080/02786826.2018.1462473 .
Cordero	Linear	2018	Modelling soiling rates in Chile	AOD	A linear correlation is found in between AOD and soiling rates. Ground-measurements outperformed satellite-derived data.	Cordero RR, Damiani A, Laroze D, MacDonell S, Jorquera J, Sepúlveda E, et al. Effects of soiling on photovoltaic (PV) modules in the Atacama Desert. Sci Rep 2018;8:1–14. https://doi.org/10.1038/s41598-018-32291-8 .
You	Semi-Physical	2018	Modelling the soiling loss profile for seven cities worldwide	PM50-20, Vd	The soiling accumulation is calculated based on the deposition velocity, calculated from the local conditions.	You S, Lim YJ, Dai Y, Wang CH. On the temporal modelling of solar photovoltaic soiling: Energy and economic impacts in seven cities. Appl Energy 2018;228:1136–46.



						https://doi.org/10.1016/j.apenergy.2018.07.020 .
Zhou	Semi-Physical	2019	Modelling soiling loss based on particle deposition estimation	PM, Rainfall	The soiling losses are estimated using a Community Multiscale Air Quality (CMAQ) model. The estimated PV panel transmittance is lower compared to on-site measurements.	L. Zhou et al., 'The impact of air pollutant deposition on solar energy system efficiency: An approach to estimate PV soiling effects with the Community Multiscale Air Quality (CMAQ) model', <i>Sci. Total Environ.</i> , vol. 651, pp. 456–465, Feb. 2019, doi: 10.1016/j.scitotenv.2018.09.194.
Micheli	Linear	2019	Rank the severity of the average soiling losses of 41 soiling stations in the USA using environmental parameters.	PM10, PM2.5, Rainfall	The work confirms that PM10 and PM2.5 are the best soiling predictors, followed by parameters describing the average and maximum length of the dry periods. However, it found that the results could be significantly affected by the environmental parameters sourcing and processing methodology.	Micheli, M. G. Deceglie, and M. Muller, 'Predicting photovoltaic soiling losses using environmental parameters: An update', <i>Progress in Photovoltaics: Research and Applications</i> , vol. 27, no. 3, pp. 210–219, Mar. 2019, doi: 10.1002/pip.3079.
Shapsough	Linear & ANN	2019	Modelling the soiling loss profile of a PV installation in the UAE	Irradiance, Rainfall, Exposure time	A multi-linear and an ANN models were used to estimate the performance of a soiled PV module, with no significant difference between their results.	S. Shapsough, R. Dhaouadi, and I. Zualkernan, 'Using Linear Regression and Back Propagation Neural Networks to Predict Performance of Soiled PV Modules', <i>Procedia Computer Science</i> , vol. 155, pp. 463–470, 2019, doi: 10.1016/j.procs.2019.08.065.
Micheli	Geo-spatial	2019	Estimating average soiling loss from nearby data	Nearby soiling data, site's characteristics	The average soiling loss of a site can be estimate using soiling data from nearby sites, by using spatial interpolation.	Micheli L, Deceglie MG, Muller M. Mapping Photovoltaic Soiling Using Spatial Interpolation Techniques. <i>IEEE J Photovoltaics</i> 2019;9:272–7. https://doi.org/10.1109/JPHOTOV.2018.2872548 .
Laarabi	ANN	2019	Modelling the soiling rate of a site in Morocco	Irradiance, Ws, Wd, Ta, RH, Rainfall	A 6-35-1 ANN model is implemented and validated. A sensitivity analysis shows that relative humidity, first, and second, wind direction are the two most impactful parameters.	Laarabi B, May Tzuc O, Dahlioui D, Bassam A, Flota-Bañuelos M, Barhdadi A. Artificial neural network modeling and sensitivity analysis for soiling effects on photovoltaic panels in Morocco. <i>Superlattices Microstruct</i> 2019;127:139–50. https://doi.org/10.1016/j.spmi.2017.12.037 . https://doi.org/10.1002/pip.2860 .



Toth	Linear	2020	Modelling the soiling loss profile for a site in Colorado, USA.	PM10, PM2.5, Rainfall	A soiling estimation model is developed, and its results are compared for the PM measurements of two devices: a traditional PM monitor and a low-cost device.	Toth S, Hannigan M, Vance M, Decglie M. Predicting photovoltaic soiling from air quality measurements. IEEE J Photovoltaics 2020:1–6.
Coello	Semi-Physical	2020	Modelling the soiling loss profile for nine soiling stations in the USA	PM10, PM2.5, Rainfall, tilt angle	The soiling loss is estimated based on the PM concentrations and the deposition velocities. Of the different approaches used to estimate the deposition velocity, setting its value equal to the value of a fixed settling velocity returned the best results.	Coello M, Boyle L. Simple Model For Predicting Time Series Soiling of Photovoltaic Panels. IEEE J Photovoltaics 2019;PP:1–6. https://doi.org/10.1109/jphotov.2019.2919628 .

4.2 Snow Models

Snow modelling can be divided into two branches: direct energy loss prediction (consisting of stochastic and curve-fitting methods), and snow coverage prediction (consisting of threshold-based, and first principle methods). In the direct energy loss approach, stochastic methods use only historical PV array output data, whereas curve-fitting methods develop empirical correlations between array output and weather data. By contrast, models that estimate energy losses by predicting the shedding of snow from PV panels are more complicated. Here, threshold models define limits that, if surpassed, result in snow sliding off a module at a defined rate. One threshold-based algorithm, the Marion model, is implemented in a popular PV simulation software developed by the National Renewable Energy Laboratory (NREL). First principle models can also simulate snow shedding but are even more complex using energy balance equations to model melting and sliding. Overall, there are at least 11 models to quantify energy losses due to snow. Some have been validated at multiple sites, often in the United States, while others remain relatively untested. There is no consensus as to which model is most accurate and more validation work is needed at different latitudes, tilt angles, and mounting configurations [97].

4.2.1 Estimating Energy Losses - A Canadian Case Study

Although many snow loss models for PV systems are available, few comparative studies have been performed. As a preliminary work, the performances of two snow-shedding models – Marion et al. [100] and Townsend and Powers [101] (see Chapter 4.2.3) – were compared for simulated PV arrays at different tilt angles and latitudes in order to create energy loss contour maps across Canada using irradiance and snowfall data from 190 combined weather stations. Energy losses for the Marion model were substantially higher than the Townsend and Powers model, and results showed significant geographic differences using the same data. The Marion model predicted peak losses at high latitudes in the Arctic Circle whereas the Townsend and Powers model showed the greatest energy losses in northern Quebec. The two models were compared to a real PV array operating in the Northwest Territories. The energy losses due to



snow predicted by the two models highlight the need for more validation by field data and the determination of latitude/tilt/technology specific snow shedding constants.

4.2.2 Meteorological Weather Station Data Selection

In order to estimate snow losses on PV arrays in Canadian climates for a given longitude and latitude, meteorological weather station data for solar insolation and ambient temperature were combined with data for fresh snowfall. Insolation and ambient temperature data were collected from the Canadian Weather Energy and Engineering Data Sets (CWEEDS) [98]. The parameters relevant to snow simulations that were provided by CWEEDS stations were hourly global horizontal, direct normal, and diffuse horizontal insolation, as well as dry bulb ambient temperature. South of 58°N, there were 492 weather stations containing at least 10 years of data between 1998 and 2014. North of 58°N, there were 95 CWEEDS stations divided into two solar irradiance data sets: from 1998-2014 there were 23 sites using solar irradiance estimated by the MAC3 model from hourly cloud layer weather observations, and from 2005-2017 there were 72 sites using SUNY/NASA polar orbiting satellite-derived data.

Snow data in this study were taken from precipitation stations measuring daily fresh snowfall by ruler, of which 1100 sites were available with data between 1968 and 2018. Each CWEEDS station was examined to determine whether there was at least one precipitation station within a five km radius with at least five years of overlapping data. Of the original CWEEDS locations, 190 met the proximity condition and were matched with nearby precipitation stations (Figure 20). For these matched stations, hourly irradiance and ambient temperature data were combined with snow depth data.



Figure 20: CWEEDS stations with combined precipitation data for 190 locations.

4.2.3 Snow Loss Simulation using the System Advisor Model

Simulation of snow loss was performed at hourly intervals using two models: the Marion [99] and the Townsend and Powers models [100]. Although other models have been developed, these two were chosen because they have been the subject of validation studies. The Marion model is integrated into the SAM software. For this report, the Townsend and Powers model



was coded in Matlab and was based on the outline provided in the snow shedding study for Truckee, California [100]. A separate version of the Marion model was also coded in Matlab in order to alter snow sliding coefficients.

For each time step, the Marion model checks if new snowfall has occurred by comparing with the previous time step. If fresh snowfall has occurred, the array is assumed to be completely covered. If there was no snowfall, the snow conditions on the array from the previous time step are used. When fresh snowfall is detected, an hour-by-hour modelling occurs starting with the first daytime hour.

The Townsend and Powers model differs from the Marion model in several ways. Instead of considering sliding of snow for hourly time steps, a monthly percentage energy loss is calculated based on correlations between measured and predicted monthly fractional energy loss.

The Townsend and Powers model takes into account array-specific geometry such as clearance distance above the ground, and the piled snow angle beneath the array [100].

The Marion model requires ambient temperature, plane of array irradiance and snow depth. In addition to these data, the Townsend and Powers model requires relative humidity. The Marion model can also be adjusted, by means of the snow sliding coefficient, to take into account snow shedding for different mounting configurations. The Marion model considers snow sliding to be the dominant removal mechanism and does not take into account melting or removal of snow by wind. Furthermore, the Marion model simulates shedding using time steps according to data collection frequency (minutely, hourly, daily), whereas the Townsend and Powers model aggregates data into monthly averages. To some extent, because both models rely on empirically derived constants, they are location, technology, and mounting configuration specific.

4.2.4 Energy Loss Due to Snow: Model Comparison

Snow loss estimates as a percentage of annual energy output were generated for 45° and latitude tilt using the Marion model and Townsend and Powers' model for both rooftop and ground-mounted systems. The results of these models are summarized as a single country-wide average snow loss based on all available years in Table 4. For the Marion model, the snow sliding coefficient was 1.97 for rooftop systems and 6.0 for ground-mounted. For the Townsend and Powers model a residential system with a clearance of 0.1 m above the rooftop was compared to a ground-mounted system with 2.0 m clearance.

Table 4: Annual average energy loss due to snow across all sites with median in brackets.

Array Orientation	Marion	Townsend and Powers
Tilt = 45°	Roof: 14.9% (13.7%)	Roof: 4.9% (4.4%)
	Ground: 10.1% (8.5%)	Ground: 2.3% (2.0%)
Tilt = latitude	Roof: 14.8% (13.8%)	Roof: 3.7% (2.3%)
	Ground: 10.5% (8.7%)	Ground: 1.7% (1.2%)

As shown in the country-wide averages, the differences between the two models are substantial even though they use the same annual weather files. Gridding was selected for the creation of snow loss contour maps in order to extend estimates from specific stations to a country-



wide level. A commercial software used in the geological sciences for 3D mapping, Surfer 17, was used for the analysis. Automatic gridding (contouring) takes randomly spaced data and extrapolates using overlaid orthogonal lines – which define cells and nodes. An algorithm is used to estimate values for all nodes. It must be noted that algorithms may also introduce noise, unrealistic features independent of real data, and values which may be incorrectly extrapolated into regions where data are non-existent or sparse [101]. The contour maps were created for 45° tilt and tilt at latitude assessing both roof and ground-mounted configurations for each snow shedding model. The results are shown in Figure 21, Figure 22, Figure 23 and Figure 24. In general, the Marion model predicted increasing energy losses at higher latitudes with annual loss ranging from nearly zero in warmer regions up to a maximum of 42% for a few stations within the Arctic Circle. Energy losses for ground-mounted systems were lower than rooftop arrays. Differences between latitude and 45° tilt scenarios were relatively small. By contrast, the Townsend and Powers model showed drastically lower losses particularly at high latitudes. The discrepancies between the two models remain a subject of further study.

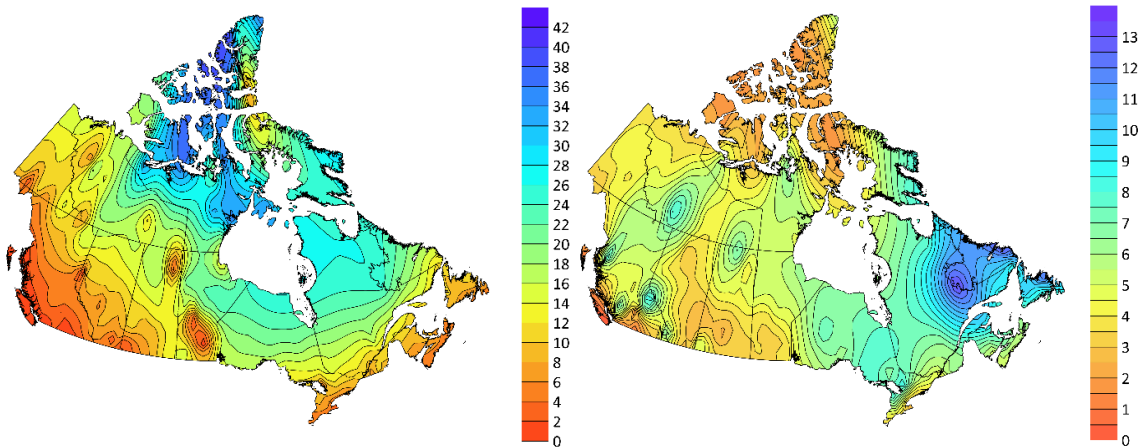


Figure 21: Tilt = 45°, rooftop array annual average energy loss [%]: Left: Marion, Right: Townsend and Powers.

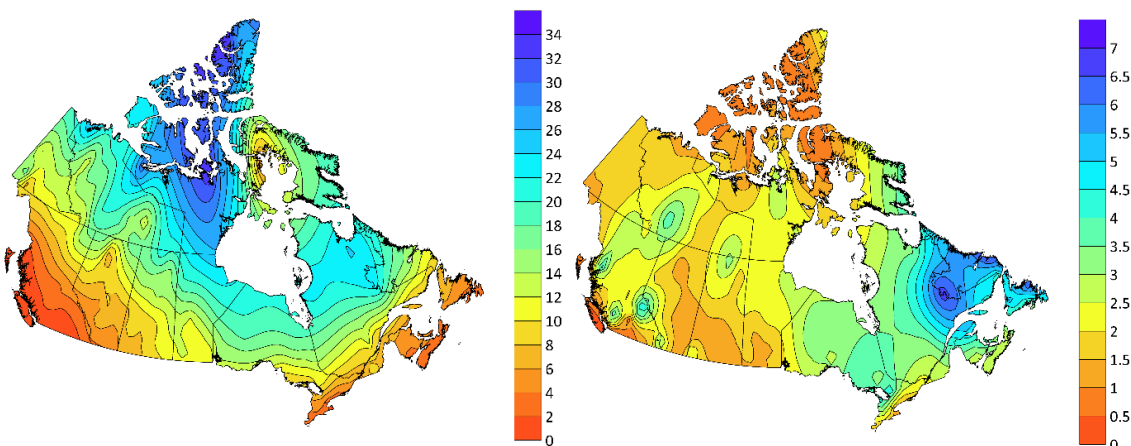


Figure 22: Tilt=45°, ground mounted array annual average energy loss [%]: Left: Marion, Right: Townsend and Powers.

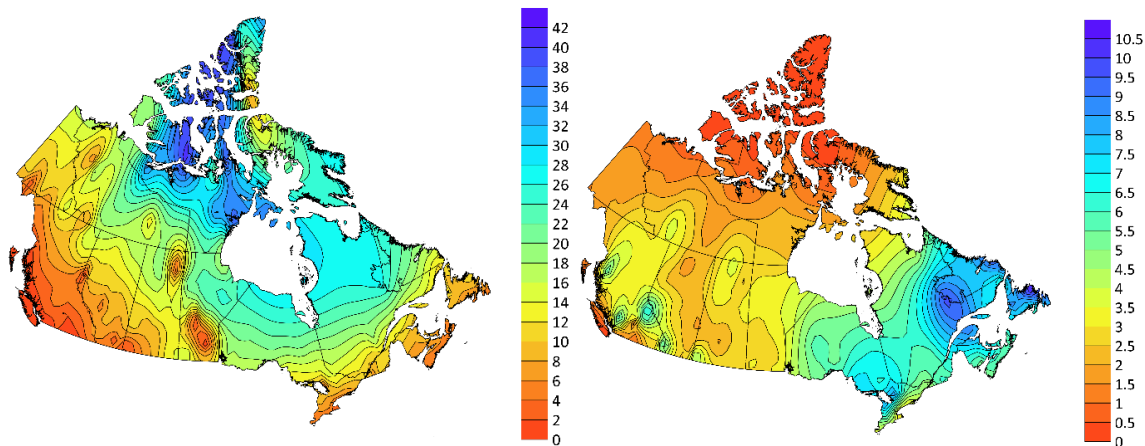


Figure 23: Tilt = latitude, rooftop array annual average energy loss (%): Left: Marion, Right: Townsend and Powers.

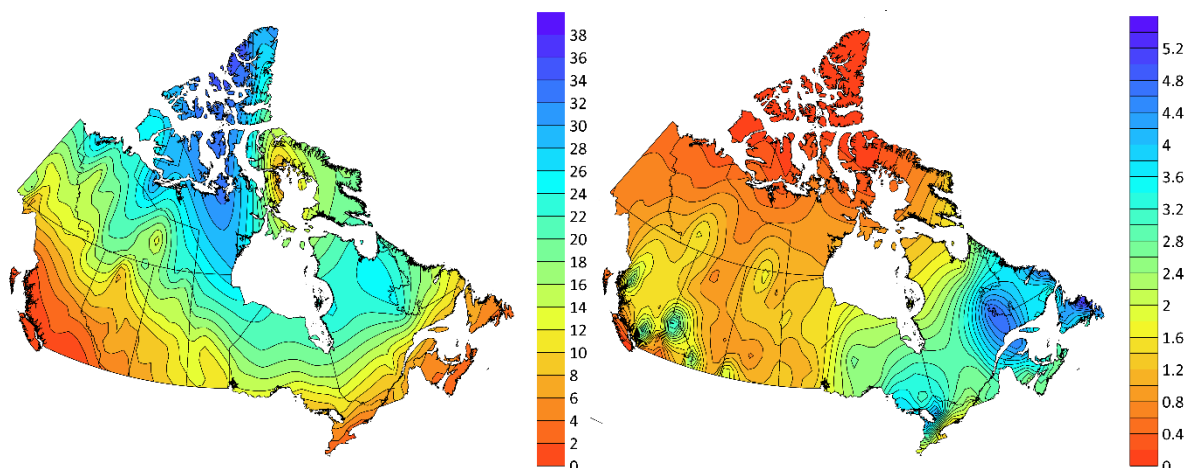


Figure 24: Tilt = latitude, ground-mounted array annual average energy loss [%]: Left: Marion, Right: Townsend and Powers.

While using a monthly average simplifies the collection of precipitation data, it may also mask the complex process of snow accumulation and shedding that can occur on an hourly time scale. The discrepancy between the two models highlights the need for more validation using real site data. Fitting coefficients used in both models were determined using site data from Colorado, Wisconsin, and California. These coefficients could be expanded to reflect site-specific geographical conditions, mounting configuration, and module technology. As shown in Figure 20, the distribution of combined weather stations with snow shedding data are concentrated at lower latitudes, with relatively few stations north of 60°N.

4.2.5 Model Validation by Comparison with PV Array Data

In order to compare the models with a real test case, snow losses for a 104 kW array in Fort Simpson, Northwest Territories, were analysed. The Fort Simpson array has a tilt angle of 35°. The effects of snow were quantified by comparing the measured monthly yield to the estimated monthly yield [102] [99]. The estimated monthly yield was determined as a function of array insolation, irradiance-weighted module temperature, power temperature coefficient, and system performance ratio at standard test conditions according to IEC 61724-1 (Edition 2).



To validate the snow loss models, Fort Simpson power output data and weather station insolation from 2015 to 2018 were used to estimate snow loss. Next, the Marion model and Townsend and Powers model were run using combined CWEEDS and precipitation weather station data from the nearby airport. The total percentage snow losses for three years of operation are shown in Table 5.

Table 5: Annual average energy loss due to snow at Fort Simpson with median in brackets.

Array Orientation	Year	Marion	Townsend and Powers	Empirical
Tilt = 35° Ground-mounted	2015	11%	2.2%	8%
	2016	17.4%	2.6%	12%
	2017	20.4%	2.5%	15%

These results show that the Marion model overestimated and the Townsend and Powers model underestimated snow loss. On average, the Marion model was closer to the empirically determined losses than the Townsend and Powers model. More work is needed to understand the causes of discrepancy and validate models with more sites.



5 ESTIMATION OF ENERGY AND REVENUE LOSSES OF SOILING AT UTILITY SCALE

5.1 Economic Impact of Soiling

Soiling affects PV systems worldwide, and its effects change depending on the location, on the time of year, and on the characteristics of the site and of the systems. Recently, it was estimated that in 2018 soiling caused the loss of at least 3% to 4% of the annual PV energy production [6]. This corresponded to an economic loss on the order of 3 to 5 billion € (Figure 25). These losses are expected to increase up to 4% to 5% and 4 to 7 billion € by 2023 due to a number of factors. First, more PV modules are being installed in high-insolation regions, such as China or India, which are also those that generally are more exposed to soiling. Second, the reduced price of electricity will make cleanings “less convenient” because the revenues for any kWh of recovered energy will be lower. Finally, under the same amount of soiling, more efficient modules are subject to larger energy losses compared to less efficient PV modules.

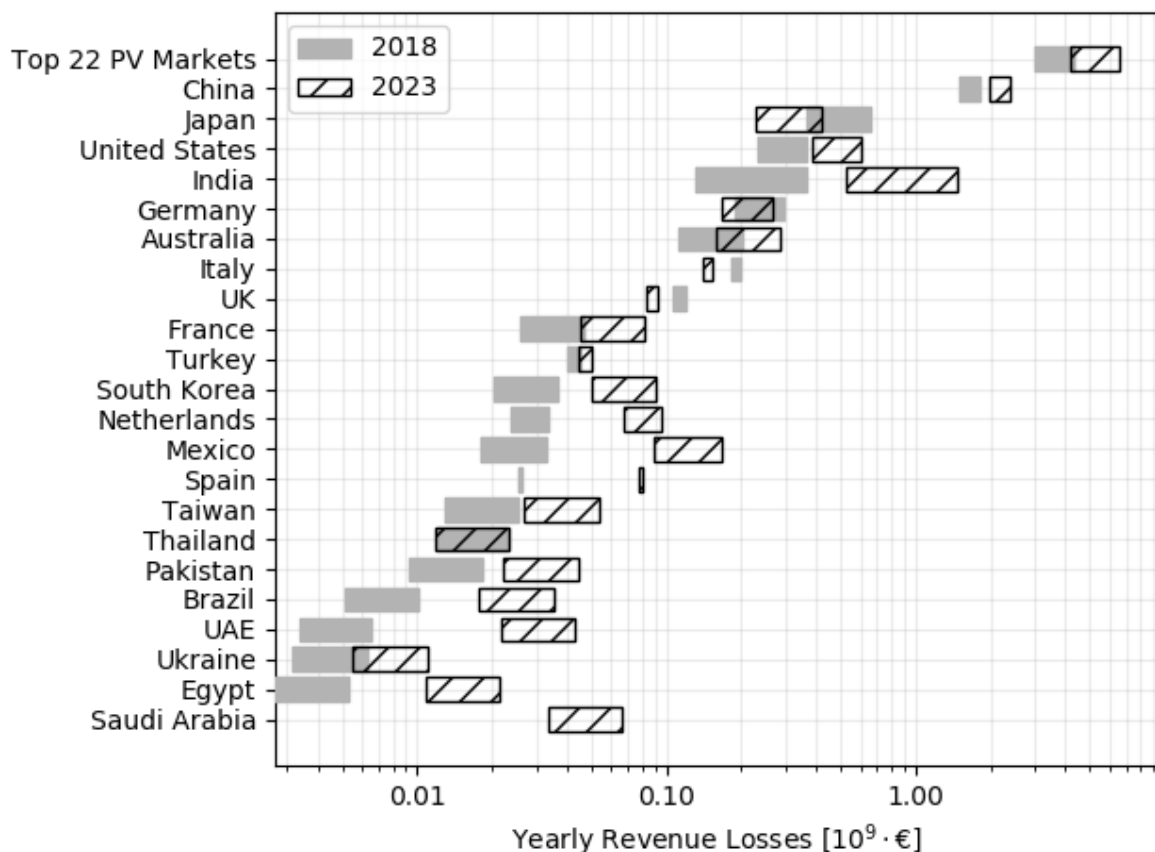


Figure 25: Global Economic Losses: Economic losses per country in 2018 and in 2023 for the top 22 PV markets. Data and methodologies from [6].

The previously mentioned work takes into account an optimal cleaning schedule scenario, where all the PV systems are operated to minimize the financial soiling losses, intended as combination of revenue losses and cleaning expenses. In a real world, the losses are expected



to be higher, as many systems do not operate at the optimal cleaning schedule. For example, the increasing share of rooftop installations might contribute to further raising the global impact of soiling.

Cleaning a PV module has a cost, which is the combination of the cost of labour and the cost of the materials. This is generally expressed in currency per unit of surface as it represents the expense needed to clean a m² of PV module (Figure 26). Factors such as the availability and the cost of resources (e.g., water) and the cost of workforce as well as the accessibility of a site can affect the cleaning costs. The expense per cleaning a full PV site (U) can then be calculated depending on the system size (C) and on the PV module types, as follows:

$$U = u \cdot A_{tot} = \frac{u \cdot C}{P_{mod}/A_{mod}} \quad (12)$$

where

- u is the cost per cleaning (in €/m²)
- P_{mod} = power rating
- A_{mod} = surface of each PV module.

The equation shows that the cost U lowers while the efficiency of the modules increases, as, for the same power capacity, higher efficiency modules have less surface to be cleaned.

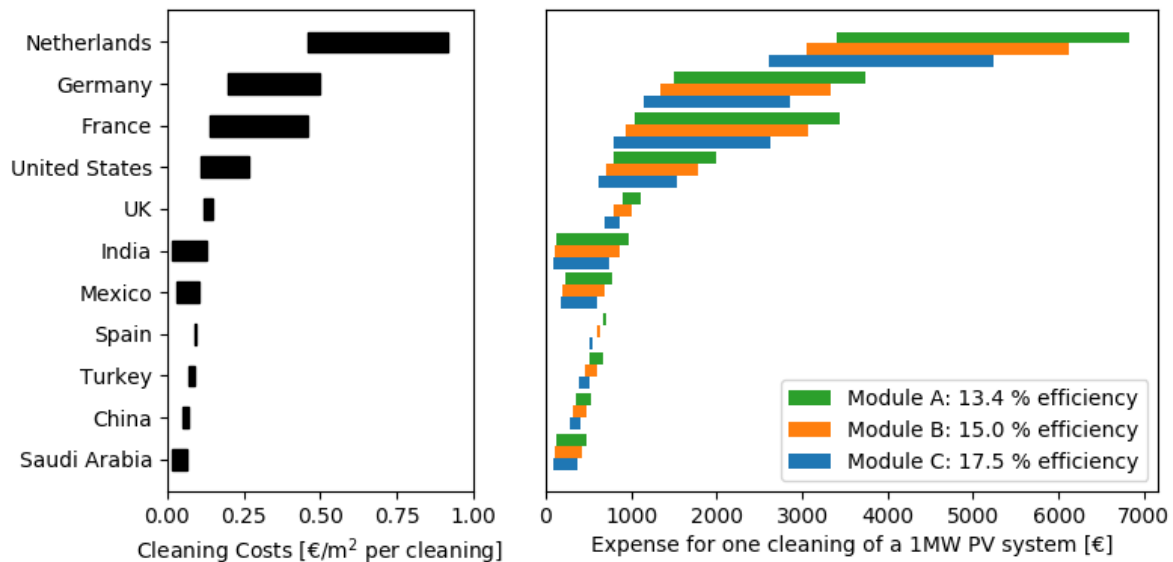


Figure 26: Cleaning Costs and Expenses. Left: PV cleaning costs for representative markets, adapted from Ilse et al. Right: Expenses for cleaning a one MW system, depending on the PV module's efficiency.

Cleaning a PV module that has no or limited soiling on its surface is an unnecessary expense, because the cleaning expense only leads to no or limited energy gain. On the other hand, not cleaning a soiled PV module is also a loss of money. For this reason, PV systems should be operated as close as possible to the optimal cleaning schedule, in order to maximize the electrical performance and, at the same time, minimize the costs. Mani and Pillai [103] compiled a



list of cleaning routine recommendations based on the location, the climatic zone, and the weather conditions of the PV sites. This is a useful guideline, but the cleaning schedule should be specifically redefined for each PV site, because it varies according to a number of factors [104]. In addition to the cost of cleaning and the PV module efficiency, the profitability of a cleaning schedule depends also on:

- The soiling deposition rate,
- The capacity factor of the system,
- The price of the recovered energy, in currency per kWh.

Various economic models have been proposed to identify the most convenient cleaning schedule. The most simple approach is to perform a cleaning whenever the cost of cleaning is lower than the revenue lost because of the missed energy production. A metric, named Cost of the Production Losses (CPL), was proposed by [105], to quantify the missed revenues caused by the unproduced energy due to soiling. It is obtained as the product of energy lost due to soiling and electricity selling price:

$$C_{PL} = (P_{STC_clean} \cdot \eta_{ineff} \cdot T_M) \cdot (R_S + R_{inc}) C_{PL} \quad (13)$$

$$= (P_{STC_clean} \cdot \eta_{ineff} \cdot T_M) \cdot (R_S + R_{inc})$$

where

- P_{STC_clean} is the STC power generated by a clean module
- η_{ineff} is the efficiency loss due to soiling
- T_M is the worthwhile moment to operate the cleaning
- R_S and R_{inc} = values (in €) in saving and in incentives for each produced kWh.

Using this approach, cleanings should be operated when $CPL > U$. The Cost of Production Losses equation has been modified to be applicable also to solar home systems [106].

This simple method works on matching the soiling revenue loss and the cleaning costs. In addition, ideally, the cleaning schedule should also take into account the fact that natural agents, such as rainfalls, wind or dew can have a cleaning effect on the PV modules at no cost [57], [107], [23]. For these reasons, there is room for an additional optimization of the cleaning schedule, as shown in Figure 27. In the plotted example, the optimal cleaning day would reduce the cost of soiling by 17% compared to the day in which the $CPL > U$ condition is met. The data in the figure are modelled from soiling measurements taken in a Californian site over a dry period of three and a half months, considering a hypothetical one MW PV system made of 17.5% efficient modules, a fixed daily capacity factor of 20%, a cost per cleaning of 0.2 €/m² and an electricity price of 0.09 €/kWh.

Because of this opportunity for optimization, additional models have been proposed in literature to further reduce the economic losses due to soiling. Jones et al. [56] proposed a method to minimize the total cost of soiling, intended as a sum of cleaning costs and revenue losses. A similar approach aimed to minimize the total soiling-related costs was employed by Ilse et al. [6]. From the analysis of data of a PV system in Saudi Arabia, Herrmann [108] developed a model to identify the optimal number of cleanings per year based on two parameters: average soiling rate per day and cleaning costs. Besson et al. [59] proposed a method to maximize the difference between revenues and cleaning costs:



$$\max \sum_{t=1}^T ss_t \cdot CP_t \cdot EP - x_t \cdot U \quad (14)$$

where

- ss_t = the soiling loss on day t
- CP_t = energy yield in clean conditions on day t
- EP is the electricity price
- U is the total cost of one cleaning
- x_t is the decision binary variable of the plant on day t .

In these approaches, the cleaning effects of rainfalls are also considered. You et al. [89] proposed an optimization method aimed to minimize the Net Present Value (NPV) of PV systems. All these optimization models would minimize the economic cost of soiling but, compared to the first simple method, which can be easily applied to take O&M decisions on fielded PV systems, are more difficult to use in a real case scenario, given the inter-annual variability of soiling and precipitations [87], [109].

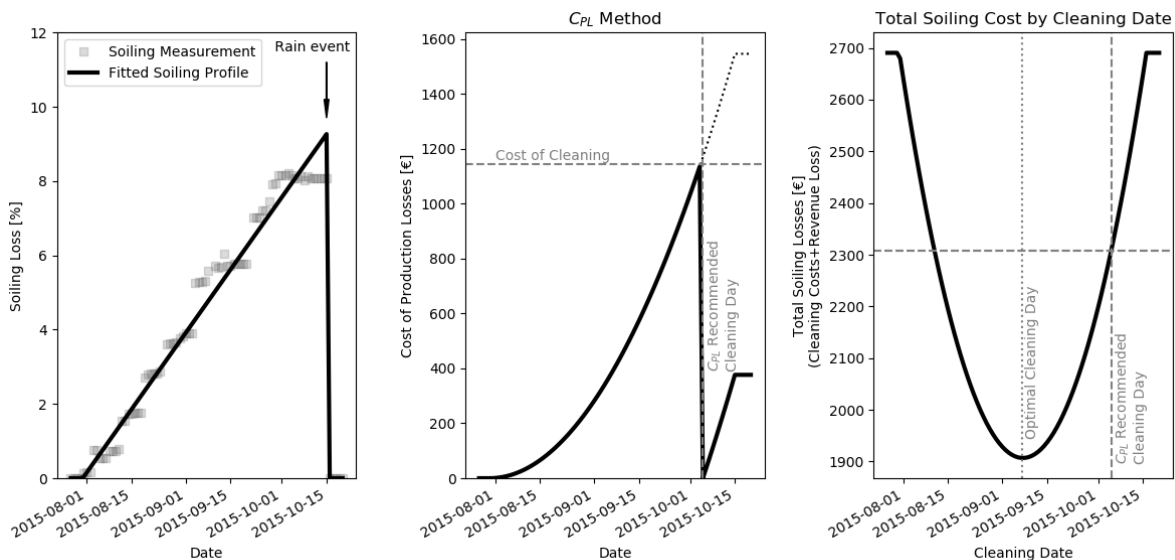


Figure 27: Comparing Models. Left: Soiling Loss during a dry period registered for a site in California ([87]). Centre: Comparing Cost of Production Losses and Cost of Cleaning to identify the most convenient cleaning day using the CPL method [105], [110]. Right: Comparing the total soiling losses for different cleaning days in a one-cleaning scenario. Considered Conditions: One MW plant with 17.5% efficient module, fixed 20% capacity factor, 0.2 €/m² cost per cleaning and electricity price of 0.09 €/kWh.

5.2 Soiling Losses Worldwide: Resources and Variability

Many publications have now been presented on PV soiling losses and related topics. However, many of these are independent case studies, and soiling information is often not reported in a systematic way. Various metrics are indeed used to quantify soiling, and, in some cases, the same metrics have slightly different definitions. For example, annual soiling ratios have been



reported both as simple averages of daily value and as irradiance-weighted averages of daily values.

In an effort to gather all this information, some resources have been made available to show soiling data from different locations. Several review articles have collected data published in literature [12], [11], [111], [6]. The first soiling map² has been published by the NCPRE (India) and reports the soiling rates [%/day] collected for many locations worldwide. The values are sourced from the literature, and therefore each calculated in a unique way. On the other hand, the NREL soiling map³ shows 83 soiling data measured at PV systems and soiling stations located in the USA. In this case, soiling is quantified using a systematic approach, but it is different for soiling stations and PV systems [3]. These resources are of value, because they can be used to estimate soiling for sites where no soiling data are available. Indeed, it is possible to estimate the soiling losses for a site through spatial interpolation techniques, given one or more soiling data from nearby locations [94]. The uncertainty in the estimation was found to lower if sites with similar characteristics (e.g., tracking type or mounting type) were compared.

None of the resources listed before currently takes into account the temporal and spatial variability of soiling. Indeed, nearby systems can soil differently and even soiling within the same site can change significantly. This can be the result of several factors, ranging from the climatic conditions to the system characteristics and the PV module design [23]. Gostein et al. [51] showed that the losses within the same site can vary by a factor of 2x. In a more recent study, conducted for two sites in California, it was found that even the soiling rate can vary by factors of 2x or 3x. The non-uniformity can depend on the spatial distribution of soiling “emitters” and on the prevailing wind direction.

5.3 Case Study: Long-Term Soiling Losses in a Moderate Climate

Soiling is generally assumed to be an issue only for arid or desert regions. In addition, PV systems in rainy locations might be easily considered to be constantly washed by the regular precipitations. The example that follows, instead, shows how soiling can slowly build up also in locations, such as Switzerland, commonly considered as soiling-free.

The PV-Laboratory of Bern University of Applied Science (BFH) Burgdorf has operated a test centre for PV-systems with a solar generator of 60 kWp, since 1994. The system consists of 1056 framed modules Siemens M55HO mounted in summer 1993 with a tilt angle of 30° and the long side in horizontal position. This solar generator is split in two parts of 30 kWp called “Tiergarten West” and “Tiergarten Ost”.

The solar generator is on top of the building of the department of electrical engineering of BFH Burgdorf, about 10 m over ground in a town of about 15'000 inhabitants. In the region surrounding this town, there are light industries and forests and farms causing biological pollution (with pollen) especially in spring. The most important external source of unusual pollution is a railway line (Bern-Zürich) at a distance of less than 100 m of the PV system. As the railway station of Burgdorf, where many trains stop, is less than one km away, many trains are braking or accelerating when they pass the building. The region is pretty humid, natural rainfall is more than 1'000 litres per m² a year and is distributed sufficiently over the whole year. These conditions made natural cleaning considered to be sufficient before installation of the plant.

While in the years 1994 up to 1996 only in spring a clearly visible pollution was observed, in course of 1997, with a rather dry and sunny period from the end of July until the beginning of November, a development of a permanent pollution strip (compact pollution up to 1 cm,

² http://www.ncpre.iitb.ac.in/ncpre/pages/SERIIUS_Soiling_rate_of_the_World.html

³ <https://www.nrel.gov/pv/soiling.html>



followed by a strip of visible, but not compact pollution) close to the lower edge of the module frame was registered. The influence of this polluting strip on array performance was found to be especially severe on the PV modules of the main generator (with the long side in horizontal position), because of the very small distance between the cells and the frame (1-2 mm). A loss as high as 10% built up until spring 1998 [112]. Until that time, artificial cleanings were performed only on the irradiance sensors and not on the PV modules.

Because of the significant impact of soiling, a periodical cleaning schedule was then established, and cleanings were performed in the summer of 1998, 2002, 2006, 2010, 2012, 2016 and 2020.

String IV-Measurements of the 30 kWp “Tiergarten West” installation were performed some days before and after each cleaning. Depending on the weather conditions and actual generator soiling, the average “gain” due to the cleaning varies from few precents up to 10% (Table 6).

Table 6: Percentage calculations of the performance gain were made for the years 2002 to 2020 from string IV measurements.

Year	1998	2002	2006	2010	2012	2016	2020
Increase in %	10.0%	9.3%	3.2%	9.9%	2.3%	9.9%	5.4%

To investigate the long-time effect on the performance of the installation, the generator correction factor k_G is calculated from the monitoring data which is a measure for different operation losses including soiling.

Figure 28 shows the qualitative progression of the measured losses due to soiling, as well as the respective gain after cleaning the installation. The values of k_G have been averaged for one year for the summer season from April to September that periods of snow coverage are excluded. In case of cleaning this season is divided into the months before and after cleaning. In 2020 it was cleaned end of August. The k_G data point of Period 8 consists only of the measured point in September 2020.

For the cleanings until 2010 a clear increase of k_G as effect of the cleaning can be seen. From 2012 on no longer-lasting performance gain can be found. It seems that the modules are getting faster back to a normal equilibrium soiling degree. It might be, that the glass surface of the module has changed over time due to aging of the modules or inadequate cleaning.



**PV-System Tiergarten West, BFH-TI, Burgdorf:
Trend of the generator correction factor in summer (April-September)**

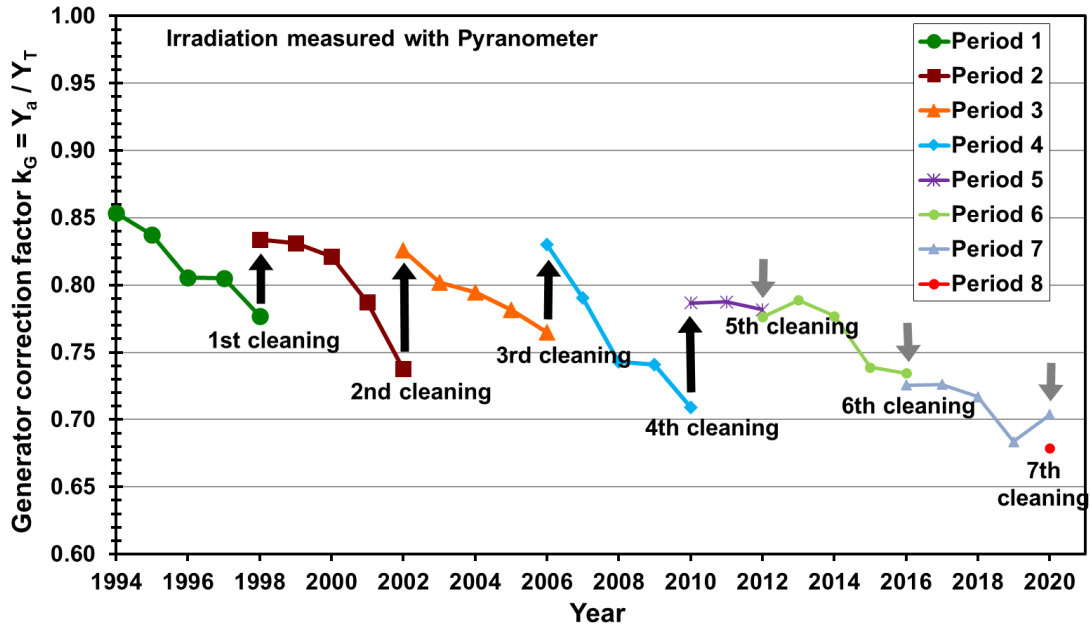


Figure 28: The performance ratio of the 30 kWp “Tiergarten West” installation from 1994 to 2020.

As shown, soiling can slowly build up throughout the years even in those locations frequent natural cleaning events occur. For this reason, annual, or at least periodical, manual cleanings should always be performed on PV systems, to remove any hard-to-remove soiling that is not washed away from natural events and to prevent the creation of hard bonds between soiling and the surface of the modules [91].



6 MITIGATION OF SOILING LOSSES IN PV SYSTEMS

Generally speaking, soiling mitigation methods can be classified into preventive and corrective measures. Preventive measures fall into the responsibility of engineering, procurement, and construction (EPC), in terms of site and module selection, anti-soiling coating applications, site adaption, etc, whereas corrective measures fall into the competence of O&M, such as choosing the right cleaning technology. Several authors have summarized mitigation strategies, e.g. AlDowsari et al. [113], Ilse et al. [6], together with a techno-economic assessment of losses and mitigation strategies.

Cleaning can be subdivided into manual-, semi- and fully automated cleaning, with respective water consumption. Costs, potential damages and influence of micro-climates vary considerably. There is consensus that there is no “one-method-fits-all” approach, because soiling strongly depends on local conditions.

Anti-Soiling Coatings (ASC) hinder the deposition of particles, and are described by particle adhesion physics, electrodynamic shields that use electrostatic forces to move particles away. Ilse et al. [6] also suggest implementing dew mitigation, as dew is a major factor in cementation and caking processes that might lead to crusts that cannot be easily removed. Lastly, site adaptation, new module- and plant designs (e.g., vertical bifacial modules facing east-west), and tracking solutions (e.g., nightly stow-away) have the potential to further mitigate soiling.

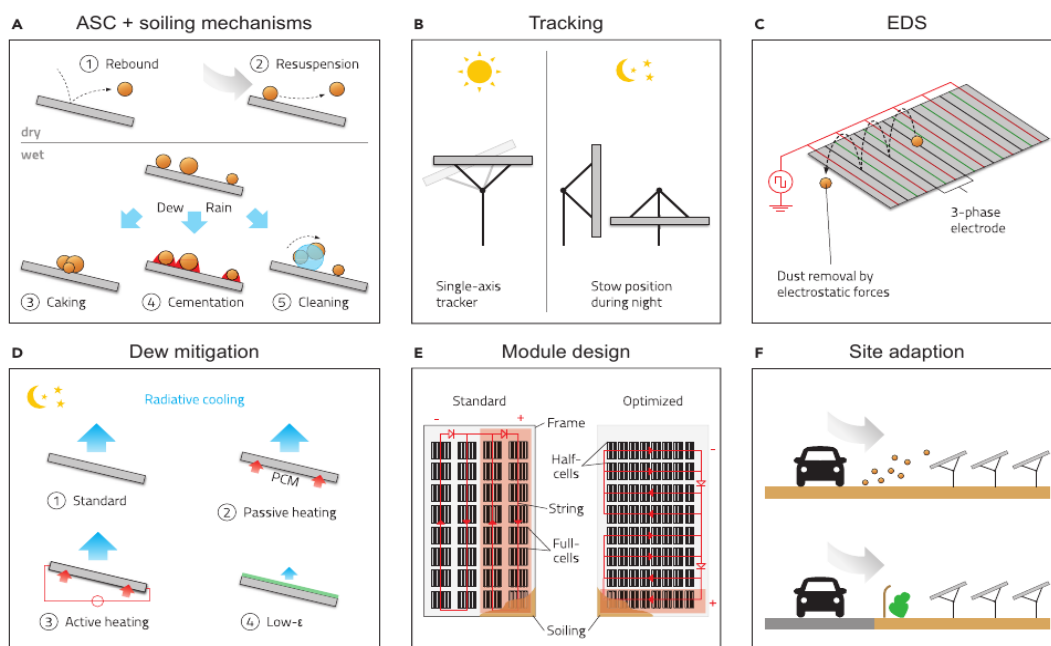


Figure 4. Schematic Illustration of Soiling Mitigation Technologies

(A) Important soiling mechanisms which could be addressed by anti-soiling coatings (ASCs).

(B) Single-axis tracking and optimization of night stowing position.

(C) Working principle of EDS (standing wave version).

(D) Dew mitigation by low- ϵ coatings and active and passive heating.

(E) PV module design approaches for soiling loss reduction: the red overlay indicates lost cell strings dew to soiling.

(F) Site adaption.

Figure 29: Soiling mitigation approaches apart from cleaning [6].



6.1 Preventive Mitigation Methods

6.1.1 Site Assessment, Adaption and Planning

From the beginning of the design and construction phase, soiling considerations should be an integral part of system design. Knowledge about local meteorological conditions like main wind direction, rain frequencies, relative humidity and dew occurrence will help in adapting systems to minimize soiling. For example, nearby dirt roads can be lined with vegetation in order to deflect dust gusts. Frameless modules may make it easier for soiling to be removed, and an optimized module design with bypass diodes can minimize the effect of partial shading by heterogenous soiling. As illustrated by examples in chapter 6.2.3, single- and double-axis trackers may be beneficial as well.

6.1.2 Anti-Soiling-Coatings

Hydrophilic/Hydrophobic Coatings

Passive preventive methods, also known as easy-to-clean, self-cleaning, or anti soiling, are based on coatings that can be classified as hydrophobic, hydrophilic or photocatalytic.

Hydrophobic coatings with easy-to-clean surfaces have low surface energies, resulting in water-repellent surface properties with high contact angles, which lead to droplet formation. These water droplets are then meant to roll-off and collect dust particles from the surface. By applying a specific microstructure, they can be tuned towards a superhydrophobic surface with a contact angle (CA) of more than 150° , often referred to as a lotus effect, inducing a self-cleaning functionality. Such coatings are based mostly on fluoropolymers or hydrophobic functionalized silica.

Hydrophilic coatings with self-cleaning surfaces, on the other hand, attract water due to high surface energies. Therefore, they show low contact angles, which lead to water spreading across the surface. If a CA of less than 10° is achieved (superhydrophilic), a complete wetting is guaranteed under the assumption that the angle of inclination and amount of water are sufficient. The coating materials are based on silicon dioxides or titanium dioxide. Coatings based on the latter material offer both photocatalysis, which prevents decomposition of organic contaminants under UV irradiation and improves mitigation, and superhydrophilicity, which facilitates the washing of contaminants from the surface by rainwater [114], [87]. Typically, hydrophilic ASCs are deposited by sputtering or wet chemical processes (e.g., roller coating).

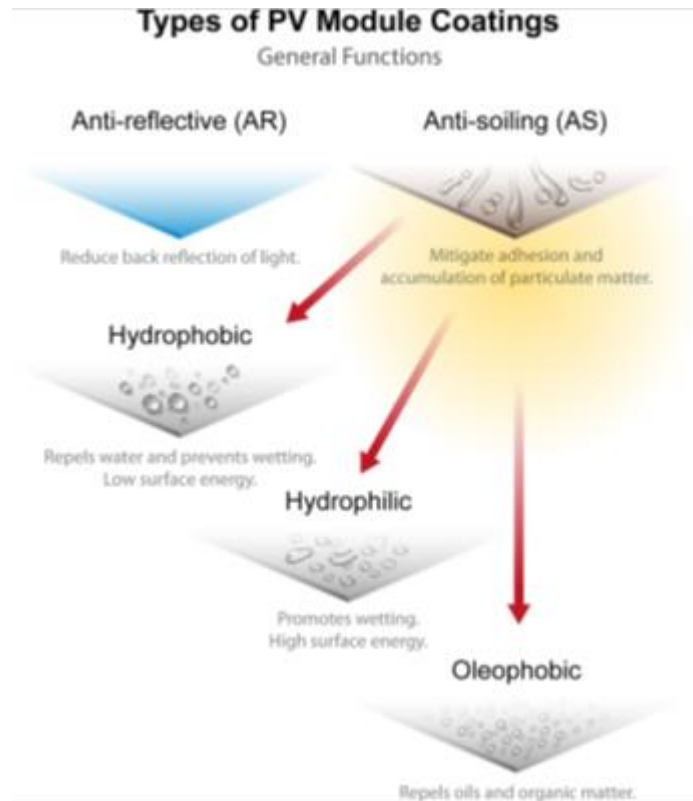


Figure 30: Different types of AS Coatings [115].

There is not agreement as to whether hydrophilic or hydrophobic ASCs are effective [116]. For instance, even if hydrophobic coatings make PVs easier to clean, they won't necessarily result in anti-soiling properties [117]. In fact, under certain circumstances, coatings can actually increase soiling when compared to uncoated glass. The benefit of ASCs must therefore be individually assessed for each target location in a technical-economic evaluation, taking into account realistic climatic conditions, cleaning cycles, manufacturing costs and other factors [87], [6]. On the other hand, Ilse et al. [6] show that the application of ASCs might enable PV array operators to increase the time between cleaning cycles, thereby reducing the associated costs. Depending on local weather conditions, cost reductions of 20-50% can be achieved with ASC alone.

From investigations in outdoor and laboratory tests, five dry and wet soiling mechanisms have been identified for arid regions [23]: rebound, resuspension, caking, cementation, and water cleaning. To minimize soiling with ASCs, each of these mechanisms could be addressed. However, restrictions resulting from physical phenomena must be taken into account. These include location factors such as fouling rates and periodic weather fluctuations. Another important issue is the general physics of particle adhesion, in particular of dust particles with diameters smaller than 20 μm , which typically cannot be removed by wind and contribute to a large proportion of soiling when combined with dew [6], [50], [118], [119].

In terms of optimized cleaning processes for ASC-equipped PV modules, Lorenz et al. [120] simulated the influence of soiling for a rainy and a dry year based on a reference model, as shown in Figure 31. The reference represents a typical year in Riyadh, Saudi Arabia based on empirical data from 1985 to 2010. As shown in Figure 41, a surplus of 3.2% of the annual economic yield can be achieved during a typical year, while a surplus of 3.34% and 3.24% can be achieved during dry and rainy years, respectively.

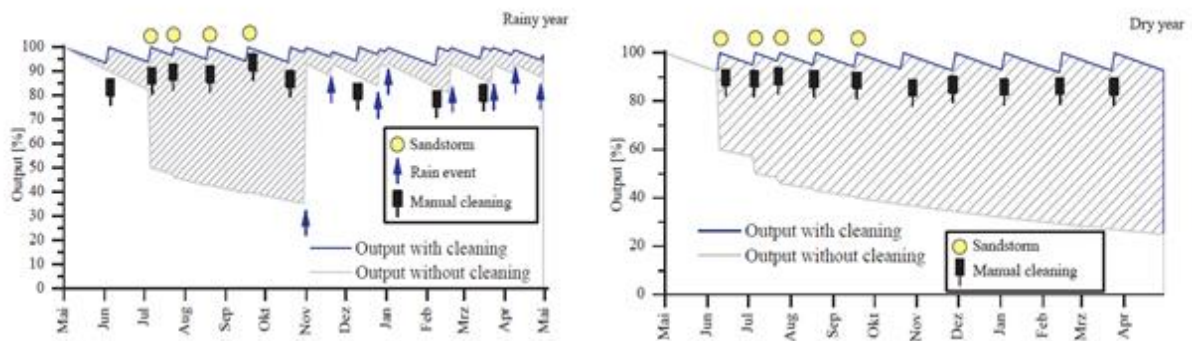


Figure 31: Optimized cleaning processes for ASC equipped PV modules, influence of Soiling [120].

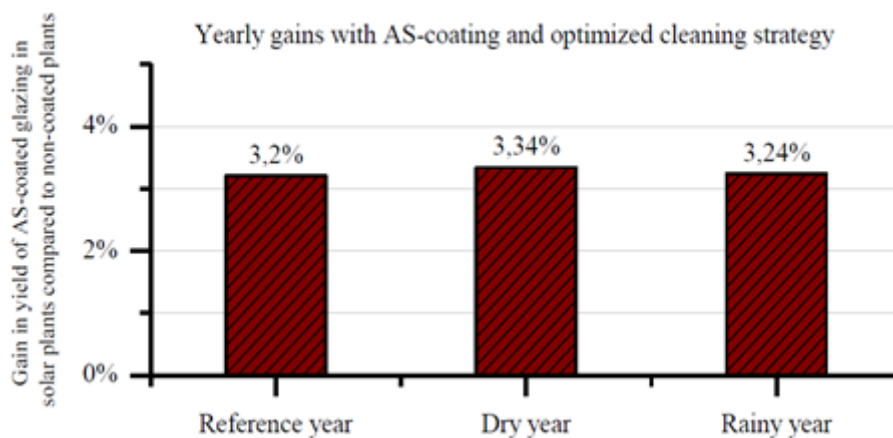


Figure 32: Yearly gains with ASCs and optimized cleaning strategy [120].

Based on transmission data, the tendency towards easier cleaning characteristics resulted in less power loss. Therefore, the advantages of an ASC are the reduction of cleaning processes due to natural cleaning methods. It is again noteworthy that, to achieve such advantages, the ASC needs to be carefully chosen based on local conditions. Further, a long lifetime cannot be guaranteed for all climatic regions, and some ASCs could increase transmission losses by themselves [8].

On the other hand, investigations showed enormous efficiency losses due to heavy soiling, up to -80% within six months [68] without an ASC. Mondal et al. [121] summarize the loss of performance up to 20% depending on test sites and other boundary conditions. However, profits from the use of ASCs are mainly achieved through savings in cleaning costs and must therefore cost less than one €/m² after 10 years in relation to an ROI [6].

The effects of abrasion cannot be predicted, since in addition to cleaning processes, abrasive sandstorms (dust composition, shape, and size) and the environment also have an impact on the service life of ASCs. Investigations of the percentage area covered by ASCs from different coatings (hydrophilic porous silica and hydrophobic polymers) in two distinct regions with different cleaning methods – dry brush, low pressure water spray and wet sponge, and rubber



squeegee – have shown that in some cases considerable damage was caused by dry brush due to the abrasive nature of the contamination [115].

Recently, a study accomplished in Denmark, which represents coastal climate, suggests that besides the combined outdoor stress, which is difficult to reflect in indoor tests, the lifetime of ASCs is also influenced by the quality and homogeneity of the surface [122]. If the surface is damaged prior to the application, the degradation accelerates the damage, e.g., by blistering.

Nevertheless, there are many standard methods to test the lifetime in advance, e.g., IEC 62788-7-3 or VDI 3956-1, but the choice of cleaning method and materials has to be adapted to the climate, soil type and soil texture, and soiling mechanism.

6.1.3 New Module- and Plant Concepts

It is widely reported that the loss in transmission due to soiling is a strong function of the tilt angle of the glass [123], [12]. Specifically, soiling loss is the lowest for a tilt angle of 90°. Gravitational force on soil particles is an important factor influencing the settlement of dust on surfaces and can partly explain the tilt angle dependence. Formation of dew on the sunny side of the PV modules, typically during the night, enhance the adhesion of the dust to the glass surface. These observations suggest that (i) vertically mounted solar panels would suffer the least from soiling, (ii) soil deposition on the rear side of a laterally mounted bifacial module would be negligible, and (iii) flipping monofacial modules sunny side down during the night could reduce soil deposition and adhesion. In this sub-chapter we discuss the effectiveness of these methods based on field experiments. The reduction in soiling by these methods is also quantified.

The experiments were conducted at a test site on the rooftop of an 8-storey building on the campus of IIT Bombay, Mumbai, India [124], [125]. Geographical coordinates of the site are 19.13°N, 72.19°E, and Mumbai has a warm and humid climate. The modules' current-voltage characteristics were periodically measured using a multi-channel curve tracer (Daystar MT5 3200). Pairs of crystalline silicon modules were used for assessing the soiling losses, one of each pair was cleaned every day and the other was left to soil. Soiling loss is characterized by the following equation,

$$\text{Soiling Loss (\%)} = \left(1 - \frac{\text{Energy}_{\text{Soiled}}}{\text{Energy}_{\text{Cleaned}}}\right) * 100 \quad (15)$$

Where:

- Energy was obtained by integrating the instantaneous power measured over the day
- Soiling rate is defined as the slope of soiling loss versus number of days.

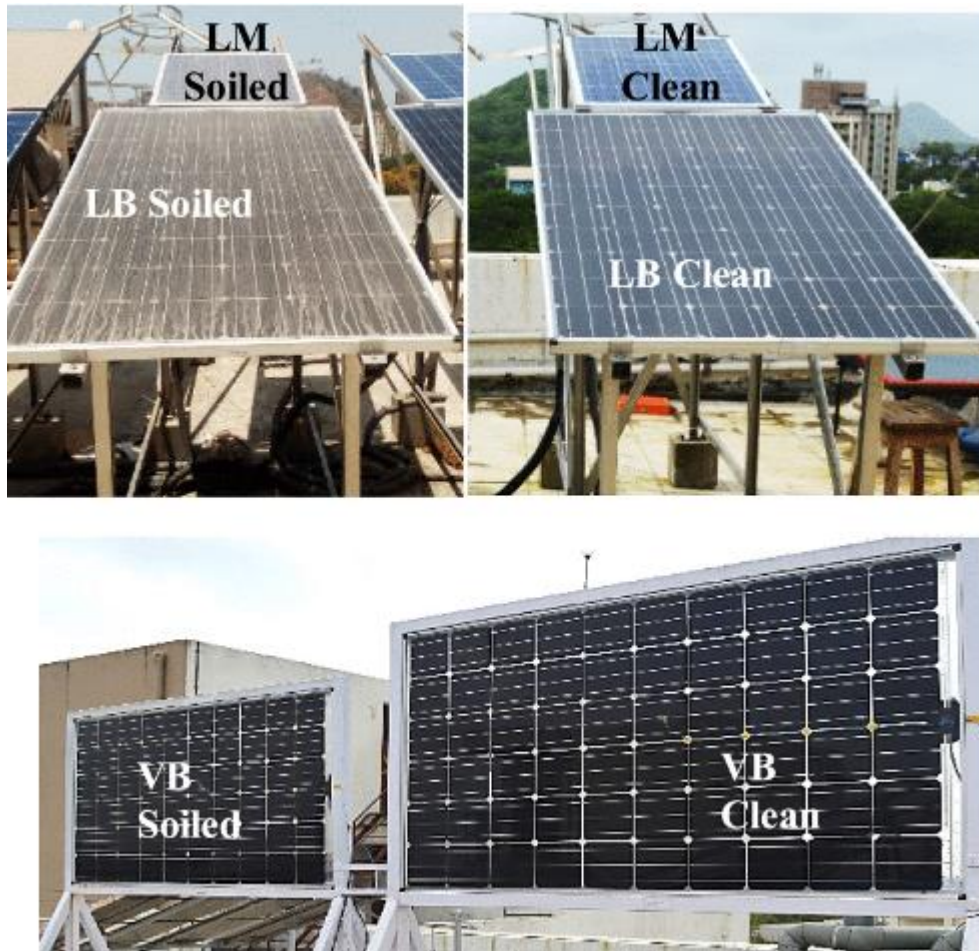


Figure 33: Experimental installation with vertically mounted bifacial modules.

(i) East-West Oriented Vertically Mounted Bifacial Modules

Even though vertical mounting of modules may reduce soiling losses, such a mounting would result in low energy yields in the case of monofacial modules, as the modules would produce substantial energy only during half of the day. This issue is partly addressed by bifacial modules with high bifaciality. If the bifacial module is vertically mounted with east – west orientation, the east facing side would produce substantial energy in the forenoon and the west facing side would be the major energy producer in the afternoon.

In our experiments, we used two monofacial modules (100 Wp, measured at STC) and four bifacial modules (nominal bifaciality of 90%; front-side 229 Wp and back-side 209 Wp, measured at STC). Both the monofacial modules and two of the bifacial modules were installed with 19° tilt, and they are referred to as Latitude mounted Monofacial modules (LM) and Latitude mounted Bifacial modules (LB) respectively. Two of the bifacial modules were installed with the front side facing the west with a tilt of 90°, and they are referred to as Vertically mounted Bifacial modules (VB). The experiment was carried out during December 2017 to April 2018.

Photographs of the experimental installations on the 20th day of the experiment are shown in Figure 33. The uncleaned vertically mounted bifacial module experienced visibly less soiling than the uncleaned laterally mounted modules. Figure 34 shows the power production profile of the cleaned vertically mounted bifacial module on a typical day of the experiment.

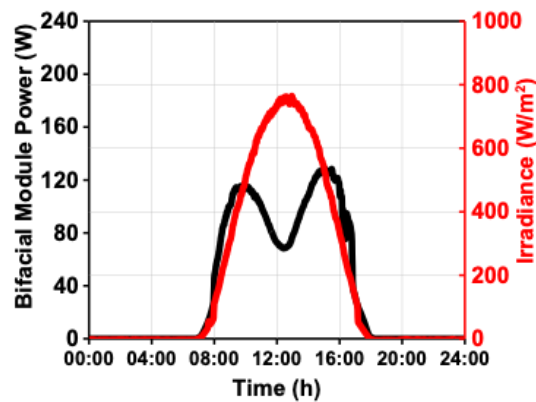


Figure 34: The power produced by the cleaned vertically mounted bifacial module on a typical day of the experiment.

Figure 35 (a) shows the soiling loss as a function of the date of experiment for the three pairs of installations. The soiling rate is seen to be 0.45%/day for the LM, and this is consistent with the experiments we had conducted at the same location since 2013 [126], [127]. The soiling rate is seen to be 0.32%/day for LB. This is because soil deposition on the rear side of the module is negligible compared to that on the front side, and hence the contribution of the rear side of the bifacial module to energy generation is not reduced substantially by soiling. This effect was less pronounced for bifacial modules with lower bifaciality [124]. It is likely that locations with high albedo, for example white sand deserts, would benefit more from this effect. In the case of vertically mounted bifacial modules, the soiling rate is seen to be about 0.02%/day, negligible compared to that observed for the modules installed at the latitude angle.

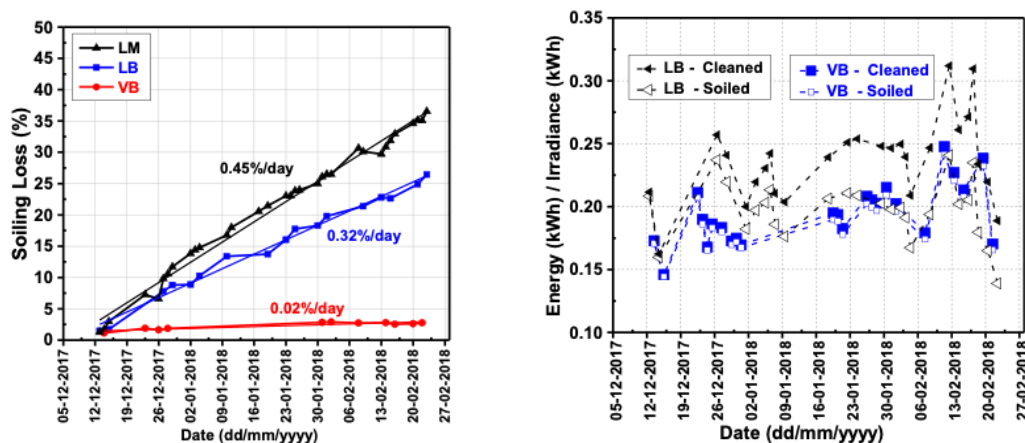


Figure 35: a) Soiling loss for the 3 different types of installations. b) Normalized energy produced by bifacial modules mounted with latitude tilt, and tilt of 90°. The daily irradiation measured at the location is also plotted for reference.

Figure 35 (b) shows the energy produced by the LB and VB modules normalized to the irradiance (in kWh) for each day. The normalized energy produced by the cleaned LB is seen to be always higher than the VB. However, the energy produced by the soiled LB, though initially higher than the VB, decreases as time progresses due to soiling and eventually crosses over and becomes lower than the energy produced by the VB. The crossover is seen to occur approximately after seven weeks of field exposure.



(ii) Reduction of Soiling by Flipping Monofacial Modules upside down during the Non-Sunshine Hours

In this experiment, conducted from early March to mid-April, 2016, modules with a nameplate rating of 90 Wp were used. One module was mounted at latitude angle throughout the experiment and cleaned every day. Another module mounted at the latitude angle was not cleaned. A third, inverted module was mounted on a structure that enabled, through the manual operation of a lever, for the module to be flipped face-side down. During daylight, this module was positioned at the latitude angle, and was flipped upside down during the night. This module was also not cleaned. Figure 36 shows the third module in the two positions.



Figure 36: The photograph on the left shows the inverted module during the day, and the photograph on the right shows it during the night.

Figure 37 shows the soiling loss as a function of the date of experiment for the fixed and inverted modules. The soiling rates were estimated as 0.45%/day and 0.14%/day by linear regression. The proposed mechanism results in a significant reduction in the soiling rate, and hence could result in a significant reduction in the cleaning frequency. Fall off from dust when the module is flipped, lower deposition of dust on the glass that is facing down during the night, and lower rate of adhesion of dust due to lower dew formation on the down facing glass during the night, are potential reasons for the lower soiling rate on the inverted module.

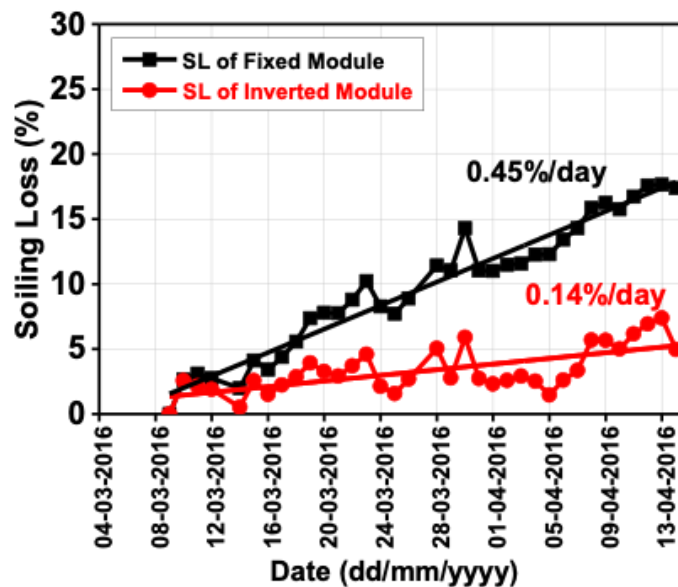


Figure 37: Soiling losses in a module fixed with a tilt of latitude angle during the entire experiment, versus that in a module which was stowed in sunny side down position during non-sunshine hours (inverted module).

The following conclusions can be drawn from these experiments:

- Bifacial modules mounted with fixed tilt at the latitude angle suffer from lower losses due to soiling than monofacial modules mounted similarly. This is due to the low or negligible soiling of the rear side of the bifacial module. This effect is more pronounced with higher bifaciality and can be anticipated to be more pronounced in a location with higher albedo.
- Bifacial modules mounted vertically suffer from negligible soiling losses compared to bifacial modules mounted at latitude angle. In Mumbai, the energy yield of a vertically mounted bifacial module exceeded that of a bifacial module mounted at latitude tilt, after seven weeks of operation in summer months, when both modules were not cleaned. However, shading in arrays of such modules and appropriate structural designs would pose challenges when scaling up.
- Flipping monofacial modules upside down during non-sunshine hours can significantly reduce the soiling rate, significantly reducing (in some cases completely eliminating) the need for cleaning. This scheme could be implemented by suitably modifying the installation structures, especially in tracking systems.

6.2 Corrective Mitigation Methods

6.2.1 Overview of Cleaning Techniques

Especially in arid regions with hardly any rainfall and nightly dew formation, it might become mandatory to actively clean modules. The market for cleaning solutions is still growing worldwide. Solutions include manual, semi-automated, and fully automated systems, applying rotating brushes and varying amounts of demineralized water.



From an analysis of the literature, Mondal et al. [121] suggest a classification of cleaning techniques based on climatic conditions (Table 7).

Table 7: Proposed cleaning techniques for weather conditions, adapted from Mondal et al. [121].

Weather/Area	Cleaning technique applied
Desert	Vibration of surface and aerodynamic streamlining
Dry	Electrostatic biasing, autonomous robotic cleaning, sprinkler
Rainy, humid	Special techniques are not required, but can be combined with anti-reflective coating
Cold, moist	Autonomous/robotic cleaning, sprinkler, and anti-reflective coating
Snow	Stowing/inverting, anti-reflective coating
Hot, arid, sunny	Electrostatic biasing, autonomous/robotic cleaning, sprinkler
Cloudy, shaded	Autonomous/robotic cleaning, sprinkler, aerodynamic streamlining

More commonly, cleaning devices have been divided into four categories:

- Manual devices such as dust brooms and water brushes.
- Truck-mounted devices, which may include a water tank.
- Semi-automatic systems that use portable robots, which can be moved from row to row. These systems can be battery-powered or wired, and they can be rail-mounted, frame-mounted or freely movable.
- Fully automatic systems that are designed to regularly clean one row of modules. These systems are often solar-powered, and they can be rail-mounted, frame-mounted or freely movable.

Especially for high pressure water cleaning, it has to be noted that module manufacturers typically specify a maximum pressure with which modules can be cleaned. Warranties may be voided if these values are exceeded. Chapter 6.2.4 summarises the results from module cleaning tests and the effects that these simulated cleaning cycles have on float glass, with or without anti-reflective coatings and/or structured glass.

Kurz [131] concludes that “cleaning can be a “make or break” factor for competitive PV projects, as the production gains enabled by cleaning grow in importance as error margins are shrinking, with dry robotic cleaning to be the most robust technology currently on the market. Presumably, these technologies will further improve as they mature, and other technologies like automated drones will further enhance planning and operation of cleaning equipment.



Table 8 compiles a non- exclusive list of cleaning solution providers in the four categories. This market is rather dynamic and dedicated fairs show new developments every upcoming season. The Uniform Resource Locator (URL) is given where details to the solutions were available.



Table 8 Non-exclusive list of available cleaning solutions, sourced from [128], [121], [129].

Manually	URL with further information, where available
Reach-IT Pro	
Kärcher	https://www.kaercher.com/int/
Unger	https://www.ungerglobal.com/en/applications/solar-cleaning
Cleantecs	https://www.cleantecs.com/en/products/solar-cleaner
IPCEagle	https://www.ipcworldwide.com/us/product/solar-panel-pure-water-cleaning-system/
Truck mounted	
SunBrush	https://sunbrushmobil.info/the-mobil-sunbrush/?lang=en
SolarCleaningMachinery SCM	http://scmsolar.com/
MERLO	
Rolhus	
BITIMEC	bitimec.com
Digcher	
Metalmeccanica	
hycleaner	https://hycleaner.eu/en/produkte/hycleaner-black-solar-2/
Drone mounted	
BladeRanger	http://www.bladeranger.com/
SolarBrush	https://www.aerialpower.com/solarbrush/
Semi-Automatic Robots	
Sunpower	
Exosun	
SolarCleaningMachinery SCM	
Chemik	
Serbot	
Helios	http://www.pv-roboter.de/
Gekko Solar32	www.serbot.ch/images/documents/TD_GEKKO%20Solar_En_20-13_06_06.pdf
Fully automated	
Eccopia	http://www.ecoppia.com/technology/
Sol-Bright	
Nomadd	http://www.nomaddesertsolar.com/the-nomadd-technology.html
Serbot	
WashPanel	http://www.washpanel.com/prodotti.php
Nozzle Sprayer	
Heliotex's 'automatic solar panel cleaning system	https://www.solarpanelcleaningsystems.com/photos.html?galItem=63&galAlbum=2&galTag=



6.2.2 Electrodynamic Cleaning of Systems

The solar power industry needs a more cost-efficient, fully automated, water-saving and time-saving solution to clean dust and sand off PV panels. The solution must not damage the panel surface and reduce power loss in desert areas where panels need faster, regular cleaning due to frequent sandstorms and higher atmospheric dust concentration. For these reasons, the Electrodynamic Cleaning System (EDS) is a promising technology to clean dust off of solar panels, solar reflectors (mirrors) and glass surfaces, especially in arid regions.

The EDS consists of a contactless cleaning solution using an electrodynamic cleaning based on the charging of sands particles. Dust particles are evacuated from the module surface via travelling waves controlled by high voltage (in the order of kV) electric pulses applied in dedicated electrodes integrated below the front glass of the solar panel (Figure 38). Parallel electrodes are embedded into the surface of the glass or the polymer, and then an electronic circuit creates travelling waves that levitate and repel the dust particles via the Coulomb force away from the surface.

Masuda et al. [130] were the first to demonstrate particle transportation based on a variable electric field.

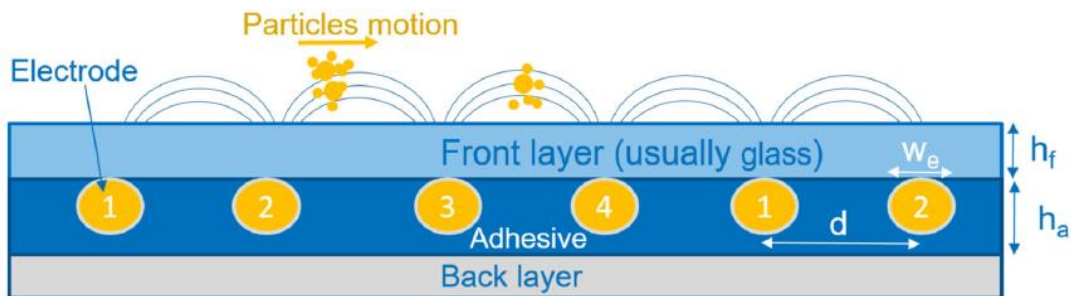


Figure 38: EDS cross-section scheme of an electrodynamic system (EDS) for dust cleaning using four wire electrodes to create the travelling wave [131].

Practically, the EDS charges dust particles, alternating the application of high voltages on several independent electrodes and creating a traveling wave that moves the particles on the surface. The electrodes can have various designs according to the final application (see Figure 39).

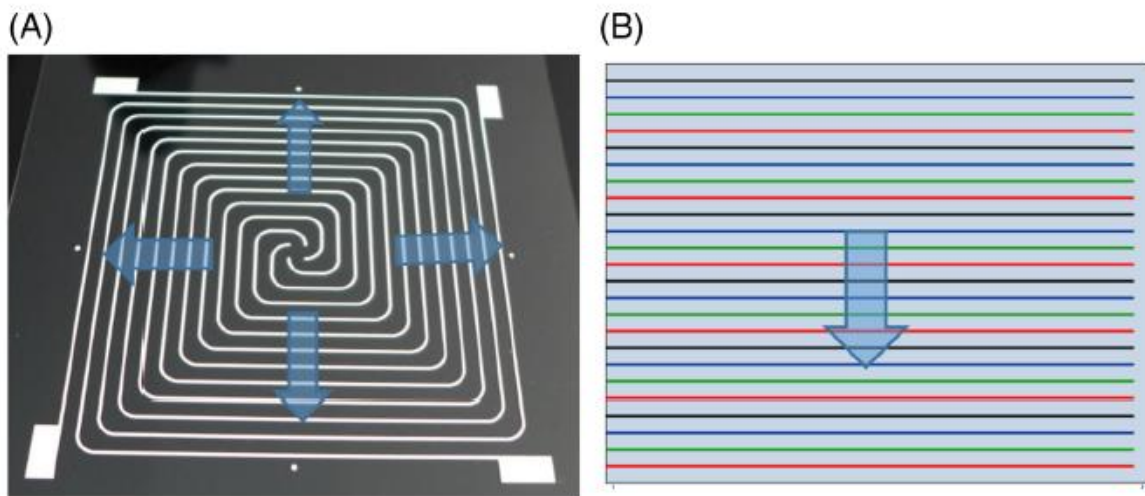


Figure 39: a) Picture of spiral electrode design. b) Scheme of wire electrode design. Arrows represent the particle motion directions [131].

The company CleanFizz SA tested a small pilot module in the King Abdullah University of Science and Technology (KAUST) in Thuwal, Saudi Arabia (see Figure 40). Built-in sensors measure luminosity, humidity, surface temperature, and other essential parameters. Their results indicate that the EDS removes more than 90% of accumulated dust within the first 20 seconds of each operation. Each cleaning consumes about seven Watts (about 3% the power of a standard PV panel). In the case of solar plants, a tracker could be used during the cleaning session in order to remove more dust more quickly.

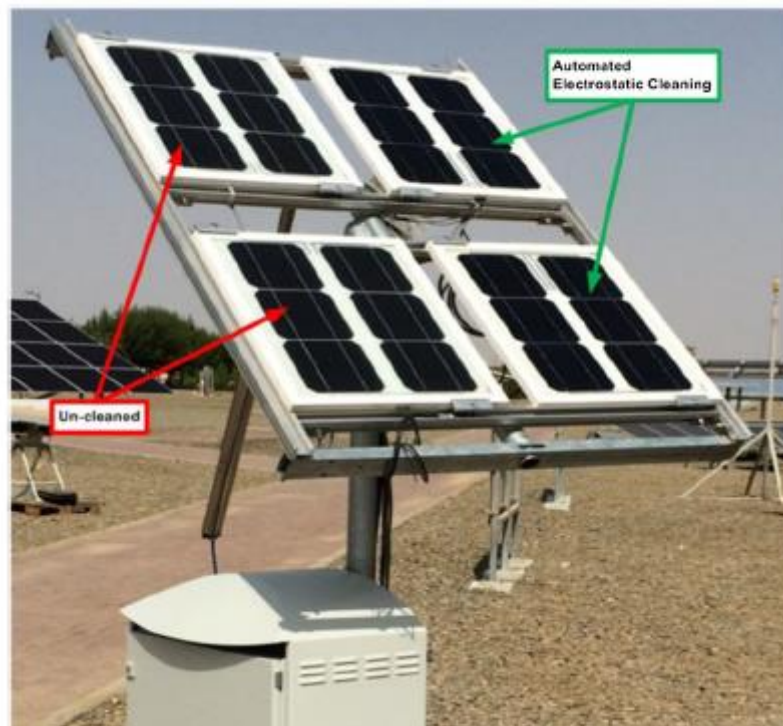


Figure 40: KAUST Pilot field test of the electrodynamic cleaning system from Cleanfizz at KAUST in Saudi Arabia [131].



According to their results, the EDS reduced power loss due to soiling by 36% when compared to an uncleaned reference module, while the energy consumption to operate the EDS is less than 0.1% of the produced energy; the cleaning sequence occurs six times per day, and for each sequence only 10% of the PV module's generated power is used, which is therefore equivalent to a total of about 20 seconds of generation loss per day. These first field results demonstrate the functionality of the electrodynamic approach and the negligible energy level required to power such functionality.

In these test field conditions; the EDS will cost \$10 to \$20 per 72-cell module, which is about 10% to 20% of the module cost [131].

6.2.3 Tracking Strategies: Single and Double Axis Tracking Systems

Nightly stow-away of modules that are mounted on single- or double axis trackers are an easily implemented solution to mitigate soiling. Since soiling largely depends on inclination angle, a nightly "parking position" is a practical approach. Case studies from the Atacama Desert show that tracking solutions could also account for local conditions, e.g., daily morning fog and wind from the Pacific.

Figure 41 shows the daily performance ratios on single and dual axis trackers during the dry winter months of 2017 in Pretoria, South Africa. The suspended particulate matter in the air during winter is caused by increased biomass burning for heat [132], so the likelihood of soiling losses increases. The 558 kWp single axis tracker system (two trackers) and the 200 kWp dual axis tracker system (17 trackers) sit adjacent to one another on the south side of the N4 highway within the campus of the Council for Scientific and Industrial Research (CSIR). Neither system was cleaned during the three-month dry season of 2017, during which no rain fell, so this time frame provides a reasonable dataset to compare soiling rates. The daily Performance Ratio on the dual-axis tracker decreased by 0.4% per week, while the Performance Ratio on the single axis tracker decreased by 1.2% per week in 2017. Soiling rates in 2019 measured in the range of 1.5% to 1.8% per week on the single axis tracker.



Figure 41: Daily performance ratio trends for single axis and dual-axis trackers during the 2017 dry season illustrates higher soiling rates on the single axis tracker.

The difference in soiling rates between the single and dual axis trackers may be explained by several mechanisms, and the analysis of happenstance data is insufficient to determine which



factor may be dominant. Wind may be lifting soil and dust one or two meters above ground resulting in greater soiling rates on the single axis tracker mounted closer to the ground (need reference). The modules on the single axis tracker come within 0.5 meters of the ground while the modules on the dual axis tracker come within three (3) meters of the ground. The orientation of the array during operation may be a more likely explanation, as tilt angle has a strong impact on soiling rates (need reference). During the winter months, the single axis tracker continues to follow the same daily path through horizontal at solar noon as it does during summer months. The dual axis tracker changes its path every day of the year, and the orientation at solar noon is near zero (0) degree tilt in summer months and near fifty (50) degree tilt in the winter months at solar noon. The dual axis tracker spends more time at steeper tilt angles during the winter months, so the effective area of the array is smaller compared to horizontal orientation and less dust and particulate matter will be deposited due to the force of gravity. The model is analogous to the cosine loss for current generation due to the angle of incidence between the direct beam sunlight and the plane of array. If the dual axis trackers could be stowed in a vertical position during night-time, the soiling rate may be reduced even further.

6.2.4 PV Module Cleaning Tests

More and more PV systems are installed in deserts with hot and dry climates. The loss of performance due to soiling can be in the order of 1% per day in some deserts [8]. This high yield loss must be reduced by regularly cleaning the PV modules. Only dry cleaning is economical, as natural cleaning with rainwater is not possible. During cleaning, small dust particles can cause scratches on the glass surface, which reduce the optical properties of the glass coating or the mechanical forces caused by cleaning can damage the cells inside the module.

The cleaning process involves a cleaning device, PV modules, the soiling and possibly water and cleaning agents. To qualify a cleaning process, an accelerated test should be performed with the planned components.

Except for simple manual cleaning with linear brushes, nearly all cleaning devices use rotating brushes. Some prototypes have also been developed using ultrasound and electrical forces or high-pressure air [133]. Typically, the brushes are manufactured with split bristles of polyamide (PA) or polyester (PE). The length of the brushes varies from 50 cm up to more than six m. The brush diameter can be up to 50 cm. For automatic systems, the cleaning time for one module takes about one to two seconds. Brushes with closed EVA foam or PE microfiber felt are also used to reduce scratches caused by dirt accumulated in the bristles.

Cleaning devices must be certified regarding accident prevention, electrical safety and electromagnetic compatibility (EMC). The evaluation of a cleaning device can be carried out with the machinery directive [134]. The test of the cleaning device should also include tests of power and water efficiency, the robustness of the machine in harsh environments (e.g., dust, sandstorms, high temperatures, strong wind) and a review of the functional datasheet (e.g., climbing slope, cleaning area, cleaning speed).

There is no international performance and functionality standard with pass/fail criteria for the cleaning of PV modules. However, test standards for the cleaning of cars, window glass or the abrasion resistance of paints or coatings could be applied. A practical test is the configuration simulation with the expected dust exposure, the intended module type and cleaning device, and the expected number of cycles.



Modules in temperate climates with rain must be regularly cleaned, because biofilms are difficult to remove, especially those caused by animals or industry. Cleaning should be done once or twice a year with water. To avoid residues on the glass after drying, rainwater or deionised water with or without cleaning agents must be used. The temperature of the water must be close to the module temperature to avoid thermal shocks. Shading of the modules can cause hot spots. For a reliable test, 50 cleaning cycles should be simulated.

In addition, the removal of cleaning resistant-dirt must be tested. The performance and the functionality of the cleaning device can be tested on an outdoor test field or in the laboratory. The analysis of a reference test plant with natural or artificial soiling is also useful. Standards describe artificial soiling for glass, with soiling, drying and UV exposure cycles [135], or for headlights [136]. Dry abrasives, such as Arizona test dust [137], quartz sand, and wet slurries consisting of Arizona test dust or quartz flour [138], are also used for abrasion tests.

Cleaning agents should be tested for ecological sustainability and functionality and the effect on PV modules. Analogous to salt mist corrosion testing, continuous and cyclic tests with wet and dry phases can be carried out.

In dry regions, access to suitable cleaning water is limited. But even in dry deserts, dew can form during the night, reacting with the dirt and the glass surface, which can lead to a cementation of the soiling. For this reason, some power plants carry out daily cleaning during the night. For an operating lifetime of 25 years, 10,000 cleaning cycles must be simulated. This high number of cleaning cycles is typical for fully automatic systems. Weekly or monthly cleaning, which often occurs when sensors measure that the soiling ratio is below approx. 95%, can be performed with other types of cleaning: manual, truck-mounted or semi-automatic systems. The effectiveness and the destructive effect of a cleaning device should be tested, taking into account the soiling conditions and the cleaning frequency specific to a particular PV plant.

In addition, the evaluation of reference plants can show failures of solar cells caused by mechanical stress or partial shading (hot spots). Also, effects of the frame and clamps can be determined.

The draft standard for PV abrasion IEC 62788-7-3 [139] defines procedures for erosion and abrasion tests. The tests are designed to test small glass samples with standardized brushes smaller than those used for PV module cleaning. The apparatus includes a linear abrasion mechanism and an abrasive dispenser (slurry or dry abrasive). An enclosure is recommended for the apparatus to prevent spilling or spraying of dry or wet slurry abrasives, and to prevent the possibility of silicosis (with ventilation, for dry abrasives). The test methods are intended to imitate damage mechanisms that may occur during the cleaning of photovoltaic modules.

Two cleaning tests are described, one with a waving brush and one with a rotating brush. A linear abrasion apparatus fulfilling the requirements of the wall paint test standards ASTM D2486 [140] or DIN 53778-2 [141] were used. The brush block was 3.5 cm x 8.5 cm in area. The brush bristles consisted of Nylon 6.12, 0.23 mm in diameter that extend 3.8 cm from the brush block (Figure 42). In Figure 43, the results for three glass types are shown.

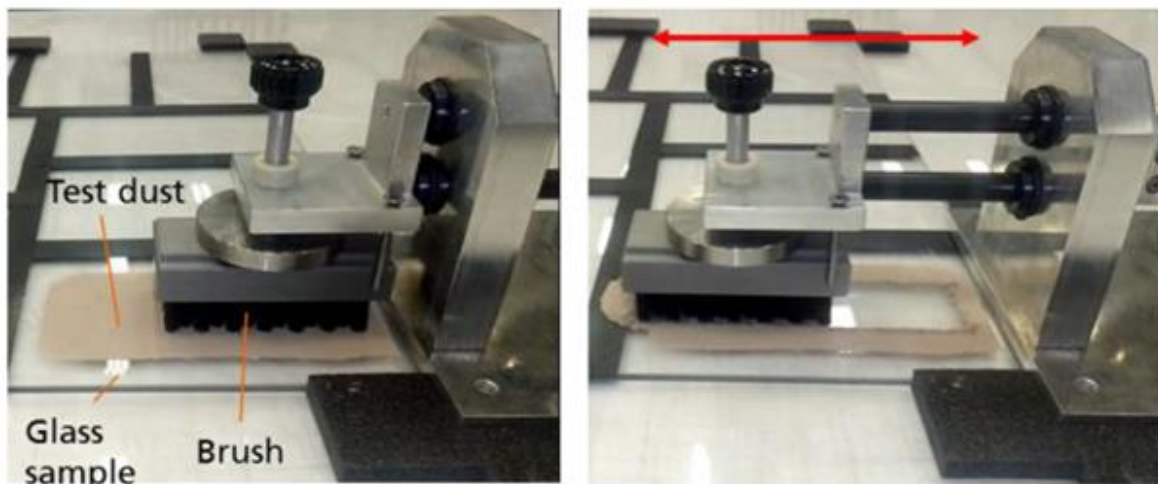


Figure 42: Set-up of linear abrasion test with a brush according to ASTM D2486 [142].

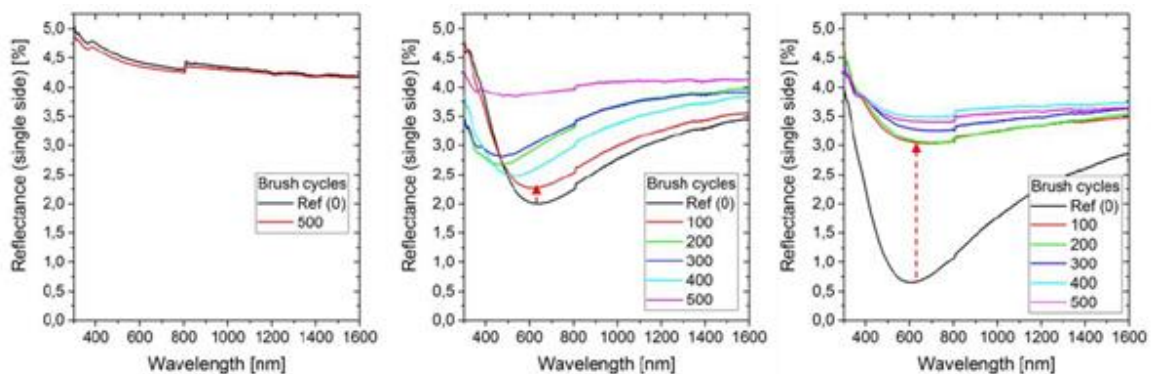


Figure 43: Spectral reflectance of 3 glass types: a) float glass without ARC, b) float glass with ARC and c) structured glass with ARC - after up to 500 linear abrasion test cycles with a brush according to ASTM D2486 [142].

For the rotary abrasion test, an apparatus similar (but smaller in scale) to ISO 20566 [138] was used. The brush block was a round cylinder at least 3.5 cm in length and 2.4 cm in diameter. The brush bristles consisted of Nylon 6.12, 0.23 mm in diameter that extend 3.8 cm from the brush block. The bristle profile was round, with no taper or other change in geometry along the length. Under the brush, the test panel holder with the test sample was moved in both directions depending on the rotation of the brush. The spray jet struck the brush directly.

IEC 62788-7-3 can mainly be used for the evaluation of glass coatings. For the evaluation of PV cleaning devices, set-ups with one to three PV modules and the original brush with the typical operating parameter (e.g., speed, rotation and pressure) were used.

A typical test procedure of cleaning sustainability of PV modules is

- Preconditioning (Soft cleaning, light soaking)
- Initial measurement (visual inspection, Pmpp, electroluminescence)
- Special measurement (reflectance)
- Testing (accelerated cleaning)
- Final measurement (visual inspection, Pmpp, electroluminescence)



- Special measurement (reflectance)

Ferretti compared two cleaning devices [143], a manually driven cleaning device working with water and a cleaning test set up with a rotating dry microfiber felt. Eight modules with anti-reflection coatings were tested. Several module types showed strong deviations in reflection after the cleaning, indicating removal of the ARC. Reflectance measurements after cleaning with a nylon brush after spreading of fine and coarse sand [144] showed less abrasion than with the TABER abraser [145] in dry conditions.

A proposed pass/fail criterion for PV module cleaning tests, especially for glass coatings, is a maximum gain in reflectance of 30% [146]. This criterion can be used for PV modules and glass sheets with a light trap on the back side. It is much harder than the most common pass/fail criterion for testing PV modules with a maximum power loss of 5%. For standard glass with 4% reflectance, this means a power loss of 1.2%. For ARC glass it is even harder. The hemispherical reflectance can be measured in the laboratory with an integrating sphere. Measurements in the field are possible with a small hand-held spectrometer. The repeatability of the measurement must also be taken into account.

Tests with full-size structured glass sheets without and with ARC were carried out without abrasive. After 10,000 cycles and an enlargement of the brush pressure with additional weights on the brush, no abrasion effect was measured for glass without ARC, but a significant effect for coated glass was detected (see Figure 44). The abrasive force due to cleaning is parallel to the glass surface. In comparison with sand abrasion tests with abrasive forces normal to the surface, the effect on the uncoated glass is minor [147].

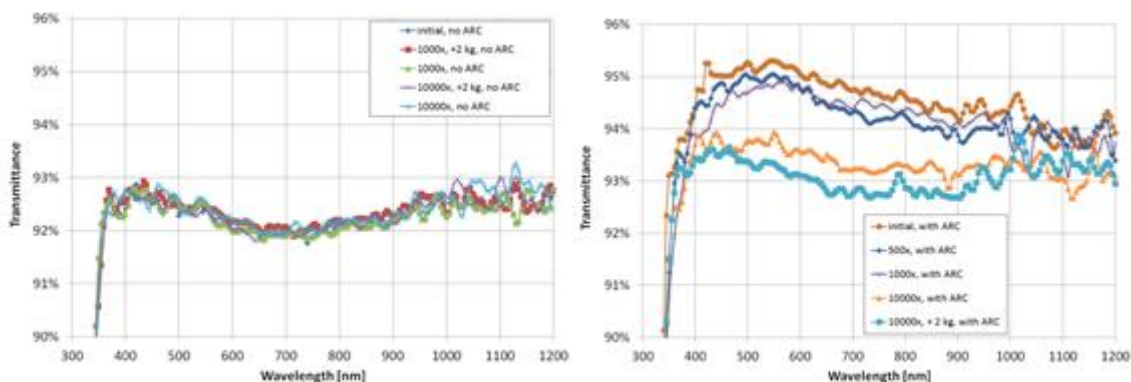


Figure 44: a) Structured glass without ARC b) Structured glass with ARC: Spectral transmittance of structured glass without and with ARC after cleaning test with up to 10000 cycles and optionally with additional 2 kg weight. No effect was measured for glass without ARC. A significant effect was measured for glass with ARC.

Ferretti et al. [146] tested ARC coated glass sheets with a focus on the ARC abrasion and scratches on the glass surface. To simulate sandstorms every three days and 25 years of operation, 3,100 cleaning cycles were performed. For the soiling, fine (0.18 mm diameter) and coarse sand (0.38 mm diameter) has been spread on the glass sheets with a 60% glass coverage. Structured and float glasses with different coatings were tested under the same conditions. For checking the impact of different brushes, two types of brushes have been used for the cleaning, one made of polyester and the other one of nylon. Reflectance measurements and visual inspections were carried out every 500 cleaning cycles. For both brushes a continuous increase in reflectance with an increasing number of cycles could be observed, indicating



that the ARC had been removed. For the nylon brushes, the increase in reflectance was higher. The results showed that fine sand had a higher abrasive effect than coarse sand.

Dusts of different regions and materials were investigated for soiling and cleaning abrasion [50]. The abrasive effect of test dusts (diameter = 20 μm) mainly consisting of corundum was stronger than of quartz as Arizona test dust and calcite.

A new standard (DINspec4867 [148]) is under development for testing with full-size brushes and original tempered module glass sheets. It is based on ISO 20566, which is for testing the scratch resistance of coatings for cars (see Figure 45).



Figure 45: Laboratory car wash for testing the scratch resistance of coatings in accordance to ISO 20566 [149].

6.3 Generic “Best-Time-to-Clean” Models

As stated above, soiling has a daily and seasonal variability and a dependence on local conditions. All these factors have a significant impact on the short-term soiling losses, which makes these more difficult to predict than the average annual losses [87].

Monitoring the degree and duration of soiling is important from an O&M perspective. In addition to maintenance, knowing the best time to clean the modules will help maximise economic viability. This cleaning time is informed by the rate and degree of soiling on the module, as well as the economic implications of cleaning the modules. To determine the best time to clean, either quality real time data or a good soiling model are needed to predict future soiling.



There are a range of approaches to the modelling and prediction of the soiling rates, as we discussed in Chapter 4.1. One is to use the average monthly soiling rate to calculate the daily soiling rate [63]. The cumulative soiling can be calculated by summing the daily soiling rate for each day at the site without any rain. When there is more than 1mm of rain per day, the soiling level can be reset to zero [63]. This approach can use a small amount of soiling data and historical rainfall data at the site to predict future soiling levels. Other approaches use artificial neural networks to calculate soiling based on a range of environmental conditions [1]. This is computationally more complex but does allow more accurate predictions of soiling rates between individual cleaning events based on local environmental factors. An example of the cumulative cleanliness index determined from this approach is shown in Figure 46.

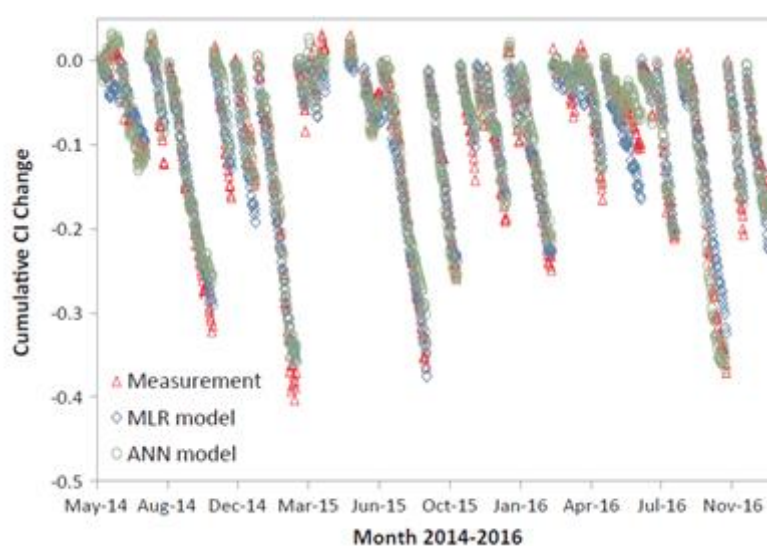


Figure 46: Cumulative cleanliness index as predicted by advanced neural networks [1].

There are also a range of approaches for cleaning frequency optimization. In areas of light to moderate soiling, heavy rainfall is considered effective at removing soiling and restores the modules power output [64], thus making it unnecessary to regularly clean. Where the power output of the modules drops below a desired output due to the long-term build-up of hard to remove soiling, then cleaning becomes necessary [64]. The cleaning can be done manually [150] and is conventionally done with water, which can be quite an expensive and time consuming process [64]. Other cleaning solutions use automated systems to remove soiling which have a high capital cost. The determination as to whether cleaning is cost effective will depend on the soiling rates, electricity prices and labour costs of the location. There are reports that in some regions of mid to north Europe that cleaning PV modules is not cost effective due to lower soiling rates and high rainfall [151]. While in regions in southern Europe it makes economic sense to clean the modules [151]. Other studies suggest a simple and regular weekly cleaning cycle as good practice [103].

As the recommended time to clean will vary based on many factors at the site location it can be a significant challenge to determine the best time to clean, yet it is an important factor in minimising economic losses. The best time to clean, or cleaning interval, is reliant on the power output of the plant, electricity tariffs, soiling rates and cost of cleaning [56]. Determining the best time to clean is done by balancing the total cost of cleaning against the cost of energy lost



to soiling. Jones, Baras et al. (2016) have developed a detailed model for determining the optimum cleaning interval (t_c) for a system based on the following parameters:

- Cost of cleaning operation at the start of the interval (C_c)
- The value of the energy lost due to soiling over the interval between cleans (V_L)
- The value of energy sold over the interval (V_S)
- The power loss due to soiling ($L_s(t)$)
- The power generated by the plant without soiling ($P(t)$)
- Electricity Tariffs ($R(t)$)

Jones, Baras et al. [56] have derived a solution for this:

$$\frac{V_L + C_c}{V_S} = \frac{L_s(t_c)}{1 - L_s(t_c)} \quad (16)$$

Where:

- $L_s(t) = 1 - e^{(-at)}$ and
- a is the average loss coefficient per hour for all months.

This average value is used in other modelling approaches as well [63]. However, different environmental conditions may have an impact [56]. A better approach may be to use seasonally variable soiling rates from real time data or modelled data [1]. This may yield more accurate results. Example outputs from the model developed by Jones [56] are shown in Figure 47. The optimal cleaning interval varies throughout the year, with a longer interval recommended in the middle of the year for this particular site.

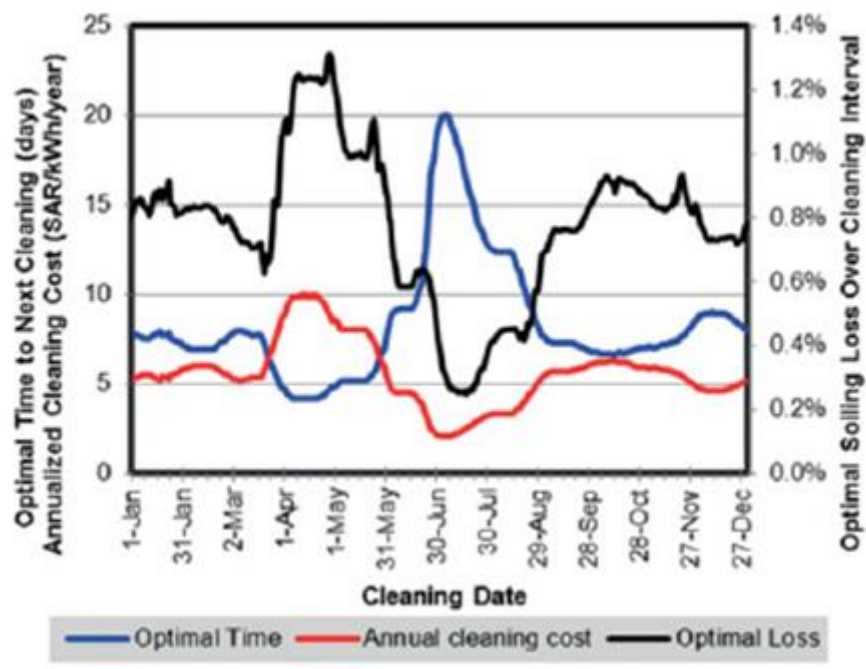


Figure 47: Example calculations of the optimal cleaning interval over the course of the year. Source: [56].

The model developed by Jones [56] can be used to determine the optimal time to clean based on several economic factors. To use these models, it is recommended to collect real time soiling data. This can be collected for the site and used to determine monthly averages, which the model [56] can use to calculate the best time to clean. This approach should be an accurate way of optimising the cleaning interval, however there are some general guidelines for cleaning in different climates proposed by Mani [103], as shown in Table 9, which can also inform O&M decisions.

Table 9: General recommendations for cleaning in different climates, reproduced from [103].

Climatic zone and characteristics	Conditions influencing PV performance and dust deposition	Recommended cleaning cycle to mitigate impact of dust
Group-I: Low latitudes – comprise mainly the wet, wet–dry and the dry tropical climate		
Wet tropical Average temperature: 20–34°C Annual precipitation: >250cm Latitude range: 108S to 258N	Low latitudes require low tilt in PV systems for maximum solar gain, but lower tilts will tend to accumulate higher dust deposition. Tilts higher than latitude recommended to reduce dust accumulation. High annual precipitation could minimize dust accumulation	High annual precipitation could reduce dust accumulation (by periodic washing). Weekly cleaning recommended during dry spells and may be altered based on intensity of dust accumulation



<p>Wet–dry tropical Temperature range: 20–30°C Annual precipitation: >150cm Latitude range: 158 to 258 N and S</p>	<p>Trade winds dominate during the dry season; blow from the north-east in the northern hemisphere and vice-versa PV systems with higher tilt recommended PV panels to be oriented to benefit from the cleaning effect of prevalent wind</p>	<p>Weekly cleaning recommend for moderate dust accumulation; daily cleaning recommended in case of intense dust accumulation</p>
<p>Dry tropical Temperature range: 20–49°C Annual precipitation: 15cm Latitude range: 158 to 258 N and S</p>	<p>Regions prone to dusty desert environments and frequent dust storms (for any PV configuration) Low humidity and rainfall Availability of intense solar radiation – PV system may be optimized to maximize harnessing solar energy</p>	<p>Cleaning to respond to intensity of dust accumulation–minimum weekly cleaning recommended Immediate cleaning subsequent to dust storms Adoption/application of dust-repelling coatings may be looked into</p>

Group–II: Mid-latitude climate – comprise mainly the steppe, the Mediterranean, the grasslands and the moist continental climate

<p>Steppe climate Temperature range: -4 to 40°C Annual precipitation: less than 10cm in dry regions to 50cm in moist steppes Latitude range: 358 to 558 N</p>	<p>High latitudes require high tilt in PV system; a lower fixed tilt angle is recommended to optimize year-round solar gain Dust generally tends to fall off with the increase in the tilt angle</p>	<p>With an arid climate with little rains and high tilt angle a moderate cleaning cycle (weekly) could be adequate With lower tilt angle (to maximize solar gain) a more frequent cleaning cycle (depending on dust intensity) might be beneficial.</p>
<p>Mediterranean climate Temperature range: 10 – 40°C Annual precipitation: 42cm Latitude range: 308 to 508 N and S</p>	<p>High latitudes require high tilt in PV system; a lower fixed tilt angle is recommended to optimize year-round solar gain Dust generally tends to fall off with the increase in the tilt angle</p>	<p>Cleaning is recommended once in a week or 2 weeks depending upon the rate of dust accumulation on the surface. Regions with higher dust accumulation (proximity to industries) a daily cleaning may be beneficial.</p>
<p>Grassland climate Temperature range: -4 to 22°C Annual precipitation: 81cm Latitude range: 308 to 558 N and S</p>	<p>High latitudes require high tilt in PV system; a lower fixed tilt angle is recommended to optimize year-round solar gain Dust generally tends to fall off with the increase in the tilt angle Higher precipitation would aid in cleaning the PV panels</p>	<p>A less intense (weekly or bi-weekly) cleaning cycle might be adequate Regions prone to higher dust (due to human activities) might require weekly cleaning</p>



Group–III: High latitude climate – comprises mainly the taiga and the tundra type of climate

<p>Taiga climate</p> <p>Temperature range: -22 to 16°C</p> <p>Average annual precipitation: 31cm</p> <p>Latitude range: 508 to 708 N and S</p>	<p>High latitudes (close to vertical) require high tilt in PV system; sun tracking mechanism may be required to effectively harness solar energy</p> <p>Lower ambient temperature improves PV performance</p> <p>Dust generally tends to fall off at near-vertical tilt angle. Dust is a less critical factor in comparison to maximizing solar gain</p>	<p>Weekly cleaning cycle should be adequate</p> <p>Clearing of snow accumulation needs to be addressed immediately (more frequently)</p>
<p>Tundra climate</p> <p>Temperature range: -22 to 6°C</p> <p>Average annual precipitation: 20cm</p> <p>Latitude range: 608 to 758 N</p>	<p>High latitudes (close to vertical) require high tilt in PV system; sun tracking mechanism may be required to effectively harness solar energy</p> <p>Dust generally tends to fall off at near-vertical tilt angle</p> <p>Lower ambient temperature improves PV performance. Susceptibility to fine-dust collection</p>	<p>Weekly cleaning is recommended, and adjusted based on type (fine/coarse) of dust accumulation</p> <p>Clearing of snow accumulation needs to be addressed immediately (more frequently)</p>

6.4 Snow Impact Mitigation Strategies

Improving array performance during the winter months also requires snow removal. While passive snow shedding from a module surface is a complex process consisting of sliding, melting, and removal by wind, sliding generally occurs best at tilt angles of at least 45°. For sites experiencing heavy snowfall, angles of 60° or more are recommended. Snow shedding is also dependent on racking configuration. The several centimetres of space between adjacent modules along the top and sides can hinder sliding. The distance between the bottom edge of a module and the ground is also important.

Providing a clearance of at least a meter between the array and ground gives space for snow to pile. In cases with inadequate clearance, such as roof-mounted modules, snow will build up at the bottom of the module frame. Similarly, the discontinuity of a frame protruding a few millimetres above the cover glass can provide a foothold for snow and ice. The greater the weight of snow above the bottom of the frame relative to the frame length, the less likely an accumulation along the bottom edge will be able to support the weight of snow above it. For this reason, it is suspected that mounting modules with their shorter dimension parallel to the ground (portrait rather than landscape configuration) will encourage snow shedding. Similarly, larger modules will shed better than smaller ones. Using frameless modules is, of course, ideal for snowy sites.



Other methods of snow removal include manual cleaning, which may be possible if there are regular site visits. However, manual cleaning is time consuming, may not provide much additional energy gain, and may damage modules. Passive melting technologies, such as ice-phobic coatings or nano-textured glass, are under investigation to test their durability and operation under different conditions. Active melting technologies such as reversing the current flow through the array are also available. Field comparisons of different removal techniques are needed to quantify the benefits of different approaches.

Lastly, the electrical interconnection of modules can also affect energy losses. For example, as shown in Figure 48, a typical 72 cell module has three bypass diodes organized into sub-strings consisting of 24 cells. Since snow sheds from top to bottom, it may be advantageous to place modules in landscape rather than portrait orientation so that some bypass diode cell strings can be completely uncovered even if snow remains on the surface.

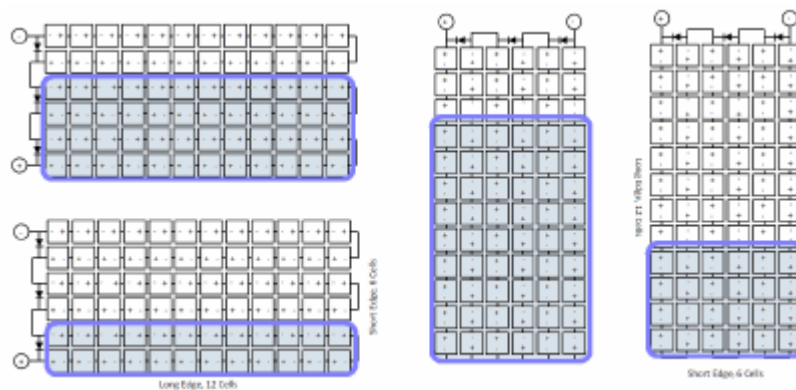


Figure 48: Electrical diagram of 72 cell module with bypass diodes, and example of progressive snow shedding in landscape and portrait orientations (snow layer movement down the module surface shown in blue). Snow shedding in landscape orientation can completely uncover bypass diode strings even with the module is still partially covered in snow.

However, although the landscape orientation may allow more uniform exposure of bypass diode strings, it will likely also hinder snow shedding compared to a portrait orientation due to greater build-up along the bottom frame. For series-connected modules, in the rare case that the junction box does not contain a built-in bypass diode, modules should be series-connected in groups of horizontal rows rather than vertical columns. Lastly, if a tracking system is used, modules can be stowed in the vertical position overnight to encourage shedding. Some operators may turn off their trackers during the winter months, when insolation is low, thus reducing reliability issues and power consumption by fixing the array at vertical tilt facing due south in the northern hemisphere or due north in the southern hemisphere. A tracking system adds additional complexity for remote locations and may not perform as well in cold climates due to motor malfunction or obstruction of the sun-tracking sensor by snow. See Chapter 7 for more details.



7 SNOW SHADING OF PHOTOVOLTAIC SYSTEMS

7.1 Introduction

Commensurate with the precipitous drop in the cost of installed photovoltaic (PV) systems and favourable economic projections relative to fossil fuels, solar systems are proliferating across northern regions, where minimal irradiance and persistent snowfall in winter have traditionally inhibited solar deployment. Accompanying such growth, however, is the increasing recognition that, although PVs can perform well and be economical in colder climates, snow adhesion to the module surface, also known as snow shading, causes significant energy losses.

The problem is widespread: snow occurs across most of the northern hemisphere and also at high elevations in both hemispheres and can persist on solar panels for days to weeks, depending on prevailing climatic conditions and also on the design of the PV array. While more data are needed to quantify losses regionally and globally, snow shading is clearly detrimental to PV performance, decreasing energy output and increasing the levelized-cost-of-energy. Monthly energy losses, which translate into revenue losses, can be as high as 100%, and yearly measured losses, under extreme conditions, can reach 34%, although average annual losses worldwide are estimated to be on the order of 10% or less [152], [99], [153], [154], [155], [100].

At the same time, PV growth in northern regions is expected to continue at a high rate.⁴ Germany, for example, added 2.72 GW of solar in the first eight months of 2019 and has a goal of 98 GW total installed capacity by 2030. Norway commissioned 23.5 MW of solar in 2018, a 29% increase over the previous year⁵. Sweden and Finland, where solar is viewed as a competitive cost system, have also seen increased growth. Sweden now has an estimated 200 MW of solar, mainly north of Stockholm [156]. In the US, four of the top ten states for solar growth are located above 40°N, and more than 7 MW of solar has been installed to date in Alaska at latitudes above 66°N. Canada has seen a 182-fold increase in solar capacity in just 13 years. Russia commissioned 75 MW of solar in 2019 in its Far East region, at an approximate latitude of 54°N [157]. Other areas that consistently see snow in winter and are also accelerating PV deployment include Japan, China, and the Czech Republic. This anticipated growth has put pressure on the solar industry to reduce snow shading and increase solar performance in winter.

To support those objectives, research is needed in five primary areas related to snow soiling and PV performance: energy losses, performance modelling, system and component reliability, design optimization, and O&M best practices (Figure 51). In addition, this chapter provides an overview of the underlying factors that influence snow shading and identifies opportunities for minimizing snow losses from PV systems at northern latitudes. Not covered in this chapter is the topic of storage, which can help support better load management in regions that have dramatic annual shifts in irradiance. Rooftop PVs are also not extensively covered in this chapter, neither residential nor commercial, largely because 1) many of the same principles that apply to utility-scale installations are applicable at other scales and 2) the economic drivers are very different.

⁴ Growth projections have been revised as a result of the COVID-19 pandemic, which is estimated to reduce the growth of global solar by 17% in 2020, with a rebound expected thereafter. [Wood Mackenzie]

⁵ pic.twitter.com/dC3YE8PfuJ, Berentsen, SolarPowerEurope (June 2022)

⁶ Reference: http://acep.uaf.edu/media/293024/2020-Net-Metering-Update_20200309Final.pdf (June 2022)



7.2 Performance Factors for PV Systems at High Latitudes

The operating conditions in higher latitude regions of the world are harsh and unpredictable: precipitation may range from freezing rain to heavy snow; temperatures may reach lows in the vicinity of -40°C and see dramatic swings; snow depths may reach a meter or more and high irradiance events can occur. To understand the capacity for PV growth in areas that regularly see snow, it is first necessary to understand the availability of solar resources as well as the climatic conditions that detract from – and contribute to – a PV system's operating efficiency.

A. Solar Resource Availability

Energy generation from PV systems in cold climates introduces both challenges and benefits. On one hand, the contributions of low temperature and albedo on an array's performance ratio during the winter season boost performance; on the other, the sun's higher angle-of-incidence, which is determined by the tilt of the earth's axis relative to the sun, and the lower irradiance intensity received by a PV system, result in losses relative to standard test conditions (STC). With greater angles-of-incidence, less light is coupled onto the cells. For most crystalline silicon modules, however, angle-of-incidence losses remain negligible until a threshold of approximately 60° is reached. On the winter solstice in Fairbanks, Alaska (64.8°N), for example, the sun rises only about 2 degrees above the horizon, providing less than four hours of dim light. In contrast, the sun's elevation at the summer solstice peaks at close to 49 degrees above the horizon, providing more than 19 hours of daylight. Northern latitudes also see a large range in the solar azimuth (the sun rises in the northeast in the summer and in the southeast in the winter), and the average annual insolation may therefore approximate, or even exceed, annual insolation at lower latitudes.

High latitude sites often experience prolonged periods of weak sunlight during the winter, whereas high altitude sites often have high irradiance levels throughout the season, although PV installations at high altitudes are relatively uncommon. For irradiance below around 200 W/m^2 , as is typical for an average of nine months a year in Fairbanks [158], the linear relationship between power output and irradiance breaks down and there may be a slight reduction in performance relative to standard test conditions. Such reductions are technology dependent, but one study has shown larger losses for thin-film CdTe and CIS modules relative to crystalline silicon due to lower shunt resistance [5]. Nevertheless, the combined winter reductions due to angle of incidence and low light are generally only 3% or 4% of annual energy production because summer insolation is so much higher.

The large range in azimuth has sparked interest in dual-axis trackers populated with bifacial modules in northern climates [159]. However, with fixed installations not all the direct insolation can be utilized, since the sun at times can be behind the modules.

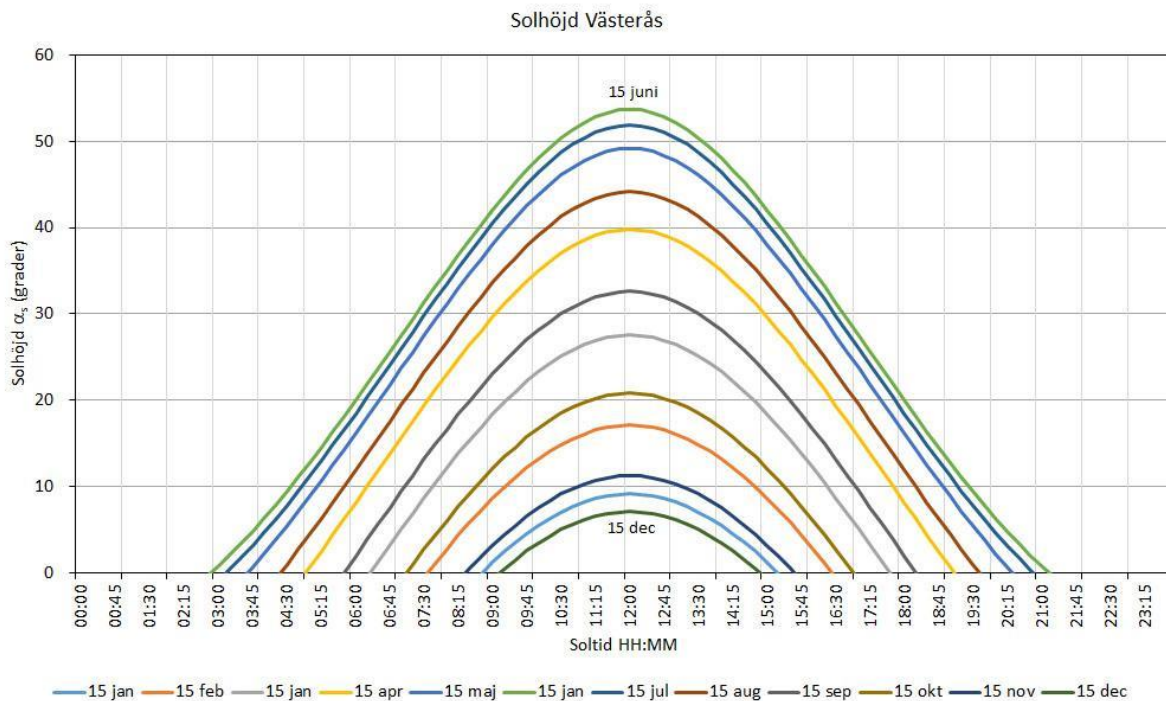


Figure 49: Seasonal variation in solar elevation in Sweden shows the sun never rises above 10 degrees and for only six hours in mid-December; in contrast, in mid-June the sun reaches an elevation of almost 55 degrees and remains above the horizon for about 18 hours. This difference becomes even more extreme at higher latitudes (Note axis labels are in Swedish).

B. Ambient Temperature

While irradiance is the dominant determinant of solar performance, temperature is also an important variable. Conversion efficiencies increase linearly as cell temperatures decrease. As a result, PV systems at high latitudes, where year-round operating temperatures are relatively cool compared with lower latitudes, can perform relatively well on an annual basis. Crystalline-silicon (c-Si) cells, for example, show a linear response of roughly a 0.34%-0.38% increase in efficiency per decrease in degree C and are most efficient on high-irradiance, below-freezing days [SINGH16], but will still perform better on a relatively cool summer day, in Sweden than on a sweltering hot day in Cairo, for example. The temperature coefficients for cadmium telluride (CdTe) and copper indium selenide (CIS) cells are slightly less than for C-Si: 0.32%/°C in the range of 25-75°C and 0.33%, respectively, as stated by the largest manufacturers of these thin-film technologies^{7,8}.

C. Albedo

The presence of persistent snow cover for several months each year also contributes to the efficiency of PV systems at northern latitudes. White substrates, which are highly reflective, can produce albedos approaching unity, and can therefore boost the performance of both mono- and bifacial PV systems, but have the greatest impact on bifacial PV. However, since

⁷ <http://www.firstsolar.com/>

⁸ <http://www.solar-frontier.com/>



snow is refreshed with each winter storm, it can out-perform other white substrates because any soiling from airborne particulates is masked by the new snow.

Both snow depth (typically accumulative) and the snow's crystalline structure (which changes with temperature and age) contribute to its reflectivity, which influences how much reflected radiation hits the front and back sides of an array, with the latter being the primary driver of bifacial gains. The in-plane insolation shows a strong dependence on tilt angles, and is quite low at moderate angles, as shown in Figure 50, for example.

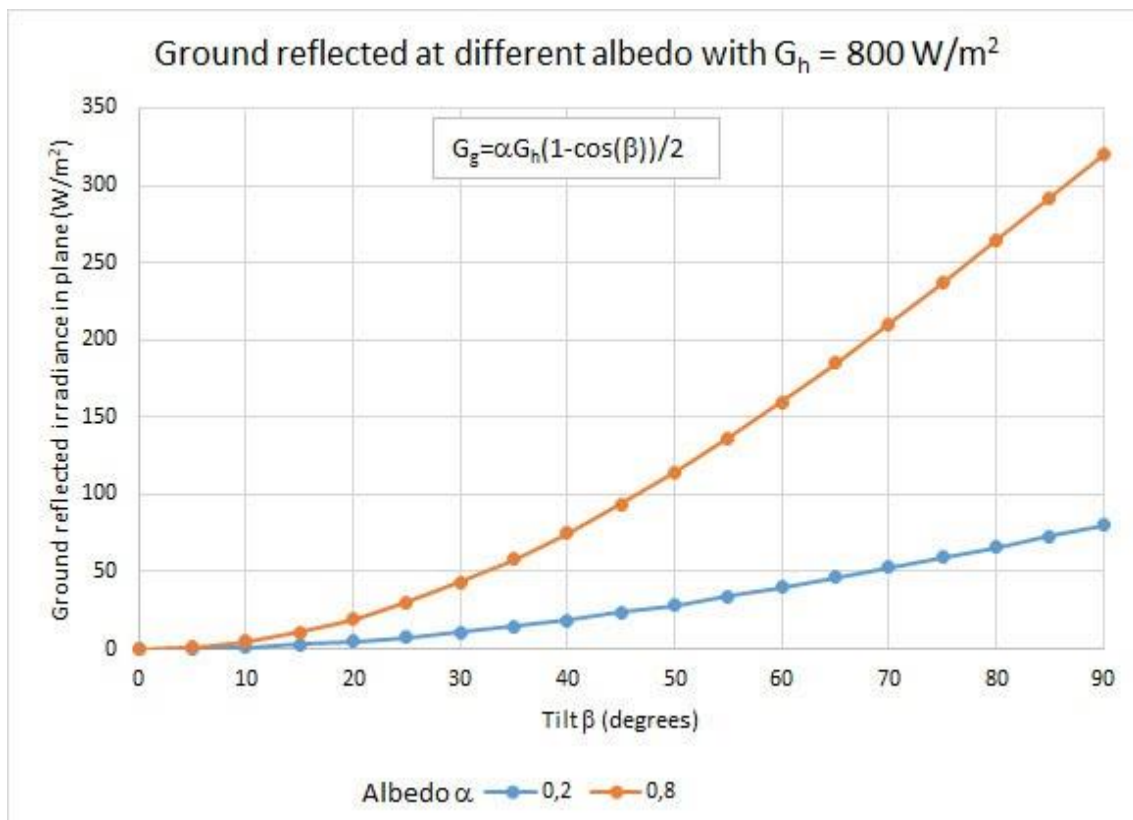


Figure 50: Ground reflected irradiance – calculated as function of module tilt angle (β) and different albedo (α) at horizontal irradiance (G_h) of 800 W/m^2 , using formula $G_g = \alpha G_h (1 - \cos(\beta)) / 2$.

7.3 Global Distribution of Snow

To correlate snow cover in different regions of the world with PV output, one can determine the number of days with snow cover and snow depth per day for each region of interest. Maps of snow cover are produced by different meteorological institutes in the world for different time periods with daily and average yearly statistics.

In Europe, at latitudes less than 60°N , snow cover persists for durations of up to 160 days per year in mountainous regions such as the Pyrenees, across the Alps of Switzerland, and in the Carpathian range in Eastern Europe. In contrast, Great Britain, France, and Spain are largely snow-free year-round.



In the Nordic countries of Norway, Sweden and Finland, the number of snow days per year varies from around 60 days to more than 200 days at latitudes 60°N and higher. In particular, Sweden has a marked distribution from south to north. Measures of daily snow depth (snow cover >1 cm) during the winter can be found on the Swedish Meteorological and Hydrological Institute (SMHI) website⁹, which shows a range in average maximum snow depth of 0.4 to 1.3m, depending on latitude.

According to the World Meteorological Organization (WMO), the average number of days per year with snow in Sweden varied from 25 days in the south to more than 225 days in the northern mountains for the period of 1961-1990, a ninefold difference for a small country that runs 1,574km in length. The number of snow days in Norway, neighbour to Sweden, is generally higher. This increase can be attributed to more extensive mountainous areas, where the altitude lowers the average annual temperature range, as well as to the higher precipitation from low-pressure systems entering from the Atlantic Ocean. The differences in snow days within Sweden and among the Nordic countries suggest that quantifying snow losses from PV systems must be region-specific, as would the economic calculations of any snow-mitigation strategy.

But another trend has emerged from Scandinavia that cannot be overlooked as a contributor to PV performance: global climate change. In both Sweden and Norway, the number of days with snow cover has decreased in recent decades^{10 11}, a trend that is especially noticeable in the southern half of Sweden. The relative variation in snow days between different winters is also greater in the south than in the north. This variation was especially noticeable in the warm winter of 2019-2020, when large parts of southern Sweden experienced unusual conditions with few days of snow cover. The trend to fewer snow days suggests snow losses will further diminish as the climate warms but also suggests that snow as a contributor to the performance of bifacial PV may be over-estimated in regions that traditionally have had more persistent snow.

⁹ <https://www.smhi.se/>

¹⁰ SMHI. Klimatindikator – antal dagar med snötäcke. Updated 3 July 2019. Available: <https://www.smhi.se/klimat/klimatet-da-och-nu/klimatindikatorer/klimatindikator-antal-dagar-med-snotacke-1.91081>. [Last accessed 20-Apr-2020].

¹¹ MOSJ. Environmental monitoring of Svalbard and Jan Mayen. Duration of snow cover on land. Available: <http://www.mosj.no/en/climate/land/duration-snow-cover.html>. [Last accessed 20-Apr-2020].



7.4 Focus Areas for Snow Research

To further the growth of solar in regions that see persistent snow in winter, research is needed in four primary areas, as illustrated in Figure 51.

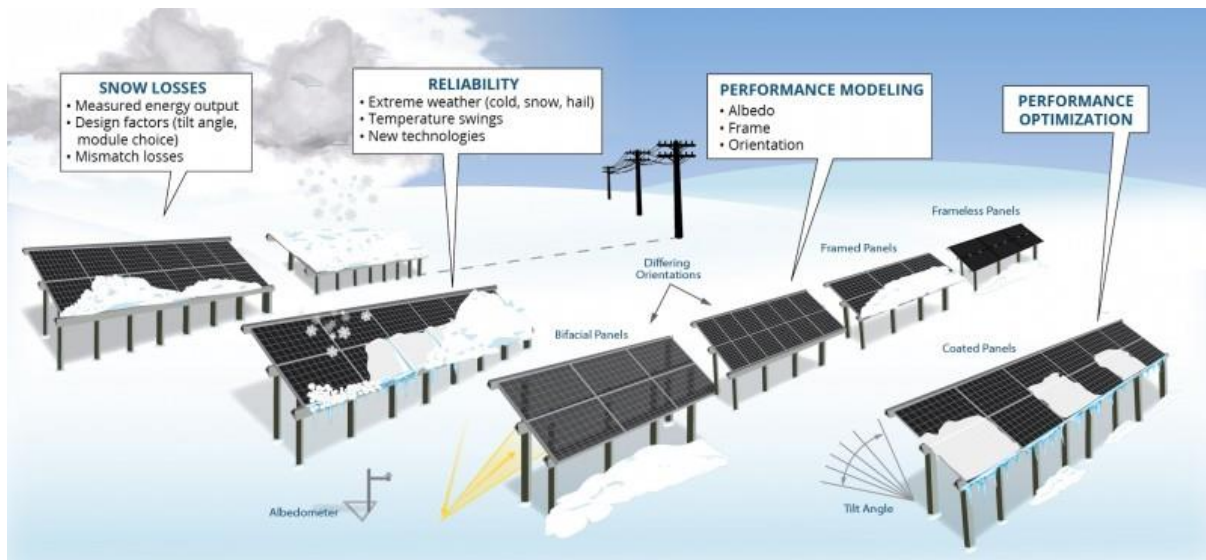


Figure 51: Research challenges related to snow. Operational issues related to snow include energy loss, reliability, performance modelling and performance optimization¹².

1. *Snow-Loss Metrics*: Estimates of monthly and annual energy losses attributed to snow are based on relatively small datasets and lack the metadata needed to develop mitigation strategies. A concerted effort is needed to quantify snow losses not only regionally and globally, but to correlate those losses with technological and design choices.
2. *Reliability*: Snow and ice adhesion to a PV array creates thermo-mechanical load stress, exacerbated by extreme winter storms and freeze/thaw cycles that can crack solar cells, distort module frames, and damage coatings, resulting in under-performing and failed modules. Data on thermo-mechanical loading and associated reliability issues, linked to specific module and system designs, are needed.
3. *Predictive Modelling*: Snow shading of modules creates significant energy losses but such losses in the absence of more detailed performance models are hard to quantify and almost impossible to predict, making accurate LCOE calculations and advance resource planning challenging for developers, investors and asset owners. Although forecasts can be made one to two weeks in advance, attempts to predict snowfall that far in advance have a high rate of error. More accurate models that take into account snow shedding variables such as module architecture are needed.
4. *Design Optimization*: Designing systems that shed snow quickly is of great value to the industry. A PV system's design can impact snow losses, underscoring the need to better quantify the energy implications of technological choices in snowy regions. Demonstration projects that can quantify the energy advantages (i.e., snow-shedding capabilities) of certain designs are needed.

¹² <https://energy.sandia.gov/Snow>



5. *Best O&M practices*: See Report IEA-PVPS T13-25:2022 “Guidelines for Operation and Maintenance of Photovoltaic Power Plants in Different Climates“, which covers O&M for residential, commercial and industrial installations at northern latitudes.

7.5 Snow-Loss Metrics

7.5.1 Methods for Measuring Snow

Snow that adheres to the surface of a PV module, like other forms of soiling, decreases or often eliminates the solar irradiance reaching a cell and – depending on its uniformity – introduces mismatch challenges and triggers the re-routing of electricity through bypass diodes. Unlike other forms of soiling, however, deep snow and ice can apply both static and dynamic thermo-mechanical stress to modules, introducing reliability concerns. The need to quantify snow accumulation and its impact on array performance is therefore important, not only for LCOE calculations, but also for system sizing, yield forecasting, and service life prediction. Yet no standard method for measuring snow depth on a module exists nor are estimates of snow load for IEC certification (IEC 61215) representative of actual snow loading, as the latter is based on uniform horizontal loads and therefore atypical of most PV systems.

Measuring snow is hard for several reasons. To begin with, snow depth is not static. Rather, it is constantly changing, either through replenishment or through reduction/compaction. Snow can be removed from an array by wind and by sublimation; it can also compact as temperatures warm and partial melting occurs. In addition, existing models do not take into account snow density, although the latter is an indication of both age (snow tends to compact over time) and the crystalline structure of the snow, both of which have different sliding and transmissivity coefficients. Finally, snow shedding often occurs at different rates across a PV array, creating uneven snow depths at both the module and array level, which also increases measurement uncertainty, as shown in Figure 52. Snow models do not take this uneven distribution into account, but instead rely on data from snow gauges or heated rain gauges, which assume uniform accumulation.



Figure 52: Uneven snow shedding across PV arrays can make snow depth a challenging indicator of performance.

Traditional methods for estimating snow depth on a PV panel include using data from weather stations in the Global Historical Climatology Network (GHCN), which supports a database of daily climate data from surface stations around the world that follow a common set of quality assurance standards. Alternatively, one can rely on measuring sticks installed onsite, although this approach requires active monitoring either by a person or a camera and can be affected by drifting snow, which introduces measurement uncertainty. Heated rain gauges, with a tipping bucket, are more accurate as they capture snow as it is falling. However, they measure snow as a liquid and so give no information about actual depth, only the quantity of moisture that has fallen. Moreover, the above methods all measure snow on a horizontal plane and not at the tilt angle of a PV array.

Newer approaches include the use of electronic snow depth sensors with two different physical principles: ultrasonic and laser systems. At the moment, ultrasonic sensors are much more common. Their measurement cone, which depends on the beam width and height of the sensor above the target, is wider than that of the new laser sensors, and has a depth accuracy of around ± 10 mm. Ultrasonic sensors typically operate at 50 kHz, but because the speed of sound in air changes significantly with temperature, ambient temperature measurements are needed to compensate for any fluctuations. In contrast, laser snow sensors, which are relatively new to the market, measure snow depth to an accuracy of around ± 5 mm, but have a small measurement point size, which can be detrimental to accurate snow depth measurement if the snow surface is uneven. To address this problem, some manufacturers are introducing multi-point measurements. A remaining drawback to laser-based sensors, however, is the need for power to heat the laser diode to ensure efficient operation and long life. This power requirement may make stand-alone operation of laser sensors in remote areas more challenging. Otherwise, both laser-based and ultrasonic sensors are mostly maintenance-free. A list of manufacturers is given in Table 10.



Table 10: A partial list of several products available for measuring snow depth. All equipment prices in this report are approximate. The manufacturer should be contacted for exact costs.

Snow Sensors					
Manufacturer	Campbell Scientific	Campbell Scientific	Lufft	Judd LLC	Sommer Messtechnik
Model name	SR50AT	SDMS40-L	SHM 31	UDS	USH-9
Method	Ultrasonic	Optical	Optical	Ultrasonic	Ultrasonic
Beam width	30 degree	Multi-point	Single point	22 degrees	12 degrees
Power supply	9 to 18 VDC	12 to 15 VDC	12 to 24 VDC	12 to 24 VDC	9 to 27 VDC
Maximum power consumption	4.5 W	30 W	18 W	0.6 W	1 W
Output options	SDI-12, RS-485, RS-232	SDI-12, RS-485, RS-232	SDI-12, RS-485, RS-232	RS-232	SDI-12, RS-485, RS-232
Snow depth Accuracy	± 10 mm	± 3 mm	± 5 mm	± 10 mm	± 10 mm
Approximate Cost: Euro / USD	€ 1386 / \$ 1574	€ 2358 / \$ 2678	€ 2749 / \$ 3121	€ 622 / \$ 704	€ 1725 / \$ 1959

Several methods specific to the snow load on PV systems are being developed. To calculate the amount of snow on a tilted array, one can deploy several techniques:

- 1) Measuring sticks that are affixed to a module installed at the tilt angle of the PV system but left in open circuit.
- 2) Displacement sensors that measure module displacement as a function of mechanical (weight) loading, although the depth has to be modelled. The sensors can be affixed to the back of modules, but they should be evenly distributed to capture data on the non-uniformity of the weight load, including build-up at the lower edge.
- 3) Stereographic digital images that are taken normally to the end of an array. This technique, however, requires the installation of cameras and a datalogger to store images.

In addition, a new method has recently been developed that allows one to measure the percentage of a system covered with snow (and thereby to model and predict snow-related power losses). The method relies on time-series images taken at five-minute intervals that are then binarized into snow and clear areas that can be quantified relative to one another [160]. This technique, which is still being refined, does not yet account for snow depth.

7.5.2 Predictive Modelling of Snow Losses

Snow-shading losses can be calculated by comparing expected system performance without snow with the actual performance of a system that is fully or partially covered with snow, but



those losses are historic and not predictive. Moreover, this method requires the analysis of time-stamped digital images to determine the percentage of modules covered and the changes in coverage over time relative to a heated plane-of-array pyranometer. Predicting or modelling the impact of snow, given the rapid expansion of PVs in winter climates, is essential to accurate levelized cost-of-energy calculations and to resource planning for utility-scale installations that feed into the grid.

The energy losses attributed to snow shading impact the LCOE of PVs in northern regions and also resource availability, which can be an issue especially when winter storms take down power lines.

A key challenge to the deployment of PVs in snow-prevalent areas is predicting accurate annual energy yields for PV systems, given the inherent intra- and inter-seasonal variability of snowfall and the many factors that contribute to snow adhesion to modules. Several attempts have been made to estimate yearly energy losses attributable to snow on PV panels, but the published data reflect a limited number of sites, small study sizes, and incomplete accounting of the variables that contribute to snow losses. Moreover, none of these models considers system-design factors other than tilt angle, yet design parameters can be significant contributors to a system's snow-shedding ability.

To date, several snow-loss models have been developed that express snow losses as a percentage of annual energy production [100], [161], [99]. These models take into account tilt angle, temperature, humidity, and irradiance, and they include a sliding coefficient based on the frictional resistance of waxed skis. All these models assume that the primary removal mechanism is snow sliding from the panel. In addition, no major PV modelling software product supports snow loss modelling beyond simple scaling, as in PVWatts [162]. However, Ryberg et al. [163] have incorporated the snow model from Marion et al. [99] into the National Renewable Energy Laboratory's (NREL) System Advisor Model (SAM).

There are two primary mechanisms by which snow sheds from the module surface, melting and sliding, though the two are interrelated and wind is an additional factor. Melting typically occurs when the snow layer is thin and able to melt quickly as the air temperature rises to near or above 0°C, a process that is accelerated by high solar irradiance. Snow sliding is generally triggered by a reduction in frictional forces, which may occur when a thin layer of melted snow forms at the module surface or when the weight of the snow is sufficient to overcome surface resistance, causing detachment at the snow-substrate interface. Sliding can occur relatively quickly thereafter, although snow shedding may be non-uniform if there is partial shading of the array.

Although no coefficient of friction of snow on PV modules has yet been proposed, the sliding force of snow is captured in the following equation [99]:

$$FS = \mu * m * g * \cos(\beta) \quad (17)$$

Where:

- the sliding force attributable to gravity, F_s , is determined by the static coefficient of friction for snow (μ), the mass of snow (m), the acceleration of gravity (g) and the tilt angle $\cos(\beta)$.
- μ = the static coefficient of friction for snow
- m =mass of snow



- g =acceleration of gravity
- β =tilt angle

Sliding can also occur at ambient-air temperatures below freezing if there is sufficient irradiance for some melting to occur and depending on the tilt angle. The higher the tilt angle, the likelier snow shedding will occur earlier and fully shed at a faster rate. For sites experiencing heavy snowfall, angles of 60° or more are recommended to induce sliding. More data, however, including average annual energy yields, are needed to confirm that recommendation. A study conducted in northern Sweden (latitude of 65°N), for example, suggests that module tilt is a minimal contributor to snow shedding when there is no physical impediment from the module frame. In this study by Granlund et al. [164], ten frameless bifacial modules were installed, in 5° tilt increments, from 0 to 90°. All were found to clear snow at comparable rates, with the exception of the 0° and 90° modules. The study's authors concluded that, with no significant difference in snow-shedding rates between modules installed from 25° to 80°, tilt angle should not be the primary determinant of system design in northern climates. One might assume that once a melt-layer forms, which is temperature rather than tilt-angle dependent, that the resistive forces are the same across all tilt angles. The Granlund study, however, is based on single modules and does not take into account physical factors specific to PV arrays, such as the gap between modules, the presence of a frame, or clip morphology, all of which create physical barriers to snow shedding. The study also does not take into account the depth, density or homogeneity of the snow, which can create enough sliding force to overcome the frictional force of the module surface and contribute to shedding.

To provide better estimation tools, several innovative approaches to snow-loss modelling have recently appeared in the literature. A team at the Universite de Quebec has proposed a daily snow-loss prediction model developed from four years of hourly meteorological data and multiple machine learning algorithms. The model is divided into three parts: yield, power-loss (from all sources, including snow, mismatch, DC cable losses, maximum powerpoint tracking and low irradiance), and snow-loss (the percentage of power loss attributed to snow). Like its predecessors, this model has yet to be validated for more than one site [165]. A second team, also at the Universite de Quebec, has developed an alternative model that estimates the amount of irradiance that can filter through a module when the latter is uniformly covered with snow, per the Bouguer-Lambert Law of insolation transmission and associated electrical characteristics of PV modules, but this model has also not been validated [166].

Other models have attempted to predict snow melting from a surface but they only consider horizontal surfaces [167] [168]; a more recent snow-melting model incorporates heat and mass transfer equations as well as operating parameters specific to PV systems [169]. This model assumes that melting can occur both at the module surface (the result of external heating), and at the top surface, if irradiance and ambient air temperature are high enough, with surface run-off flowing through the snow in the direction of the panel tilt. Inputs to the model include measured energy needed to precipitate snow sliding, tilt angle, snow cover measured as mass per unit area, and ambient temperature. Parameters not modelled, however, include soiling of the panel, surface topology, presence or absence of a frame and build-up of ice along the bottom frame that creates a physical barrier to sliding.



7.6 Design Optimization for Snowy Climates

Preliminary research suggests that climate-specific technological and design choices can lead to measurable efficiency gains [159]. Options to increase rates of snow shedding and/or decrease the impact of snow shading fall into the following categories:

- Module architecture (e.g., frame vs frameless, cell stringing, etc.)
- Module technology (cell size, cell design, bifacial vs mono-facial)
- System design (module orientation; height above ground; tilt angle; clip design and placement)

The choices described below are of greatest relevance to commercial and utility-scale installations; residential rooftop PV is also considered but not discussed at depth because the design options there are more limited.

7.6.1 Module Architecture

The intense focus in recent years on increasing the performance efficiency of PV modules has led to a proliferation of module technologies and designs. This section describes what is known about the performance of different module designs in snowy climates and lays out areas where more research is needed.

1. Frame Design

Module frames can function as snow dams, creating resistance that – depending on snow depth, ambient air temperature and irradiance – will slow the momentum of sliding snow and cause it to compact on the lower portion of the module, further obstructing the sliding process [170]. Although module orientation, form factor, snow depth, ambient air temperature and irradiance are contributing factors, even a low-profile frame morphology will obstruct the sliding of snow [171]. The discontinuity of a frame protruding even a few millimetres above the cover glass can provide a foothold for snow and ice. The greater the weight of snow above the bottom of the frame relative to the frame length, the less likely it is that an accumulation along the bottom edge will be able to support the weight of snow above it.

What is not clear is whether there are quantifiable differences attributable to a specific frame morphology (e.g., a bevelled edge) or frame colour, but these differences should be studied. What is clear is that frameless modules can, under the right climate conditions, shed snow more quickly than framed modules. One recent study demonstrated that an array of frameless modules produced 13% more energy than framed – but otherwise identical – modules in the month of December. More research is underway to better understand the role of ambient air temperature, which affects the rate of shedding, with the difference between the two arrays shrinking as temperatures drop, likely attributable to a higher surface adhesion at lower temperatures. Another study showed that snow, when shed quickly from the frameless panels, will form mounds on the ground. These mounds, in turn, support ever bigger mounds that can eventually obstruct the lower row of modules. By contrast, the mounds under the adjacent framed modules are much smaller, not only because some snow is retained on the lower edge of the modules but because a certain amount is removed via wind or melting before it ever reaches the ground [170].



Figure 53: Framed vs. frameless modules side-by-side PV arrays demonstrate the impact of a module frame on snow shedding. Frameless modules (right) generated 13% more energy in the month of December than the adjacent framed modules. The modules were virtually identical except for the presence or absence of a frame [170].

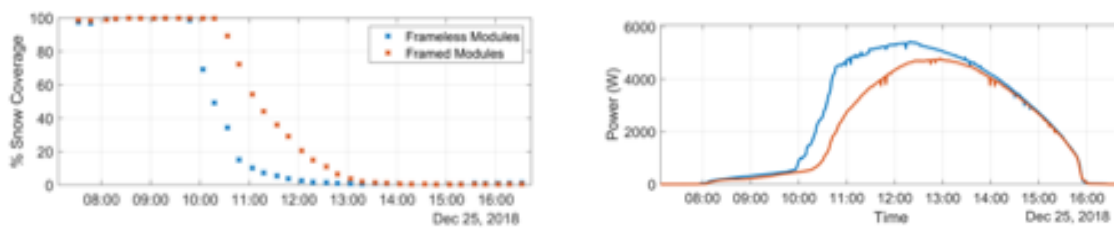


Figure 54: Difference in snow shedding and energy output are shown for the adjacent framed and frameless modules. As shown in the graph on the left, the framed modules begin shedding snow almost an hour before the frameless modules, a difference that is reflected in the power-output graph on the right [170].

Other factors must also be considered. Installation costs, for example, may be higher if taller racks are needed to avoid ground build-up. In addition, the frameless modules require more delicate handling during installation, which may also increase costs, especially for utility-scale installations. Moreover, frameless modules may have reliability issues, as they may be less resistant to the weight of larger snow loads and they may be more vulnerable in the long term to moisture ingress. That said, framed modules have their own reliability challenges: water can freeze under the frame, putting expansion pressure on both the frame and module glass. Under heavy snow loads, the load on the lower edge of the module can cause the frame to shear from the module [172]. As more is learned about the thermo-mechanical stress on modules from cold and snow, including its spatial distribution, opportunities to improve the frame design will likely arise. Possibilities include materials substitution, e.g., a composite instead of aluminium, or some type of stabilizing back bar.

2. Form Factor

Larger-format modules have a greater glass-to-frame ratio than smaller modules, and therefore have less sliding resistance, but their larger surface area also creates stress vulnerabilities that should be investigated across a range of thermo-mechanical loading conditions.



3. Cover Glass Texture and Coatings

The use of smooth versus textured cover glass is known to improve angle-of-incidence losses and, by reducing surface roughness, is likely to increase rates of snow shedding. However, further investigation is needed. The application of a snow-phobic surface film, or coating, represents another opportunity for improving shedding performance, but such coatings will need to have high optical transmissivity and sufficient durability to withstand the friction from sliding snow.

7.6.2 Solar-Cell Innovation

The solar industry is experiencing rapid technological change driven by the desire for higher-efficiency modules and lower-cost products. While the innovation taking place is not motivated by the operating climate per se but on cost reductions, many of the changes have implications for northern climates that regularly see snow. These changes are briefly discussed in this section.

Cell Size

Si-wafer based PV technology accounted for about 95% of the total production in 2019. The result of Mono-crystalline silicon solar cells is experiencing a growth phase, with ever-larger wafer sizes being introduced into the marketplace in order to boost the maximum power rating of modules and gain production efficiencies. More than 10 years ago, the prevailing cell size was 125 mm x 125 mm; by 2010, so-called M1 cells (156 mm x 156 mm) were becoming popular, followed within a few years by M2 wafers (156.75 mm x 156.75 mm); today, even larger sizes are emerging (157 mm x 157 mm) and an M6 cell (166 mm x 166 mm) is on the horizon.

But as cell size increases, negative resistive losses also increase, resulting in decreased power output. Manufacturers have compensated by moving to half-cut cells to reduce cell-to-module losses. The impact of these technological trends, combined with the shift to thinner wafers, has introduced questions regarding the wafers' increased sensitivity to the combined stressors of cold temperatures and snow load. For example, research shows that cell fragility is inversely proportional to temperature, with cell cracking more likely to occur, especially with snow weight on the module, as temperatures fall below freezing [173]. But this work needs to be expanded to emerging technologies and across a broader spectrum of thermo-mechanical-load scenarios.

Half-cut and Shingled Cells

In the past two years, the solar industry has shown significant interest in half-cut cells, which have six strings instead of the traditional four, allowing for higher voltage and more resistance to shading. On one hand, half-cut-cell modules may be the optimal choice for snowy climates because the new modules outperform traditional modules in portrait orientation when the lower half is shaded. On the other hand, half-cut cells, which are partially cut, may prove to be susceptible to cell cracking under heavy snow loads and/or extreme cold temperatures. Given the expected market penetration of half-cut cells, field data from installed systems at northern latitudes are needed.

Shingled solar cells are silicon cells that are cut into multiple parts (typically 3 or 4) and overlaid like rooftop shingles, inter-connected with electrically conductive paste. The shingling approach is seen as having several advantages: the cut cells are partially overlaid, allowing for better area utilization; the shingles are connected electrically with conductive adhesive paste,



eliminating the need for busbars and reducing shading losses; shingled modules also lack soldered ribbons, which are a known point of failure; and they can be wired in parallel, resulting in high shade-tolerance, depending on orientation. Yet to be thoroughly investigated, however, is how shingled cells perform when thermo-mechanically stressed in winter, especially if bus-bar failure is a non-issue and the shingled cells are supported by each other.

Bifacial versus Mono-facial

The rapid growth of the bifacial PV market can be explained by the relatively low cost of bifacial modules and their perceived advantages. Nowhere are those advantages more apparent than in northern regions where snow may persist on the ground for months, creating a high-albedo operating environment. One advantage of bifacial modules is that the backside does not get covered by snow, so it is possible to produce even when the front side is shaded by snow. Shading from the mounting structure might be an issue, but most racking companies are now designing racks specifically for bifacial systems.

Early studies have shown that bifacial gains in winter can be considerable, and that an outside-the-box approach to bifacial system designs may be warranted. A field study of east-west facing vertical bifacial PV arrays in Alaska, for example, demonstrated that the vertical arrays generated from 5-20% more energy than traditional designs, produced two energy peaks per day that aligned well with electric loads, and had almost no snow shading [174].

A second study of bifacial performance on a dual-axis tracker in Vermont also had impressive results. In this case, the tracker's string of bifacial modules outperformed the adjacent string of mono-facial modules by 14% over the course of a year, with highest gains in winter, as shown in Figure 55. The findings from this experiment suggest that a two-axis tracker, which maximizes irradiance normal to the array, also allows for a large optical capture area on the backside. The study demonstrated that bifacial modules will shed snow at a faster rate than monofacial modules, likely because the increased backside irradiance increases the module temperature [159].

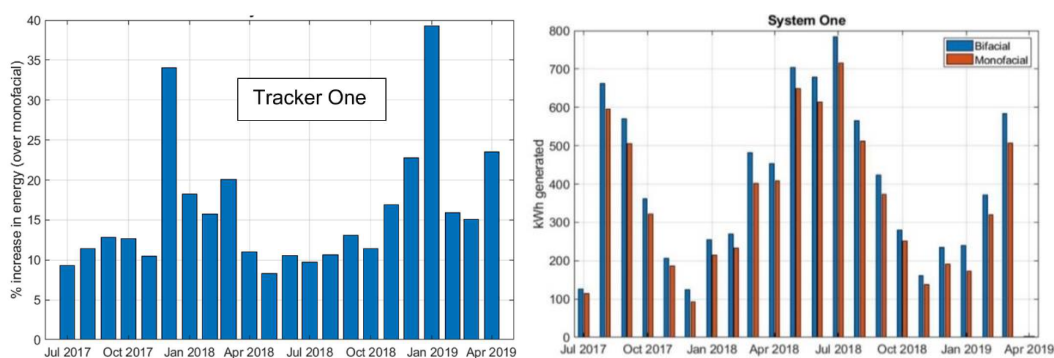


Figure 55: String of bifacial modules installed next to a string of mono-facial modules, on a two-axis tracker, showed an average annual energy gain of 14% compared with the monofacial modules [159].



7.6.3 System Design

Tilt Angle

Tilt angles tend to roughly correlate with latitude (hence the term “latitude tilt”), with fixed-tilt angles in far northern utility- and commercial-scale installations as high as 45°. Choice of tilt angle is generally based on angle-of-incidence and inter-row shading calculations. In Sweden, for example, the optimal tilt for a latitude of 60N is from 40-45 degrees, assuming the array is facing due south. To date, little attention has been paid to the impact of tilt angle on snow shedding, as it reflects multiple variables that are being researched but are not yet well understood [100]. However, this study indicated that annual energy losses decreased dramatically, from 34% to 5%, as tilt angle increased from zero to 45 degrees for unobstructed systems.

Module Orientation

Module orientation is thought to contribute to snow shedding, but this assumption needs to be better quantified. Preliminary work suggests that the length of vertical glass relative to the length of the horizontal frame allows for greater sliding momentum that will propel snow beyond the frame edge. For this reason, mounting modules with their shorter dimension parallel to the ground – in portrait rather than landscape configuration – is thought to encourage snow shedding, but module stringing and the location of bypass diodes must also be taken into account [160].



Figure 56: Two adjacent PV systems set at the same tilt angle but with different module orientations create an ideal experimental set-up for investigating the impact of orientation on snow shedding. As shown above, orientation can impact shedding rates, although more research is needed to investigate temperature-dependency and the role of bypass diodes [160].

Module Clips

Both inter-modules spacing on a rack and the location, size, and profile of module clips can have a measurable impact on snow shedding. Snow that builds up in the several centimetres of space between adjacent modules creates a physical impediment that can hinder further sliding; similarly, clips can function as snow dams, holding snow on the module surface that can shade all three module strings. An example of the clip effect can be seen in Figure 57. The



influence of the module frame and other design features on snow shedding are discussed in the previous section.



Figure 57: Module clips. The photo demonstrates how a module clip can create a physical barrier that prevents snow from sliding from the module surface.

Array Height

Height is another important contributor to snow losses. If a PV array is set too close to the ground, and if snow sheds too quickly and/or too often, and without significant melting, snow will accumulate on the ground, forming piles that can engulf the PV array, reducing its power output and introducing reliability concerns, from mechanical loading to moisture ingress. Providing a clearance of at least a meter between the array and ground gives space for snow to accumulate without reaching the lower edge of the array, although the elevation should also take local snow and wind conditions into account. In cases with inadequate clearance, such as roof-mounted modules, or even ground-mounted systems that experience extreme snow events, snow will build up at the bottom of the module frame but is something to generally be avoided (see Figure 58).

That said, more research is needed in this area to determine the trade-offs regarding engineering and installation costs of higher racks versus the energy lost from snow build-up from the ground.

Ground-Mounted Systems

In northern regions where snow accumulates throughout the four to six months of winter and the ground freezes to a depth of two metres or more, most PV installations are seasonal activities owing to the cost and complexity of winter installations. Even then, installing the foundations for array-racking in cold climates can be difficult depending on whether the terrain is rock, permafrost, or a mixture of sand and clay. Also concerning is the height of the water table, which can create frost heaves in winter, thus requiring relatively deep pile-driven posts. If frost heaves are a concern, foundations should extend below the frost level; otherwise, the pilings may shift as the soil expands and contracts during seasonal freeze and thaw.

For sites with permafrost, foundations can be anchored directly into the frozen soil, assuming the permafrost is stable and shows no signs of melting. A thawed layer of soil can be excavated during the summer down to the permafrost layer. Exposed to the ambient air, a 30 cm depth of permafrost will thaw and can be removed creating a cavity into which a steel platform can be installed and topped with insulating foam. The excavation is then filled in and the entire structure becomes bolted to the permafrost [3].



Figure 58: Insufficient elevation of a PV array can result in snow build-up from the ground that prevents further snow sliding.

Tracking Systems

Trackers, both single- and dual-axis, represent yet another approach to reducing snow losses. They can be tilted and/or stowed to minimize snow adhesion and/or accelerate snow shedding. But trackers require motors and controls, both of which add complexity and reliability challenges, especially in cold operating environments. Also unknown is whether snow load, combined with tracker movement, can stress the solar cells, especially at sub-freezing temperatures, resulting in cell cracking [175].

Residential Rooftop PV

In contrast, the concern for residential rooftop PV is twofold, depending on the placement of the array relative to the rest of the roof: 1) snow can shed abruptly, creating a mini-avalanche that poses a danger and 2) snow may shed from the modules but then adhere to the roofing substrate, creating a snow dam that prevents further shedding. To mitigate safety concerns, some PV companies advocate implementation of a snow guard, or physical barrier, which can be installed along the edge of the roof. In Sweden, snowguard placing is recommended 80 cm from the PV system [176].

Other options that may favour the shedding of snow include the installation of frameless modules and rooftop PV systems that are integrated or semi-integrated into the roof, lowering the array's profile and therefore reducing resistance to sliding. Solar roof tiles could be another option, although they are still not mainstream and their long-term reliability in harsh winter conditions is not yet established.

Power Electronics

Cold climates may exacerbate thermal cycling and create condensation inside electronic devices leading to performance drift or short-circuits. Circuits cooled by natural convection and radiation are preferable to fan-cooled devices, since fans may fail at low temperature and component replacement in remote locations is difficult. Electronics encased in epoxy should be pretested over a range of temperatures to ensure the difference in coefficients of thermal expansion does not cause undue stress. Liquid-crystal displays may work poorly in cold conditions. Inverters or charge controllers should ideally be in a dry sheltered environment, such as a nearby building; if not possible, they should be hung on the back of the PV rack, which will provide some shelter. However, batteries should be stored separately due to the possibility of generating corrosive vapours or hydrogen gas. Also, inverters and charge controllers also



need to be sized appropriately. The voltage of a c-Si module increases with decreasing temperature. Voltage dependence on temperature is most strongly affected by the dark saturation current, which in turn shows a temperature dependence on the intrinsic carrier concentration. While open-circuit voltage rises, short-circuit current decreases slightly at lower temperatures due to bandgap widening. Maximum power and open-circuit voltage improve by 0.3% to 0.5%, while short-circuit current drops by around 0.04% to 0.06% for every degree below standard test conditions of 25°C. The overall effect on performance at low temperature is a power gain and a slight improvement in fill factor. For example, a crystalline silicon array operating at an average temperature of 0°C will generate approximately 10% more power than an array operating at 25°C, for equal solar irradiance [4].



8 CONCLUSION

This report summarises the current state of the still-evolving field of soiling, closing the loop from physical and chemical mechanisms to measurement, modelling, economic impacts, and mitigation. In a nod to the growing popularity and viability of installations in high latitude regions, dedicated sections on snow soiling are also included. This report addresses both mineral dust particle and snow-induced shading of installations, but not anthropogenic, zoological or biological sources of PV system yield loss, such as diesel exhaust, bird droppings, moss, lichens, etc.

Particles in the range of 2 μm to 63 μm are found to be the main contributors to soiling in arid regions. Normally, such particles are water-soluble and can be removed relatively easily. However, under the influence of high humidity with subordinate phases of dryness, adhesion can increase greatly and require professional cleaning.

Soiling is also found to be highly heterogeneous, and monitoring of soiling in large-scale systems should therefore be conducted in multiple locations – as described in the monitoring standard for PV systems, IEC 61724. Regular cleaning of the irradiation sensors is also obligatory to avoid misinterpretation of performance data. When choosing soiling sensors, it is important to consider how easily such devices can be integrated into the system's monitoring infrastructure. An ideal solution should be installable with as little maintenance as possible and be able to detect heterogeneous soiling at both module and site level with high accuracy.

In the field of soiling metrics prediction, there are different models that can be divided into several classes, from semi-physical models to those that use AI methods. Their common feature is that they are very often limited to a local test area and are difficult to generalise. Globally applicable models for predicting soiling rates based on satellite data are currently quite crude. Energy losses predicted by emerging snow models as predictors for soiling phenomenon in high latitudes also show that more work and validation is still needed to understand the causes of discrepancy between the models and with empirical data.

Studies suggest that soiling of PV installations may already have caused a loss in annual PV energy production worldwide of at least 3% to 4% in 2018, corresponding to economic losses of up to three to five billion euros. Despite lower component costs and thus lower CAPEX, increasing absolute losses must be assumed, as PV installations will continue to expand in all regions.

On a global level, these economic consequences are immense. Techno-economic models, as described in Chapters 4 and 5, provide decision-making support for O&M companies. Cleaning decision timelines, especially for large plants, should be based on sound on-site monitoring, rather than on predefined operation and maintenance schedules, to minimise the costs of cleaning operations. Especially for large power plants in arid regions with correspondingly high soiling rates, the trend is clearly towards robotic or semi-robotic cleaning.

Technological advancements and lower component costs are also making PV systems increasingly attractive at higher latitudes (and altitudes), despite winter season stresses on systems caused by snow cover and low temperatures. Ongoing research projects are aimed at improvements in component reliability, predictive modelling and system design optimisation. To mitigate production losses, promising considerations for high latitude solar installations include frameless modules, steeper tilt angles, snow-shedding coatings, bifacial modules, and attention to array heights to minimize snow accumulation on the bottom edges of modules, among other factors.



In conclusion, PV soiling will continue to be a global issue, which is expected to be exacerbated by climate change with rising global temperatures and subsequent droughts. Further advancements in soiling modelling, adaptation and mitigation are critically necessary to help PV operators maximize their power generation and economic gains, in spite of the challenges posed by soiling.



APPENDIX 1: PARTICLE COMPOSITION AND SOLUBILITY

Table 11: List of some compound families with examples of their salts and possible origins.

Chemical compounds minerals family	Examples of salts	formula	most likely origins
Nitrates	Sodium Nitrate	$NaNO_3$	atmospheric (Ozone + Nitrogen + Oxygen)
	Potassium Nitrate	KNO_3	industry or intensive agriculture or road traffic
Acetates	Calcium Acetate	$Ca(C_2H_3O_2)_2$	Polymers industry
	Potassium Acetate	$K(C_2H_3O_2)$	
Sulfates	Gypsum	$CaSO_4 \cdot 2(H_2O)$	Evaporite Alteration of sulphide
	Potassium Sulfates	KSO_4	Fumarole Smogs ($H_2O + SO_2 + NO_2$)
	Sodium Sulfates	Na_2SO_4	Mirabilite or Thénardite industrial extraction Industrial production of chlorhydric acid, ...
	Ammonium Sulfate	$(NH_4)_2SO_4$	Mascagnite industrial extraction Intensive agriculture Industrial production $(NH_4)_2CO_3 + CaSO_4 \rightarrow (NH_4)_2SO_4 + CaCO_3$
Chlorate	Sodium Chlorate	$NaClO_3$	Intensive agriculture Industrial production
	Magnesium Chlorate	$Mg(ClO_3)_2$	



Silicate-Phyllosilicate	Palygorskite	$(Mg, Al)_2Si_4O_{10}(OH)_4(H_2O)$	Attapulgitic clay industrial extraction
	Kaolinite	$Al_2Si_2O_5(OH)_4$	Natural alteration of mica, or feldspaths due to water, carbonic gas or organic acids.
Halide	Halite	$NaCl$	Salt marshes
	Sodium Chlorid		Halite industrial extraction

Cementation is not a simple drying of the paste after adding water, but a complex set of chemical hydration reactions allowing the cement paste to pass from the liquid state to the solid state.

The famous Portland Cement, the basic ingredient of concrete, is a good example which can illustrate the hydration process. The study of the chemical reactions involved artificially dissociates the different mechanisms. In practice, these mechanisms take place simultaneously.

- Silicates Hydration: In this cement tricalcium silicates (Ca_3O_5Si and dicalcium silicates (Ca_2O_2Si) dissolve as ions which interacts with each other and forms silicates of hydrated calcium ($(CaO)_{1.7}(SiO_4)(H_2O)_4$) and portlandite ($Ca(OH)_2$). The hydrated calcium has the same characteristics of a gel. This is the tangle of this gel which gives the cement's robustness. The hydrates calcium molecules grow on the surfaces of non hydrated grains and fill the capillary interstices between those grains. After a few hours, the layer around the grain is thick enough to slow down the diffusion of water and ions towards the anhydric components. The hydration slows but the process can still continue for months or years.
- Aluminate's hydration: tricalcium aluminate ($Ca_3Al_2O_6$) is the more reactive compound with water. The reactions are carried out in several steps
 - Step 1: Aluminates react with gypsum to form ettringite $(CaO)_6(Al_2O_3)(SO_3)_3, 32H_2O$. A hydrates layer is covering the aluminates forming a protective cover all around the grain.
 - Step 2: When gypsum is exhausted, the sulfates concentration of the solution decreases. Ettringite become unstable and dissolve to form hydrated calcium monosulfate named AFm $(CaO)_3(Al_2O_3)(CaSO_4), 12H_2O$
 - Step 3: After a couple of weeks, ettringite has transformed totally in AFm. Over one month, reactions carry out slowly with aluminate and aluminoferrite to form aluminoferrite of hydrated calcium

The complex mechanisms behind the creation of the various hydration products that are silicates and aluminates are adsorption, hydrolysis, dissolution, solvation and crystallisation. This conclusion is probably similar for most of the soiling cementation mechanisms.



APPENDIX 2: DUST COMPOSITION SURVEY

Table 12 Some examples of dust composition for samples sieved below 38 μm from [37]. PSDA analysis is from [30].

Locality		Major 20-100%	Minor 5-20%	Trace <5%
Spain las Canarias	La Mala 29°05'50.50"N 13°27'43.92"W	Calcite ¹ , Quartz ^{2a}	Illite ^{2c}	Plagioclase ^{2b} , Aragonite ¹ , Dolomite ¹ , Hematite ³
	La Mala 29°05'49.79"N 13°27'44.83"W	Calcite ¹ ,	Quartz ^{2a}	Plagioclase ^{2b} , Aragonite ¹ Dolomite ¹ , Hematite ¹ Halite ³
	Mirador del Rio 29°13'39.86"N 13°28'20.92W	Quartz ^{2a} , Illite ^{2c}	Calcite ¹ , Plagioclase ^{2b} , Dolomite ¹ , Kaolinite ^{2c}	Hematite ⁴
	Vega de femes 28°55'22.71°N 13°45'52.71W	Illite ^{2c}	Biotite ^{2c} , Quartz ^{2a} , Plagioclase ^{2b} , Microcline ^{2b}	Calcite ¹ , Goethite ⁵ Hematite ⁴ , Illite ^{2c} Kaolinite ^{2c}
Chile	Atacama Yungay 25°56'56.89"S 70°27'45.81"W	Quartz ^{2a} Illite ^{2c}	Anhydrite ⁶ Plagioclase ^{2b} Amphibole ^{2d}	Gypsum ⁶ Montmorillonite ^{2c}
	PSDA* Antofagasta	Quartz ^{2a} Anorthite ^{2a} Orthoclase ^{2b}	Albite ^{2b}	Gypsum ⁶
USA	Arizona road undisclosed	Quartz ^{2a}		Plagioclase ^{2b} , K-feldspar (Orthoclase ^{2b})
	Yuma AZ 32°52'27.06"N 114°12'31.84W	Quartz ^{2a} , Plagioclase ^{2b}	Calcite ¹ , Muscovite ^{2c} , Kaolinite ^{2c}	Dolomite ¹ Montmorillonite ^{2c} ,



				Gypsum ⁶
	Yuma AZ 32°51'48.62"N 114°10'50.72"W	Quartz ^{2a} , Calcite ¹	Plagioclase ^{2b} , Muscovite ^{2c}	Kaolinite ^{2c} , K-feldspar (Orthoclase ^{2b}), Dolomite ¹
	FT. Carson CO 38°42'30.79N 104°47'10.56"W	Quartz ^{2a} , Plagioclase ^{2b}	Muscovite ^{2c} , Kaolinite ^{2c} , Dolomite ¹	Calcite ¹
	Dugway UT, 40°11'30.10"N 113°09'50.05"W	Quartz ^{2a} , Calcite ¹	Dolomite ¹ , Plagioclase ^{2b} , Aragonite ¹	Muscovite ^{2c} , K-feldspar (Orthoclase ^{2b}), Hematite ¹
Morocco	Lake Iriki 29°50'17.02"N 06°30'44.51"W	Quartz ^{2a} , Illite ^{2c}	Calcite ¹	Kaolinite ^{2c} Dolomite ¹
Iraq	Camp Victory 33°15'17.09N 44°13'26.87"E	Quartz ^{2a} , Calcite ¹	Kaolinite ^{2c} Plagioclase ^{2b} , Dolomite ¹	Amphibole ^{2d} , Montmorillonite ^{2c} , Halite ⁷ , Palygorskite ^{2c}

where in this table, the superscript upon each mineral refers to the Strunz mineral classification:

- ¹Carbonates
- ^{2a}Silicates:Tectosilicates
- ^{2b}Silicates:Tectosilates:Feldspathic
- ^{2c}Silicates:Phyllosilicates
- ^{2d}Silicates:Inosilicates
- ⁴Oxydes
- ⁶Sulfates
- ⁷Halide



APPENDIX 3: MACROSCOPIC, CONTROLLABLE AND MICROSCOPIC FACTORS INFLUENCING SOILING

Microscopic Approach

The first step of the microscopic approach aims to characterize the dust samples so as to determine the size distribution and the mineral composition of the dust. The separation of large-grain materials from hundredths of a millimetre to two to three mm is done using a sieve analysis. Separation of smaller particles is done by hydraulic method based on either the difference in the speed of sedimentation of particles of different sizes in water or on the ability of water jets flowing at different speeds to draw off particles of different sizes. The samples can be soaked in water to avoid disaggregation. Alternatively, aggregates may be broken down by boiling and treating samples with various agents. In order to prevent coagulation of the suspension during the analysis, stabilizers are added. Another method is laser diffraction (LD). This is a widely used technique for particle sizing from hundreds of nanometres to several millimetres. Laser diffraction measures particle size distribution by measuring the angular variation in intensity of light scattered as a laser beam passes through a dispersed particulate sample. Large particles scatter light at small angles relative to the laser beam and small particles scatter light at large angles. Using Mie light scattering theory, the angular scattering intensity data are analyzed to calculate the size of the particles forming the scattering pattern. The particle size is reported as a volume equivalent sphere diameter as shown in the Figure 59.

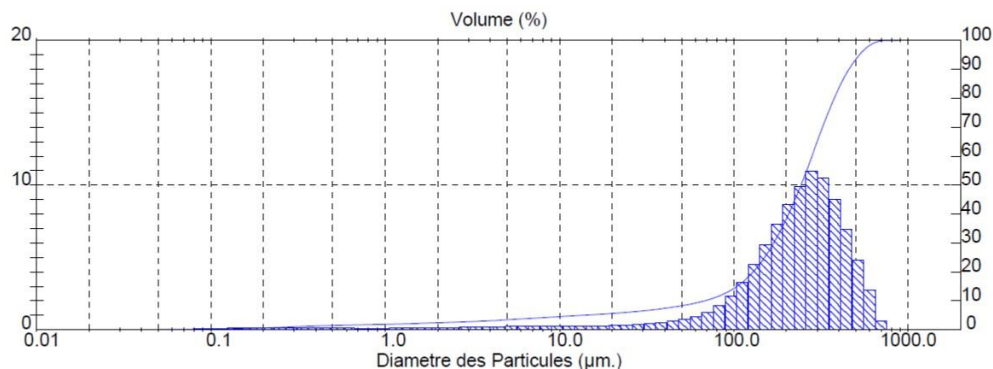


Figure 59: Size distribution of one dust sample performed by one Mastersizer 3000 instrument.

The second step of the microscopic approach aims to determine the mineral composition of the dust. This analysis can be performed by X-Ray Diffraction (XRD). Figure 60 shows one diffractogram obtained using a Panalytical Aeris instrument accompanied by the X'pert Highscore software and the PDF-4 database allowing the peaks to be assigned to the corresponding compounds.

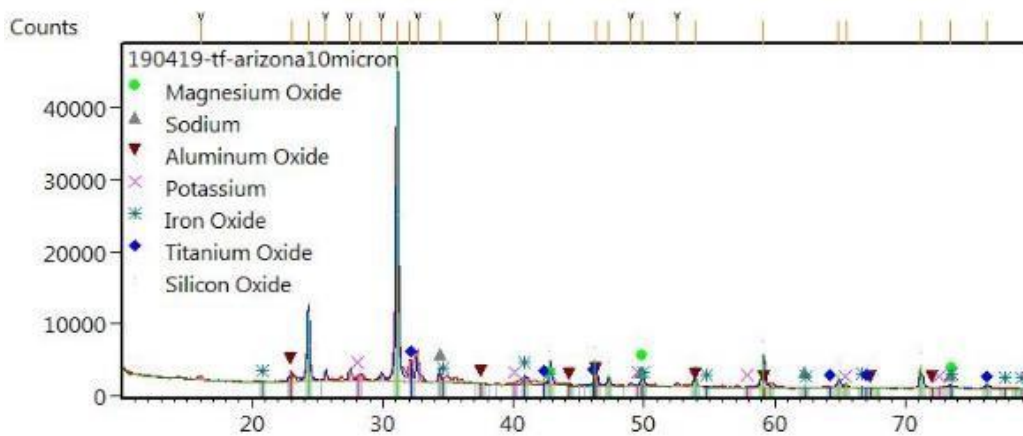


Figure 60: Diffractogram with compounds identified.

Energy Dispersive X-ray (EDX) is performed to reveal the presence and quantities of atomic elements. Even if it does not specify directly which compound, this result eliminates many mineral possibilities. EDX is coupled with Scanning Electron Microscopy, and as a consequence the EDX result is accurately localized on the dust sample. The high magnification image also gives a clear view on the shape and of the arrangement of the various dust compounds. Figure 61 shows one big (10 μm) crystallized mineral surrounded by smaller (one μm) ones, which illustrate the caking effect. The EDX measurement concentrated on a part of this mineral (red point) reveals the strong presence of Ca and Sulfur atomic elements. These two elements are in the chemical formula for Calcium sulfate (CaSO_4) which could demonstrate the presence of Gypsum or Anhydrite. This assumption should be confirmed by XRD or TEM (Transmission Electron Microscopy) or other visual inspections.

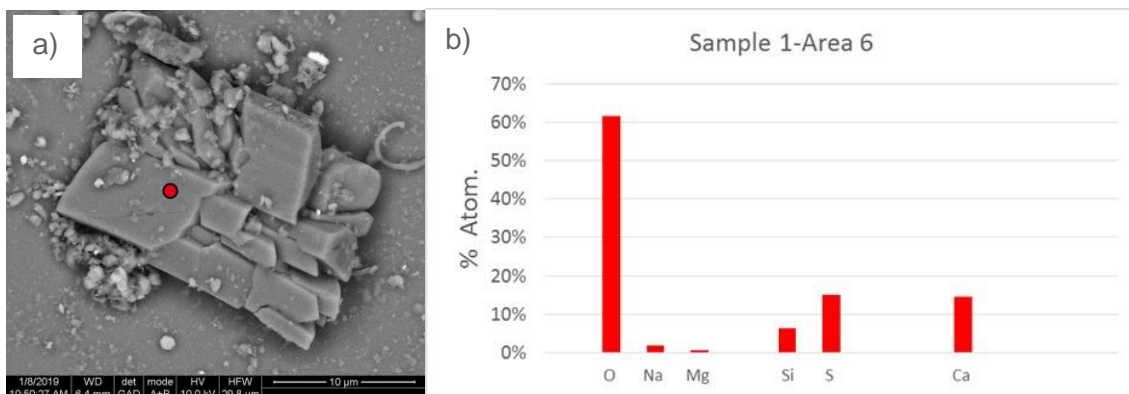


Figure 61: (left) SEM image; (right) corresponding EDX result.

Macroscopic Approach

The macroscopic approach consists in observing the influence of meteorological phenomena at the same time as the aerosol concentration. This approach can be applied at several levels depending on the accuracy of the information sought.

- In the context of multi-annual estimates, the induced loss can be quantified by taking into account only the average annual concentration of PM10 particles (airborne below 10 μm) suspended in the air, and the rainfall frequency. This approach generates uncertainties of several percent and consequently the means and resources required in the targeted area.



- In the construction of a new power plant, it is necessary to consider other meteorological parameters. A study [1] in Qatar has shown good correlations, taking into account wind speed and humidity, when one disregards exceptional events such as sandstorms.
- In order to plan cleaning or protection actions, it is mandatory to take into account additional parameters such as wind direction. Certain winds may contain more dust than others.

Controllable Approach

The controllable approach focuses on the configurations of the plant and its solar panels as well as the methods applied to maximize cleanliness. The major influencing factors are:

- Orientation of the strings of panels and choice of technology by comparing, for example, a south-facing array (northern hemisphere) or north-facing array (southern hemisphere) with an East-West orientation with bifacial technology.
- Nature of the soil, presence of particles which can be resuspended, and which can therefore cover the modules.
- Electrical architecture in the case of a very localized soiling therefore source of “mismatch”.
- Evolution of the soil albedo linked to dust in the case of the bifacial.
- Effect of tilt angle: A horizontal module will be soiled by relatively large particles, while a steeply tilted module will be soiled by smaller particles.
- Modules temperature: this parameter strongly influences the initial bonding and accumulation process.
- The surface coating of the modules: the particle size distribution influences the initial adhesion; the hydrophobic or hydrophilic characteristics will directly condition the cementation and self-cleaning processes.



REFERENCES

- [1] W. Javed, B. Guo and B. Figgis, “Modeling of photovoltaic soiling loss as a function of environmental variables,” *Solar Energy*, vol. 157, p. 397–407, 2017.
- [2] L. Micheli, D. Ruth and M. Muller, “Seasonal Trends of Soiling on Photovoltaic Systems: Preprint,” Golden, CO: National Renewable Energy Laboratory. NREL/CP-5J00-68673. , 2017.
- [3] L. Micheli, M. G. Deceglie and M. Muller, “Predicting photovoltaic soiling losses using environmental parameters: An update,” *Progress in Photovoltaics: Research and Applications*, vol. 27, no. 3, p. 210–219, 2019.
- [4] M. Gostein, K. Passow, M. G. Deceglie and L. Micheli, “Local Variability in PV Soiling Rate,” in *2018 IEEE 7th World Conference on Photovoltaic Energy Conversion (WCPEC 2018)*, Waikoloa Village, Hawaii, USA, 2018.
- [5] K. Ilse, M. Werner, V. Naumann, B. W. Figgis, C. Hagendorf and J. Bagdahn, “Microstructural analysis of the cementation process during soiling on glass surfaces in arid and semi-arid climates,” *physica status solidi (RRL) – Rapid Research Letters*, vol. Volume 10, no. Issue 7, pp. 525-529, 2016.
- [6] K. Ilse, L. Micheli, B. W. Figgis, K. Lange, D. Daßler, H. Hanifi, F. Wolfertstetter, V. Naumann, C. Hagendorf, R. Gottschalg and J. Bagdahn, “Techno-Economic Assessment of Soiling Losses and Mitigation Strategies for Solar Power Generation,” *Joule*, vol. 3, no. 10, p. 2303–2321, 2019.
- [7] L. L. Kazmerski, Diniz, Antonia Sonia A. C., C. Brasil Maia, M. Machado Viana, S. C. Costa, P. P. Brito, C. Dias Campos, L. V. Machado Neto, S. Morais Hanriot and L. R. Oliveira Cruz, “Fundamental studies of the adhesion of dust to PV module chemical and physical relationships at the microscale,” in *2015 IEEE 42nd Photovoltaic Specialists Conference (PVSC)*, New Orleans, LA, USA, IEEE, 2015, p. 1–7.
- [8] A. Sayyah, M. N. Horenstein and M. K. Mazumder, “Energy yield loss caused by dust deposition on photovoltaic panels,” *Solar Energy*, vol. 107, p. 576–604, 2014.
- [9] G. P. Smestad, T. A. Germer, H. Alrashidi, E. F. Fernández, S. Dey, H. Brahma, N. Sarmah, A. Ghosh, N. Sellami, I. A. I. Hassan, M. Desouky, A. Kasry, B. Pesala, S. Sundaram, F. Almonacid, K. S. Reddy, T. K. Mallick and L. Micheli, “Modelling photovoltaic soiling losses through optical characterization,” *SCIENTIFIC REPORTS*, vol. 10, no. 1, 2020.
- [10] M. Köntges, S. Kurtz, C. E. Packard, U. Jahn, K. Berger, K. Kato, T. Friesen, H. Liu, M. Van Iseghem, J. Wohlgemuth, D. Miller, M. Kempe, P. Hacke, F. Reil, N. Bogdanski, W. Herrmann, C. Buerhop Lutz and G. Friesen, “Review of Failures of Photovoltaic Modules,” ISBN 987 3 906042 16 9, Report IEA PVPS T13 01:2014.
- [11] S. C. Costa, A. S. A. Diniz and L. L. Kazmerski, “Dust and soiling issues and impacts relating to solar energy systems: Literature review update for 2012–2015,” *Renewable and Sustainable Energy Reviews*, vol. 63, p. 33–61, 2016.
- [12] T. Sarver, A. Al-Qaraghuli and L. L. Kazmerski, “A comprehensive review of the impact of dust on the use of solar energy: History, investigations, results, literature, and mitigation approaches,” *Renewable and Sustainable Energy Reviews*, vol. 22, p. 698–733, 2013.



- [13] J. Zorrilla-Casanova, M. Piliouguine, J. Carretero, P. Bernaola, P. Carpena, L. Mora-Lopez and M. Sidrach-de-Cardona, "Analysis of Dust Losses in Photovoltaic Modules," Linköping University Electronic Press, 2011, p. 2985–2992.
- [14] R. Appels, B. Lefevre, B. Herteleer, H. Goverde, A. Beerten, R. Paesen, K. Medts, J. Driesen and J. Poortmans, "Effect of soiling on photovoltaic modules," *Solar Energy*, vol. 96, p. 283–291, 2013.
- [15] E. Kymakis, S. Kalykakis and T. M. Papazoglou, "Performance analysis of a grid connected photovoltaic park on the island of Crete," *Energy Conversion and Management*, vol. 50, no. 3, p. 433–438, 2009.
- [16] A. Massi Pavan, A. Mellit and D. Pieri, "The effect of soiling on energy production for large-scale photovoltaic plants," *Solar Energy*, vol. 85, no. 5, p. 1128–1136, 2011.
- [17] A. Al-Otaibi, A. Al-Qattan, F. Fairouz and A. Al-Mulla, "Performance evaluation of photovoltaic systems on Kuwaiti schools' rooftop," *Energy Conversion and Management*, vol. 95, p. 110–119, 2015.
- [18] H. Qasem, T. R. Betts, H. Müllejans, H. AlBusairi and R. Gottschalg, "Dust-induced shading on photovoltaic modules," *Progress in Photovoltaics: Research and Applications*, vol. 22, no. 2, p. 218–226, 2014.
- [19] A. P. Bateman, H. Belassein and S. T. Martin, "Impactor Apparatus for the Study of Particle Rebound: Relative Humidity and Capillary Forces," *Aerosol Science and Technology*, vol. 48, no. 1, p. 42–52, 2014.
- [20] B. Figgis, A. Ennaoui, B. Guo, W. Javed and E. Chen, "Outdoor soiling microscope for measuring particle deposition and resuspension," *Solar Energy*, vol. 137, p. 158–164, 2016.
- [21] X. Li, D. L. Mauzerall and M. H. Bergin, "Global reduction of solar power generation efficiency due to aerosols and panel soiling," *Nature Sustainability*, vol. 3, no. 9, p. 720–727, 2020.
- [22] V. Masson-Delmotte, P. Zhai, A. Pirani, S. Connors, C. Péan, S. Berger, N. Caud, Y. Chen, L. Goldfarb, M. I. Gomis, M. Huang, K. Leitzell, E. Lonnoy, J. Matthews, T. K. Maycock, T. Waterfield, O. Yelekçi, R. Yu and B. Zhou, Eds., *Climate Change 2021 - The Physical Science Basis*, IPCC, 2021: Summary for Policymakers., Cambridge University Press, Cambridge, United Kingdom and New York, NY, USA, p. 3–32.
- [23] K. K. Ilse, B. W. Figgis, V. Naumann, C. Hagendorf and J. Bagdahn, "Fundamentals of soiling processes on photovoltaic modules," *Renewable & Sustainable Energy Reviews*, vol. 98, p. 239–254, 2018.
- [24] B. S. Yilbas, H. Ali, M. M. Khaled, N. Al-Aqeeli, N. Abu-Dheir and K. K. Varanasi, "Influence of dust and mud on the optical, chemical, and mechanical properties of a pv protective glass," *SCIENTIFIC REPORTS*, vol. 5, p. 15833, 2015.
- [25] S. Mariraj Mohan, "An overview of particulate dry deposition: measuring methods, deposition velocity and controlling factors," *International Journal of Environmental Science and Technology*, vol. 13, no. 1, p. 387–402, 2016.
- [26] C. R. Lawrence and J. C. Neff, "The contemporary physical and chemical flux of aeolian dust: A synthesis of direct measurements of dust deposition," *Chemical Geology*, vol. 267, no. 1-2, p. 46–63, 2009.
- [27] J. F. Kok, E. J. R. Parteli, T. I. Michaels and D. B. Karam, "The physics of wind-blown sand and dust," *Reports on progress in physics. Physical Society (Great Britain)*, vol. 75, no. 10, p. 106901, 2012.
- [28] P. Ferrada, D. Olivares, V. del Campo, A. Marzo, F. Araya, E. Cabrera, J. Llanos, J. Correa-Puerta, C. Portillo, D. Román Silva, M. Trigo-Gonzalez, J. Alonso-Montesinos, G. López, J. Polo, F. J. Batlles and E.



- Fuentealba, "Physicochemical characterization of soiling from photovoltaic facilities in arid locations in the Atacama Desert," *Solar Energy*, vol. 187, p. 47–56, 2019.
- [29] D. Olivares, P. Ferrada, C. Matos, A. Marzo, E. Cabrera, C. Portillo and J. Llanos, "Characterization of soiling on PV modules in the Atacama Desert," *Energy Procedia*, vol. 124, p. 547–553, 2017.
- [30] B. Figgis, A. Ennaoui, S. Ahzi and Y. Rémond, "Review of PV soiling particle mechanics in desert environments," *Renewable & Sustainable Energy Reviews*, vol. 76, p. 872–881, 2017.
- [31] S. Mekhilef, R. Saidur and M. Kamalisarvestani, "Effect of dust, humidity and air velocity on efficiency of photovoltaic cells," *Renewable & Sustainable Energy Reviews*, vol. 16, no. 5, p. 2920–2925, 2012.
- [32] L. Dorobantu, M. O. Popescu, C. I. Popescu and A. Craciunescu, "The effect of surface impurities on photovoltaic panels," *Renewable Energy and Power Quality Journal*, p. 622–626, 2011.
- [33] E. Urrejola, J. Antonanzas, P. Ayala, M. Salgado, G. Ramírez-Sagner, C. Cortés, A. Pino and R. Escobar, "Effect of soiling and sunlight exposure on the performance ratio of photovoltaic technologies in Santiago, Chile," *Energy Conversion and Management*, vol. 114, p. 338–347, 2016.
- [34] G. McTainsh and C. Strong, "The role of aeolian dust in ecosystems," *Geomorphology*, vol. 89, no. 1-2, p. 39–54, 2007.
- [35] K. K. Ilse, J. Rabanal, L. Schonleber, M. Z. Khan, V. Naumann, C. Hagendorf and J. Bagdahn, "Comparing Indoor and Outdoor Soiling Experiments for Different Glass Coatings and Microstructural Analysis of Particle Caking Processes," *IEEE Journal of Photovoltaics*, vol. 8, no. 1, p. 203–209, 2018.
- [36] J. P. Engelbrecht, H. Moosmüller, S. Pincock, R. K. M. Jayanty, T. Lersch and G. Casuccio, "Technical note: Mineralogical, chemical, morphological, and optical interrelationships of mineral dust re-suspensions," *Atmospheric Chemistry and Physics*, vol. 16, no. 17, p. 10809–10830, 2016.
- [37] P. Burton and B. King, "Artificial soiling of photovoltaic module surfaces using traceable soil components," in *2013 IEEE 39th Photovoltaic Specialists Conference (PVSC)*, Tampa Bay, FL, USA, IEEE, 2013, pp. 1542–1545.
- [38] P. D. Burton and B. H. King, "Application and Characterization of an Artificial Grime for Photovoltaic Soiling Studies," *IEEE Journal of Photovoltaics*, vol. 4, no. 1, p. 299–303, 2014.
- [39] P. Piedra and H. Moosmüller, "Optical losses of photovoltaic cells due to aerosol deposition: Role of particle refractive index and size," *Solar Energy*, vol. 155, p. 637–646, 2017.
- [40] F. M. Zaihidee, S. Mekhilef, M. Seyedmahmoudian and B. Horan, "Dust as an unalterable deteriorative factor affecting PV panel's efficiency: Why and how," *Renewable & Sustainable Energy Reviews*, vol. 65, p. 1267–1278, 2016.
- [41] T. Lombardo, A. Ionescu, A. Chabas, R.-A. Lefèvre, P. Ausset and Y. Candau, "Dose-response function for the soiling of silica-soda-lime glass due to dry deposition," *The Science of the total environment*, vol. 408, no. 4, p. 976–984, 2010.
- [42] A. Chabas, A. Fouqueau, M. Attoui, S. C. Alfaro, A. Petitmangin, A. Bouilloux, M. Saheb, A. Coman, T. Lombardo, N. Grand, P. Zapf, R. Berardo, M. Duranton, R. Durand-Jolibois, M. Jerome, E. Pangui, J. J. Correia, I. Guillot and S. Nowak, "Characterisation of CIME, an experimental chamber for simulating interactions between materials of the cultural heritage and the environment," *Environmental science and pollution research international*, vol. 22, no. 23, p. 19170–19183, 2015.



- [43] M. Melcher, R. Wiesinger and M. Schreiner, "Degradation of glass artifacts: application of modern surface analytical techniques," *Accounts of chemical research*, vol. 43, no. 6, p. 916–926, 2010.
- [44] E. F. Cuddihy, "Theoretical considerations of soil retention," *Solar Energy Materials*, vol. 3, no. 1-2, p. 21–33, 1980.
- [45] J. Tomas, "Mechanics of Particle Adhesion, Extended master version of Tomas 2003 and full version of review paper of CHISA event," Prague, 2004.
- [46] C. L. Perkins, M. Muller and L. Simpson, "Laboratory Studies of Particle Cementation and PV module Soiling," in *2017 IEEE 44th Photovoltaic Specialist Conference (PVSC)*, Washington D.C., USA, IEEE, 2017, p. 2294–2297.
- [47] G. Picotti, P. Borghesani, M. E. Cholette and G. Manzolini, "Soiling of solar collectors – Modelling approaches for airborne dust and its interactions with surfaces," *Renewable & Sustainable Energy Reviews*, vol. 81, p. 2343–2357, 2018.
- [48] B. Figgis, A. Nouviaire, Y. Wubulikasimu, W. Javed, B. Guo, A. Ait-Mokhtar, R. Belarbi, S. Ahzi, Y. Rémond and A. Ennaoui, "Investigation of factors affecting condensation on soiled PV modules," *Solar Energy*, vol. 159, p. 488–500, 2018.
- [49] P. Hülsmann, M. Heck and M. Köhl, "Simulation of Water Vapor Ingress into PV-Modules under Different Climatic Conditions," *Journal of Materials*, vol. 2013, p. 1–7, 2013.
- [50] K. K. Ilse, B. W. Figgis, M. Werner, V. Naumann, C. Hagendorf, H. Pöllmann and J. Bagdahn, "Comprehensive analysis of soiling and cementation processes on PV modules in Qatar," *Solar Energy Materials and Solar Cells*, vol. 186, p. 309–323, 2018.
- [51] M. Gostein, J. R. Caron and B. Littmann, "Measuring soiling losses at utility-scale PV power plants," in *2014 IEEE 40th Photovoltaic Specialist Conference (PVSC)*, Denver, CO, USA, IEEE, 2014, p. 0885–0890.
- [52] L. Micheli, M. Muller and S. Kurtz, "Determining the effects of environment and atmospheric parameters on PV field performance," in *2016 IEEE 43rd Photovoltaic Specialists Conference (PVSC)*, Portland, OR, USA, IEEE, 2016, p. 1724–1729.
- [53] B. Guo, W. Javed, B. W. Figgis and T. Mirza, "Effect of dust and weather conditions on photovoltaic performance in Doha, Qatar," in *2015 First Workshop on Smart Grid and Renewable Energy (SGRE)*, IEEE, 2015, p. 1–6.
- [54] M. Gostein, B. Littmann, J. R. Caron and L. Dunn, "Comparing PV power plant soiling measurements extracted from PV module irradiance and power measurements," in *2013 IEEE 39th Photovoltaic Specialists Conference (PVSC)*, Tampa Bay, FL, USA, IEEE, 2013, p. 3004–3009.
- [55] L. L. Kazmerski, A. S. A. Diniz, D. S. Braga, C. B. Maia, M. M. Viana, S. C. Costa, P. P. Brito, C. D. Campos, S. Morais Hanriot and L. R. Oliveira Cruz, "Interrelationships Among Non-Uniform Soiling Distributions and PV Module Performance Parameters, Climate Conditions, and Soiling Particle and Module Surface Properties," in *2017 IEEE 44th Photovoltaic Specialist Conference (PVSC)*, Washington D.C., USA, IEEE, 2017, p. 2307–2311.
- [56] R. K. Jones, A. Baras, A. A. Saeeri, A. Al Qahtani, A. O. Al Amoudi, Y. Al Shaya, M. Alodan and S. A. Al-Hsaien, "Optimized Cleaning Cost and Schedule Based on Observed Soiling Conditions for Photovoltaic Plants in Central Saudi Arabia," *IEEE Journal of Photovoltaics*, vol. 6, no. 3, p. 730–738, 2016.



- [57] A. Kimber, L. Mitchell, S. Nogradi and H. Wenger, "The effect of soiling on large grid-connected photovoltaic systems in California and the Southwest region of the United States," in *2006 IEEE 4th World Conference on Photovoltaic Energy*, Waikoloa, HI, USA, 2006.
- [58] M. G. Deceglie, M. Muller, Z. Defreitas and S. Kurtz, "A scalable method for extracting soiling rates from PV production data," in *2016 IEEE 43rd Photovoltaic Specialists Conference (PVSC)*, Portland, OR, USA, IEEE, 2016, p. 2061–2065.
- [59] P. Besson, C. Munoz, G. Ramirez-Sagner, M. Salgado, R. Escobar and W. Platzler, "Long-Term Soiling Analysis for Three Photovoltaic Technologies in Santiago Region," *IEEE Journal of Photovoltaics*, vol. 7, no. 6, p. 1755–1760, 2017.
- [60] L. Micheli, E. F. Fernandez, M. Muller and F. Almonacid, "Extracting and Generating PV Soiling Profiles for Analysis, Forecasting, and Cleaning Optimization," *IEEE Journal of Photovoltaics*, vol. 10, no. 1, p. 197–205, 2020.
- [61] M. Gostein, T. Düster and C. Thumann, "Accurately measuring PV soiling losses with soiling station employing module power measurements," in *2015 IEEE 42nd Photovoltaic Specialist Conference (PVSC)*, New Orleans, LA, USA, IEEE, 2015, pp. 2808-2810.
- [62] M. R. Maghami, H. Hizam, C. Gomes, M. A. Radzi, M. I. Rezadad and S. Hajighorbani, "Power loss due to soiling on solar panel: A review," *Renewable and Sustainable Energy Reviews*, vol. 59, p. 1307–1316, 2016.
- [63] J. R. Caron and B. Littmann, "Direct Monitoring of Energy Lost Due to Soiling on First Solar Modules in California," *IEEE Journal of Photovoltaics*, vol. 3, no. 1, p. 336–340, 2013.
- [64] J. Lopez-Garcia, A. Pozza and T. Sample, "Long-term soiling of silicon PV modules in a moderate subtropical climate," *Solar Energy*, vol. 130, pp. 174-183, 2016.
- [65] W. Herrmann, M. Schweiger, G. Tamizhmani, B. Shisler and C. S. Kamalaksha, "Soiling and self-cleaning of PV modules under the weather conditions of two locations in Arizona and South-East India," in *2015 IEEE 42nd Photovoltaic Specialist Conference*, New Orleans, LA, USA, IEEE, 2015, pp. 1-5.
- [66] M. A. Grammatico and B. W. Littmann, "Quantifying the anti-soiling benefits of anti-reflective coatings on first solar cadmium telluride PV modules," in *2016 IEEE 43rd Photovoltaic Specialists Conference*, Portland, OR, USA, IEEE, 2016, pp. 1697-1701.
- [67] M. Muller, L. Micheli and A. A. Martinez-Morales, "A Method to Extract Soiling Loss Data from Soiling Stations with Imperfect Cleaning Schedules," in *2017 IEEE 44th Photovoltaic Specialist Conference (PVSC)*, Washington D.C., USA, IEEE, 2017, p. 2881–2886.
- [68] C. Schill, S. Brachmann and M. Koehl, "Impact of soiling on IV-curves and efficiency of PV-modules," *Solar Energy*, vol. 112, p. 259–262, 2015.
- [69] "IEC 60891:2009 Photovoltaic devices - Procedures for temperature and irradiance corrections to measured I-V characteristics," International Electrotechnical Commission, 2009.
- [70] "CR-PVS1: PV Soiling Loss Index RTU (revision: 11/17)," Campbell Scientific, 2017.
- [71] L. Dunn, B. Littmann, J. R. Caron and M. Gostein, "PV module soiling measurement uncertainty analysis," in *2013 IEEE 39th Photovoltaic Specialists Conference (PVSC)*, Tampa Bay, FL, USA, IEEE, 2013, pp. 0658-0663.



- [72] A. Skoczek, T. Sample and E. D. Dunlop, "The results of performance measurements of field-aged crystalline silicon photovoltaic modules," *Progress in Photovoltaics: Research and Applications*, vol. 17, pp. 227-240, 2009.
- [73] L. Fanni, I. Pola, E. Bura, T. Friesen and D. Chianese, "Investigation of annealing and degradation effects on a-Si PV modules in real operating conditions," in *2009 24th European Photovoltaic Solar Energy Conference (EU-PVSEC)*, Hamburg, Germany, 2009, pp. 3596 - 3599.
- [74] K. Sinapis, G. Papageorgiou, K. Durose, M. van den Donker and W. Folkerts, "Outdoor degradation of CdTe modules at open circuit and at maximum power point," in *2015 IEEE 42nd Photovoltaic Specialists Conference*, New Orleans, LA, USA, IEEE, 2015, pp. 1-5.
- [75] D. van Velson, "DustIQ Soiling Measurement Instruction Manual," Kipp and Zonen, Delft, 2018.
- [76] M. Gostein, "Atonometrics white paper: specifying a soiling measurement system," Atonometrics, Austin, 2018.
- [77] *IEC 61724-1:2017, "Photovoltaic system performance - Part 1: Monitoring"*, Geneva, Switzerland: International Electrical Commission IEC, 2017.
- [78] A. A. Hegazy, "Effect of dust accumulation on solar transmittance through glass covers of plate-type collectors," *Renewable Energy*, vol. 22, no. 4, p. 525–540, 2001.
- [79] J. Cano, J. J. John, S. Tatapudi and G. TamizhMani, "Effect of tilt angle on soiling of photovoltaic modules," in *2014 IEEE 40th Photovoltaic Specialist Conference, PVSC*, Denver, CO, USA, IEEE, 2014, p. 3174–3176.
- [80] M. Waters, T. Tirumalai, M. Gostein and B. Stueve, "Soiling Rates of PV Modules vs. Thermopile Pyranometers," in *2017 IEEE 44th Photovoltaic Specialist Conference (PVSC)*, Washington D.C., USA, IEEE, 2017, p. 2923–2925.
- [81] F. Wolfertstetter, K. Pottler, N. Geuder, R. Affolter, A. A. Merrouni, A. Mezrhah and R. Pitz-Paal, "Monitoring of Mirror and Sensor Soiling with TraCS for Improved Quality of Ground based Irradiance Measurements," *Energy Procedia*, vol. 49, p. 2422–2432, 2014.
- [82] C. Chen, "CiteSpace II: Detecting and visualizing emerging trends and transient patterns in scientific literature," *Journal of the American Society for Information Science and Technology*, vol. 57, no. 3, p. 359–377, 2006.
- [83] L. Boyle, *Dissertation: Don't Soil Your Chances With Solar Energy: Experiments Of Natural Dust Accumulation On Solar Modules And The Effect On Light Transmission*, University of Colorado, 2015.
- [84] S. Toth, M. Muller, D. C. Miller, H. Moutinho, B. To, L. Micheli, J. Linger, C. Engtrakul, A. Einhorn and L. Simpson, "Soiling and cleaning: Initial observations from 5-year photovoltaic glass coating durability study," *Solar Energy Materials and Solar Cells*, vol. 185, p. 375–384, 2018.
- [85] B. Guo, W. Javed, S. Khan, B. Figgis and T. Mirza, "Models for Prediction of Soiling-Caused Photovoltaic Power Output Degradation Based on Environmental Variables in Doha, Qatar," Charlotte, North Carolina, USA, ASME, 2016, p. V001T08A004.
- [86] S. Pulipaka, F. Mani and R. Kumar, "Modeling of soiled PV module with neural networks and regression using particle size composition," *Solar Energy*, vol. 123, p. 116–126, 2016.



- [87] L. Micheli and M. Muller, "An investigation of the key parameters for predicting PV soiling losses: Key parameters for predicting PV soiling losses," *Progress in Photovoltaics: Research and Applications*, vol. 25, no. 4, p. 291–307, 2017.
- [88] R. R. Cordero, A. Damiani, D. Laroze, S. MacDonell, J. Jorquera, E. Sepúlveda, S. Feron, P. Llanillo, F. Labbe, J. Carrasco, J. Ferrer and G. Torres, "Effects of soiling on photovoltaic (PV) modules in the Atacama Desert," *SCIENTIFIC REPORTS*, vol. 8, no. 1, 2018.
- [89] S. You, Y. J. Lim, Y. Dai and C.-H. Wang, "On the temporal modelling of solar photovoltaic soiling: Energy and economic impacts in seven cities," *Applied Energy*, vol. 228, p. 1136–1146, 2018.
- [90] M. Coello and L. Boyle, "Simple Model for Predicting Time Series Soiling of Photovoltaic Panels," *IEEE Journal of Photovoltaics*, vol. 9, no. 5, p. 1382–1387, 2019.
- [91] M. H. Bergin, C. Ghoroi, D. Dixit, J. J. Schauer and D. T. Shindell, "Large Reductions in Solar Energy Production Due to Dust and Particulate Air Pollution," *Environmental Science & Technology Letters*, vol. 4, no. 8, p. 339–344, 2017.
- [92] B. Laarabi, O. May Tzuc, D. Dahlioui, A. Bassam, M. Flota-Bañuelos and A. Barhdadi, "Artificial neural network modeling and sensitivity analysis for soiling effects on photovoltaic panels in Morocco," *Superlattices and Microstructures*, vol. 127, p. 139–150, 2019.
- [93] S. Shapsough, R. Dhaouadi and I. Zualkernan, "Using Linear Regression and Back Propagation Neural Networks to Predict Performance of Soiled PV Modules," *Procedia Computer Science*, vol. 155, p. 463–470, 2019.
- [94] L. Micheli, M. G. Deceglie and M. Muller, "Mapping Photovoltaic Soiling Using Spatial Interpolation Techniques," *IEEE Journal of Photovoltaics*, vol. 9, no. 1, p. 272–277, 2019.
- [95] S. Pelland, P. Pawar, A. Veeramani, W. Gustafson and L. L. A. Etringer, "Testing Global Models of Photovoltaic Soiling Ratios Against Field Test Data Worldwide," in *2018 IEEE 7th World Conference on Photovoltaic Energy Conversion (WCPEC) (A Joint Conference of 45th IEEE PVSC, 28th PVSEC & 34th EU PVSEC)*, Waikoloa Village, HI, USA, IEEE, 2018, p. 3442–3446.
- [96] L. Zhou, D. B. Schwede, K. W. Appel, M. J. Mangiante, D. C. Wong, S. L. Napelenok, P.-Y. Whung and B. Zhang, "The impact of air pollutant deposition on solar energy system efficiency: An approach to estimate PV soiling effects with the Community Multiscale Air Quality (CMAQ) model," *Science of the Total Environment*, vol. 651, p. 456–465, 2019.
- [97] R. E. Pawluk, Y. Chen and Y. She, "Photovoltaic electricity generation loss due to snow – A literature review on influence factors, estimation, and mitigation," *Renewable & Sustainable Energy Reviews*, vol. 107, p. 171–182, 2019.
- [98] Government of Canada, "Engineering Climate Datasets", *Natural Resources Canada*, 2019.
- [99] B. Marion, R. Schaefer, H. Caine and G. Sanchez, "Measured and modeled photovoltaic system energy losses from snow for Colorado and Wisconsin locations," *Solar Energy*, vol. 97, p. 112–121, 2013.
- [100] T. Townsend and L. Powers, "Photovoltaics and snow: An update from two winters of measurements in the SIERRA," in *2011 37th IEEE Photovoltaic Specialists Conference*, Seattle, WA, USA, IEEE, 2011, p. 3231–3236.
- [101] S. A. Krajewski and B. L. Gibbs, *Understanding Contouring: A Practical Guide to Spatial Estimation Using a Computer and Basics of Using Variograms*, Colorado: Gibbs Associates, 2014.



- [102] C. Baldus-Jeursen, "Analysis of Fort Simpson Airport Photovoltaic System Performance from January 1, 2015 to December 31, 2018," Varennes, 2018.
- [103] M. Mani and R. Pillai, "Impact of dust on solar photovoltaic (PV) performance: Research status, challenges and recommendations," *Renewable and Sustainable Energy Reviews*, vol. 14, no. 9, p. 3124–3131, 2010.
- [104] National Renewable Energy Laboratory, Sandia National Laboratory, SunSpec Alliance and SunShot National Laboratory Multiyear Partnership (SuNLaMP) PV O&M, "Best Practices for Operation and Maintenance of Photovoltaic and Energy Storage Systems; 3rd Edition," 2018.
- [105] L. Cristaldi, M. Faifer, M. Rossi, M. Catelani, L. Ciani, E. Dovere and S. Jerace, "Economical evaluation of PV system losses due to the dust and pollution," IEEE Instrumentation and Measurement Technology Conference, IEEE, 2012, p. 614–618.
- [106] J. Tanesab, D. Parlevliet, J. Whale and T. Urmee, "Energy and economic losses caused by dust on residential photovoltaic (PV) systems deployed in different climate areas," *Renewable Energy*, vol. 120, p. 401–412, 2018.
- [107] F. A. Mejia and J. Kleissl, "Soiling losses for solar photovoltaic systems in California," *Solar Energy*, vol. 95, p. 357–363, 2013.
- [108] W. Herrmann, *Energy yield of PV power plants – Approaches for the determination of yield losses due to dust soiling in desert climates*, InDust Workshop 16 May 2019, Intersolar Europe, Munich, Germany, 2019.
- [109] M. G. Deceglie, L. Micheli and M. Muller, "Quantifying Year-to-Year Variations in Solar Panel Soiling from PV Energy-Production Data," in *2017 IEEE 44th Photovoltaic Specialist Conference (PVSC)*, Washington D.C., USA, IEEE, 2017, p. 2804–2807.
- [110] Faifer M., Lazzaroni M., Toscani S., "Dust effects on the PV plant efficiency: A new monitoring strategy," in *20th IMEKO TC4 International Symposium and 18th International Workshop on ADC Modelling and Testing*, Benevento, Italy, 2014.
- [111] S. C. Costa, A. S. A. Diniz and L. L. Kazmerski, "Solar energy dust and soiling R&D progress: Literature review update for 2016," *Renewable & Sustainable Energy Reviews*, vol. 82, p. 2504–2536, 2018.
- [112] H. Haeberlin and J. D. Graf, "Gradual Reduction of PV Generator Yield due to Pollution," in *1998 2nd World Conference on Photovoltaic Solar Energy Conversion*, Vienna, Austria, 1998, pp. 2764-2767.
- [113] A. AlDowsari, R. Bkayrat, H. AlZain and T. Shahin, "Best practices for mitigating soiling risk on PV power plants," Jeddah, Saudi Arabia, IEEE, 2014, p. 1–6.
- [114] W. Glaubitt and P. Löbmann, "Anti-soiling effect of porous SiO₂ coatings prepared by sol–gel processing," *Journal of Sol-Gel Science and Technology*, vol. 59, no. 2, p. 239–244, 2011.
- [115] A. Einhorn, L. Micheli, D. C. Miller, L. J. Simpson, H. R. Moutinho, B. To, C. L. Lanaghan, M. T. Muller, S. Toth, J. J. John, S. Warade, A. Kottantharayil and C. Engtrakul, "Evaluation of Soiling and Potential Mitigation Approaches on Photovoltaic Glass," *IEEE Journal of Photovoltaics*, vol. 9, no. 1, p. 233–239, 2019.
- [116] M. A. M. L. Jesus, G. Timò, C. Agustín-Sáenz, I. Braceras, M. Cornelli and A. d. M. Ferreira, "Anti-soiling coatings for solar cell cover glass: Climate and surface properties influence," *Solar Energy Materials and Solar Cells*, vol. 185, p. 517–523, 2018.



- [117] M. A. Bahattab, I. A. Alhomoudi, M. I. Alhussaini, M. Mirza, J. Hegmann, W. Glaubitt and P. Löbmann, “Anti-soiling surfaces for PV applications prepared by sol-gel processing: Comparison of laboratory testing and outdoor exposure,” *Solar Energy Materials and Solar Cells*, vol. 157, p. 422–428, 2016.
- [118] K. Ilse, M. Z. Khan, N. Voicu, V. Naumann, C. Hagendorf and J. Bagdahn, “Advanced performance testing of anti-soiling coatings – Part I: Sequential laboratory test methodology covering the physics of natural soiling processes,” *Solar Energy Materials and Solar Cells*, vol. 202, p. 110048, 2019.
- [119] K. Ilse, M. Z. Khan, N. Voicu, V. Naumann, C. Hagendorf and J. Bagdahn, “Advanced performance testing of anti-soiling coatings - Part II: Particle-size dependent analysis for physical understanding of dust removal processes and determination of adhesion forces,” *Solar Energy Materials and Solar Cells*, vol. 202, p. 110049, 2019.
- [120] T. Lorenz, E. Klimm and K.-A. Weiss, “Soiling and Anti-soiling Coatings on Surfaces of Solar Thermal Systems – Featuring an Economic Feasibility Analysis,” *Energy Procedia*, vol. 48, p. 749–756, 2014.
- [121] S. Mondal, A. K. Mondal, A. Sharma, V. Devalla, S. Rana, S. Kumar and J. K. Pandey, “An overview of cleaning and prevention processes for enhancing efficiency of solar photovoltaic panels,” *CURRENT SCIENCE*, vol. 115, no. 6, p. 13, 2018.
- [122] G. C. Oehler, F. Lisco, F. Bukhari, S. Uličná, B. Strauss, K. L. Barth and J. M. Walls, “Testing the Durability of Anti-Soiling Coatings for Solar Cover Glass by Outdoor Exposure in Denmark,” *Energies*, vol. 13, no. 2, p. 299, 2020.
- [123] H. K. Elminir, A. E. Ghitas, R. H. Hamid, F. El-Hussainy, M. M. Beheary and K. M. Abdel-Moneim, “Effect of dust on the transparent cover of solar collectors,” *Energy Conversion and Management*, vol. 47, no. 18-19, p. 3192–3203, 2006.
- [124] S. Bhaduri and A. Kottantharayil, “Mitigation of Soiling by Vertical Mounting of Bifacial Modules,” *IEEE Journal of Photovoltaics*, vol. 9, no. 1, p. 240–244, 2019.
- [125] S. Bhaduri, S. Chattopadhyay, S. Zachariah, C. S. Solanki and A. Kottantharayil, “Evaluation of Increase in the Energy Yield of PV Modules by Inverting the Panels during the Non-Sunshine Hours,” in *26th International Photovoltaic Science and Engineering Conference*, Singapore, 2016.
- [126] S. Warade and A. Kottantharayil, “Analysis of Soiling Losses for Different Cleaning Cycles,” in *2018 IEEE 7th World Conference on Photovoltaic Energy Conversion (WCPEC) (A Joint Conference of 45th IEEE PVSC, 28th PVSEC & 34th EU PVSEC)*, Waikoloa Village, HI, USA, IEEE, 2018, p. 3644–3647.
- [127] J. J. John, *Characterization of Soiling Loss on Photovoltaic Modules, and Development of a Novel Cleaning System*, Bombay, India: Indian Institute of Technology, 2015.
- [128] J. Kurz, “PV Cleaning: Choosing the Optimal Method and Frequency,” *Solar Power Europe Webinar*, p. 25, October 18, 2017.
- [129] M. T. Grando, E. R. Maletz, D. Martins, H. Simas and R. Simoni, “Robots for Cleaning Photovoltaic Panels: State of the Art and Future Prospects,” in *Actas de las IX Jornadas Argentinas de Robótica*, Córdoba, Argentina, 2017.
- [130] S. Masuda, K. Fujibayashi, K. Ishida and H. Inaba, “Confinement and transportation of charged aerosol clouds via electric curtain,” *Electronic Engineering in Japan*, pp. 92:9-18, 1972.
- [131] A. Faes, D. Petri, J. Champiaud, J. Geissbühler, N. Badel, J. Levrat, B. Roustom, A. Hessler-Wyser, N. Wyrsh, C. Ballif, G. Getaz, G. McKarris and M. Despeisse, “Field test and electrode optimization of



- electrodynamic cleaning systems for solar panels," *Progress in Photovoltaics: Research and Applications*, vol. 27, no. 11, p. 1020–1033, 2019.
- [132] S. P. Hersey, R. M. Garland, E. Crosbie, T. Shingler, A. Sorooshian, S. Piketh and R. Burger, "An overview of regional and local characteristics of aerosols in South Africa using satellite, ground, and modeling data," *Atmospheric Chemistry and Physics*, vol. 15, p. 4259–4278, 2015.
- [133] N. Ferretti, *White Paper PV Module Cleaning, Market Overview and Basics*, PI Berlin, 2018.
- [134] *European Parliament and the Council of the European Union, EC/2006/42, Essential health and safety requirements relating to the design and construction of machinery*, 2006.
- [135] *EN 1096-5:2016-06, "Glass in building - Coated glass - Part 5: Test method and classification for the self-cleaning performances of coated glass surfaces"*, 2016.
- [136] *ECE R45, Supplement 4.2, "Uniform provisions concerning the approval of headlamp cleaners and of power driven vehicles with regard to headlamp cleaners (Test Dirt: Quartz-Coal Mixture)"*.
- [137] *ISO 12103-1, "Road vehicles — Test contaminants for filter evaluation — Part 1: Arizona test dust"*, 2016.
- [138] *DIN EN ISO 20566, 2013-06, "Paints and varnishes -- Determination of the scratch resistance of a coating system using a laboratory-scale car-wash"*, 2013.
- [139] *IEC 62788-7-3 ED1, "Measurement procedures for materials used in photovoltaic modules - Part 7-3: Environmental exposures - Accelerated abrasion tests of PV module external surfaces (test of small glass samples)"*, Geneva, Switzerland: International Electrical Commission.
- [140] *ASTM D2486-17:2017, "Standard test methods for scrub resistance of wall paints"*, 2017.
- [141] *DIN 53778-2, "Emulsion paints for interior use: evaluation of cleanability and of wash and scrub resistance of coatings, 1983-08"*, 1983.
- [142] K. Ilse, *Cleaning resistance of glass coatings, Test report V403/2018 www.fsolar.de*, Fraunhofer CSP, 2018.
- [143] N. Ferretti, A. Sönmez, F. Schneider, B. Litzemberger, S. Janke, T. Weber, J. Berghold and P. Grunow, "Reflectance Measurements for Testing the Effect of Module Cleaning on the Glass Surface," *2015 31st European Photovoltaic Solar Energy Conference and Exhibition (EU-PVSEC)*, pp. 2538 - 2544, 2015.
- [144] N. Ferretti, K. Ilse, A. Sönmez, C. Hagendorf and J. Berghold, "Investigation on the Impact of Module Cleaning on the Antireflection Coating," *32nd European Photovoltaic Solar Energy Conference and Exhibition*, 2016.
- [145] *EN 1096-5:2012, "Glass in building - Coated glass - Part 2: Requirements and test methods for class A, B and S coatings. Annex E: Abrasion resistance test"*, 2012.
- [146] N. Ferretti, A. El-Issa and L. Podlowski, "Standardized Test Procedure for PV Module Cleaning Equipment," in *2019 36th European Photovoltaic Solar Energy Conference and Exhibition (EU-PVSEC)*, Marseille, France, 2019, pp. 805 - 809.
- [147] G. Mathiak, D. Grimm, L. Rimmelspacher, W. Herrmann, F. Reil, J. Althaus and A. Morlier, "PV Module and Solar Glass Trickling Sand Testing," in *2018 35th European Photovoltaic Solar Energy Conference and Exhibition*, Brussels, Belgium, 2018, pp. 1092 - 1096.



- [148] DIN spec 4867, (under development): "Reinigungsprüfverfahren für die Abrasionsbeständigkeit von Photovoltaik-Modulen - Cleaning test method for the abrasion resistance of photovoltaic modules.", 2022.
- [149] Amtec Kistler GmbH, *Laboratory car wash for testing the scratch resistance of coatings*, www.amteckistler.de, download 2020, 2020.
- [150] J. Tanesab, D. Parlevliet, J. Whale and T. Urnee, "Dust Effect and its Economic Analysis on PV Modules Deployed in a Temperate Climate Zone," *Energy Procedia*, vol. 100, p. 65–68, 2016.
- [151] B. Stridh, "Economical Benefit of Cleaning of Soiling and Snow Evaluated for PV Plants at Three Locations in Europe," *27th European Photovoltaic Solar Energy Conference and Exhibition*, 2012.
- [152] N. Heidari, J. Gwamuri, T. Townsend and J. M. Pearce, "Impact of Snow and Ground Interference on Photovoltaic Electric System Performance," *IEEE Journal of Photovoltaics*, vol. 5, no. 6, p. 1680–1685, 2015.
- [153] R. W. Andrews, A. Pollard and J. M. Pearce, "The effects of snowfall on solar photovoltaic performance," *Solar Energy*, vol. 92, p. 84–97, 2013.
- [154] G. Becker, B. Schiebelsberger, W. Weber, J. Schumacher, M. Zehner, G. Wotruba and C. Vodermayr, "Energy Yields of PV Systems - Comparison of Simulation and Reality," *23rd European Photovoltaic Solar Energy Conference and Exhibition, 1-5 September 2008, Valencia, Spain*, 2008.
- [155] T. Sugiura, T. Yamada, H. Nakamura, M. Umeya, K. Sakuta and K. Kurokawa, "Measurements, analyses and evaluation of residential PV systems by Japanese monitoring program," *Solar Energy Materials and Solar Cells*, vol. 75, no. 3-4, p. 767–779, 2003.
- [156] M. Child and C. Breyer, "Vision and initial feasibility analysis of a recarbonised Finnish energy system for 2050," *Renewable & Sustainable Energy Reviews*, vol. 66, p. 517–536, 2016.
- [157] E. Bellini, "Russian Far East sees 75MW of large scale solar come online," *PV Magazine*, 2019, Nov.1 .
- [158] D. Dissing, "Radiation climatology of Alaska," University of Alaska Fairbanks.
- [159] L. Burnham, *Performance of Bifacial Modules on a Dual-Axis Tracker in a High-Albedo Environment*, <https://www.osti.gov/servlets/purl/1641282> last accessed Dec 2022, 2019, p. 8.
- [160] J. L. Braid, D. Riley, J. M. Pearce and L. Burnham, "Image Analysis Method for Quantifying Snow Losses on PV Systems," in *2020 47th IEEE Photovoltaic Specialists Conference (PVSC)*, Virtual Meeting, IEEE, 2020, p. 1510–1516.
- [161] E. Lorenz, D. Heinemann and C. Kurz, "Local and regional photovoltaic power prediction for large scale grid integration: Assessment of a new algorithm for snow detection," *Progress in Photovoltaics: Research and Applications*, vol. 20, no. 6, p. 760–769, 2012.
- [162] A. P. Dobos, *PV Watts Version 5 Manual*. NREL/TP-6A20-62641, 2014.
- [163] D. F. J. Ryberg, *Integration, Validation, and Application of a PV Snow Coverage Model in SAM*. Report number: NREL/TP-6A20-64260., September 2015.
- [164] A. Granlund, J. Narvesjö and A. M. Petersson, "The Influence of Module Tilt on Snow Shadowing of Frameless Bifacial Modules," in *2019 36th European Photovoltaic Solar Energy Conference and Exhibition*, Marseille, France, 2019, pp. 1646 - 1650.



- [165] B. Hashemi, A.-M. Cretu and S. Taheri, "Snow Loss Prediction for Photovoltaic Farms Using Computational Intelligence Techniques," *IEEE Journal of Photovoltaics*, vol. 10, no. 4, p. 1044–1052, 2020.
- [166] S. Hosseini, S. Taheri, M. Farzaneh and H. Taheri, "Modeling of Snow-Covered Photovoltaic Modules," *IEEE Transactions on Industrial Electronics*, vol. 65, no. 10, p. 7975–7983, 2018.
- [167] X. Liu, S. J. Rees and J. D. Spitler, "Modeling snow melting on heated pavement surfaces. Part I: Model development," *Applied Thermal Engineering*, vol. 27, no. 5-6, p. 1115–1124, 2007.
- [168] S. L. Hockersmith, Experimental and Computational Investigation of Snow Melting on heated horizontal Surfaces, Oklahoma State University, Stillwater, Oklahoma, USA, 2002.
- [169] A. Rahmatmand, S. J. Harrison and P. H. Oosthuizen, "Numerical and experimental study of an improved method for prediction of snow melting and snow sliding from photovoltaic panels," *Applied Thermal Engineering*, vol. 158, p. 113773, 2019.
- [170] D. Riley, L. Burnham, B. Walker and J. M. Pearce, "Differences in Snow Shedding in Photovoltaic Systems with Framed and Frameless Modules," in *2019 IEEE 46th Photovoltaic Specialists Conference (PVSC)*, Chicago, IL, USA, IEEE, 2019, p. 0558–0561.
- [171] J. Bogenrieder, C. Camus, M. Hüttner, P. Offermann, J. Hauch and C. J. Brabec, "Technology-dependent analysis of the snow melting and sliding behavior on photovoltaic modules," *Journal of Renewable and Sustainable Energy*, vol. 10, no. 2, p. 021005, 2018.
- [172] G. Mathiak, J. Sommer, W. Herrmann, N. Bogdanski, J. Althaus and F. Reil, "PV Module Damages Caused by Hail Impact and Non-Uniform Snow Load," in *2016 32nd European Photovoltaic Solar Energy Conference and Exhibition*, Munich, Germany, 2016, pp. 1692 - 1696.
- [173] E. J. Schneller, H. Seigneur, J. Lincoln and A. M. Gabor, "The Impact of Cold Temperature Exposure in Mechanical Durability Testing of PV Modules," in *2019 IEEE 46th Photovoltaic Specialists Conference (PVSC)*, Chicago, IL, USA, IEEE, 2019, p. 1521–1524.
- [174] C. Pike, E. Whitney, M. Wilber and J. S. Stein, "Field Performance of South-Facing and East-West Facing Bifacial Modules in the Arctic," *Energies*, vol. 14, no. 4, p. 1210, 2021.
- [175] A. M. Gabor, R. Janoch, A. Anselmo, J. Lincoln, E. J. Schneller, H. Seigneur, D. J. Harwood and M. W. Rowell, "Mounting Rail Spacers for Improved Solar Panel Durability," in *2019 IEEE 46th Photovoltaic Specialists Conference (PVSC)*, Chicago, IL, USA, IEEE, 2019, p. 0131–0135.
- [176] J. S. Malmsten, "Solceller på tak" - "Solar cells on the roof", BELOK large commercial building in cooperation with Swedish Energy Agency, 2015 Dec..

